The Development and Enhancement of a Forward Mathematical Model of the Human Knee Joint

A Dissertation Presented for the

Doctor of Philosophy

Degree

The University of Tennessee, Knoxville

Seth Coomer

May 2024

Copyright © 2024 by Seth Coomer

All rights reserved.

Dedication

This dissertation is dedicated to my late father, Dr. Timothy Coomer. Dad, you have always been my greatest supporter. I always felt you understood my experience as a fellow PhD and engineering major. I could come to you with anything and always felt accepted and loved. Your perseverance in the face of the most difficult circumstances continues to inspire me to push through challenges with strength and joy. For it is in those moments where you truly learn who you are. Your example of hard work, integrity, and kindness will stay with me forever. I love you and thank you for all you did for me and your family.

Acknowledgements

I would first like to thank Dr. Richard Komistek for your wisdom and encouragement during my time at the Center for Musculoskeletal Research. You believed in me and empowered me to make this project my own. You also taught me to think about problem solving with curiosity and eagerness. Finally, you taught me that relationships are key for success in both academics and industry.

Thank you to Dr. Michael LaCour for your guidance and support during my time at the lab. As someone who has been a graduate student in CMR, I felt you understood the challenges that I faced whether big or small. Your advice on navigating the development of a mathematical model was extremely valuable to me.

Thank you to Dr. Bradley Meccia for sharing your expertise in mathematical modeling. Your patience and effective communication make you a great teacher. I'm glad we got to work closely on improving this model. You taught me everything from coding concepts to biomechanics during my time in CMR.

Finally, I would like to thank my CMR lab mates Lauren Smith, Garett Dessinger, Jarrod Nachtrab, Viet Nguyen, Thang Nguyen, Caleb Chesney, Milad Khasian, and Mike Ta. I appreciate your friendship and support during my time at CMR. Best of luck in the future.

Abstract

Degenerative joint disease, or osteoarthritis, is a common occurrence in the knee joint. This can often result in joint pain, decrease in range of motion, and ultimately disability. One way to counteract osteoarthritis is the incorporation of a total knee arthroplasty (TKA). TKAs replace the damaged bone and soft tissue surrounding the knee with metal and polyethylene components. Ideally this will improve the joint's performance and reduce pain. However, there is still a number of TKA patients who remain dissatisfied. In order to investigate this, in depth research must be done on the design and performance of TKAs.

One such way to analyze TKA performance is through mathematical modeling. Over the years a forward solution mathematical model of the knee has been developed by the Center of Musculoskeletal Research at the University of Tennessee in Knoxville. The goal of this dissertation is to build upon and further advance this previously validated forward mathematical model of the knee. This is done by creating a patellofemoral contact detection system which allows for a medial/lateral contact area split in deep flexion, developing a contact mapping algorithm which can utilize modeling results to calculate contact areas and contact stresses, and incorporating a gait activity into the model which assesses kinetics and kinematics during the stance phase of gait. This dissertation also seeks to incorporate new implant types into the model including revision TKAs and unicompartmental knee arthroplasties. Overall, utilizing the model's new capabilities allows researchers to explore various aspects of TKA design and the effects that change may have on contact mechanics and soft tissue forces.

Table of Contents

Chapter 1 Introduction 1

1.1 Basic Anatomical Definitions 1

1.2 Anatomy of the Knee Joint 1

1.2.1 Muscles of the Knee Joint 4

1.2.2 Ligaments of the Knee Joint 4

1.3 Motion of the Normal Knee 6

1.4 Total Knee Arthroplasty 9

1.4.1 Common TKA Complications 9

1.4.2 TKA Evaluation Techniques 10

Chapter 2 Background 14

2.1 Knee Implant Designs 14

2.1.1 Fixed Bearing vs Mobile Bearing TKAs 14

2.1.2 TKA Designs and Ligament Resection 16

2.1.3 UKA Designs 18

2.2 Mathematical Modeling Techniques 21

2.2.1 Inverse Solution Modeling 21

2.2.2 Forward Solution Modeling 24

2.2.3 Rigid Body Dynamics 26

2.2.4 Finite Element Analysis 28

Chapter 3 Objectives and Contributions 31

3.1 Dissertation Objectives 31

3.2 Dissertation Contributions 32

Chapter 4 Methods 35

4.1 General Mathematical Modeling Methods 35

4.1.1 Modeling Techniques to Analyze the Lower Leg 36

4.2 Modeling Human Anatomy 38

4.2.1 Modeling Bones 41

4.2.2 Modeling Muscles 41

4.2.3 Modeling Ligaments 43

4.3 Contact Detection and Contact Mapping 46

4.3.1 General Contact Detection 46

4.3.2 Contact Mapping 48

4.3.3 Patellofemoral Contact Mapping Improvements 52

4.4 Developing Solutions for New Implants 58

4.4.1 Sigma Stabilized + ... 58

4.4.2 Unicompartmental Knee Arthroplasty 63

4.5 Developing New Activities 66

4.5.1 Gait 66

4.6 Graphical User Interface 72

Chapter 5 Results and Discussion 74

5.1 Improving Soft Tissue Representations 74

5.1.1 Modifying MCL Attachments 74

5.1.2 Incorporating the Posterior Capsule 86

5.2 Incorporating New Implant Types 90

5.2.1 Sigma Stabilized + ... 90

5.2.2 Unicompartmental Knee Arthroplasty 101

5.2.3 Kinetic Comparison for UKAs 104

5.2.4 Analyzing the Role of the Cruciate Ligaments in UKA Subjects 110

5.2.5 Step Down Activity for the UKA 112

5.3 Incorporating New Activities into the Model 119

5.3.1 Gait Results 119

5.4 Contact Mapping Results 124

5.4.1 Femorotibial Contact Mapping 124

5.4.2 Cam/Post Contact Mapping 126

5.4.3 Patellofemoral Contact Mapping 126

Chapter 6 Summary 136

6.1 Assumptions 139

6.2 Limitations 140

6.3 Future Work 142

Works Cited 144

Vita 148

List of Figures

Figure 1-1: Anatomical axes and planes[9] 2

Figure 1-2: Rotational definitions of the knee (mayoclinic.org). 2

Figure 1-3: Basic anatomy of the knee joint (clevelandclinic.org). 3

Figure 1-4: Quadriceps muscles of the knee (bodyjunction.co.uk). 5

Figure 1-5: Hamstrings and gastrocnemius of the knee (physiopedia.com). 5

Figure 1-6: Major ligaments of the knee (badamuscle.com). 7

Figure 1-7: Ligaments acting on the patella (badamuscle.com). 7

Figure 1-8: Condylar motion of the normal knee [17] 8

Figure 1-9: Osteoarthritic knee before and after a TKA procedure (ufhealth.com). 11

Figure 1-10: Wear simulator applying load to TKA design [26] 12

Figure 2-1: Fixed bearing vs mobile bearing TKA designs[31]. 15

Figure 2-2: Maximum femorotibial contact stress in fixed bearing and mobile bearing designs for a) AP malalignment b) ML malalignment c) rotational malalignment (* represent statistically significant differences)[33] 17

Figure 2-3: Visualization of the PS and BCS TKA designs[39] 19

Figure 2-4: Visualizations of CR (left) and XR (right) TKA designs[37] 20

Figure 2-5: Fixed bearing and mobile bearing UKA designs. 22

Figure 2-6: Inverse solution dynamics modeling overview[49] 25

Figure 2-7: Forward solution dynamics modeling overview[49] 27

Figure 2-8: Finite element representation of the knee [54] 30

Figure 4-1: Process of the forward solution mathematical model of the knee. 37

Figure 4-2: Selected bodies and their weight percentages. 39

Figure 4-3: Forces at the patellofemoral and femorotibial joint 40
Figure 4-4: Bones and components included in the model. 42
Figure 4-5: Muscle insertions and origins. 44
Figure 4-6: Wrapping points on the femoral component. 44
Figure 4-7: Choosing a wrapping point based upon the muscle angle. 45
Figure 4-8: Ligament force equations utilized in model. 47
Figure 4-9: List of modeled ligaments and ligament properties. 47
Figure 4-10: Polynomial surfaces and point clouds utilized in patellofemoral, femorotibial, and cam/post contact types. 49
Figure 4-11: Iterations of the femorotibial contact mapping tool. 51
Figure 4-12: Strain vs axial load for polyethylene component. 51
Figure 4-13: Deformation and Stress relationship of polyethylene. 53
Figure 4-14: Visualization of increasing contact area with increased surface deformation. 53
Figure 4-15: Previously used polynomial surface on the trochlear groove. 55
Figure 4-16: Updated polynomial surface on the patella and point cloud on the trochlear groove. 55
Figure 4-17: Patellofemoral contact area split into two parts in late flexion. 57
Figure 4-18: Post shape comparison between the Sigma Stabilized + (left) and the Attune PS (right). 60
Figure 4-19: Sidewall clearance for Sigma Stabilized +. 60
Figure 4-20: Medial femoral sidewall polynomial surface for the Sigma Stabilized +. 61
Figure 4-21: The medial side post point cloud for the Sigma Stabilized + implant. 61
Figure 4-22: Equations for normal, damping, and friction forces in FSM contact detection. 62

Figure 4-23: Circle fitted to femoral condyle to identify FFC location. 65
Figure 4-24: Implanted components are placed on the bones to best recreate the native surfaces. 65
Figure 4-25: Surfaces on the bone and femoral implant to assess patellofemoral contact. 67
Figure 4-26: Knee flexion profile during gait activity. 69
Figure 4-27: Muscle force profiles utilized in gait activity. 69
Figure 4-28: Filmstrip of gait activity. 71
Figure 4-29: Visualization of the GRF location and direction during the stance phase of gait. ... 71
Figure 4-30: Visualization of the knee model GUI in Matlab. 73
Figure 5-1: Medial knee soft tissue attachment sites. 75
Figure 5-2: MRI image showing MCL attachments on femur and tibia [73]. 75
Figure 5-3: New MCL origins (left) and old MCL origins (right) for Subject 4. 76
Figure 5-4: Subject 5 updated MCL attachments. 76
Figure 5-5: Subject 6 updated MCL attachments. 77
Figure 5-6: Subject 7 updated MCL attachments. 77
Figure 5-7: Subject 8 updated MCL attachments. 78
Figure 5-8: MCL force in a CR TKA during a DKB activity[74].Each line representing a EMG measurement. 80
Figure 5-9: MCL force profiles for Subject 4 during a DKB activity with old MCL attachments (green) and new MCL attachments (red). 81
Figure 5-10: MCL force profiles for Subject 6 during a DKB activity with old MCL attachments (green) and new MCL attachments (red). 82

Figure 5-11: MCL force profiles for Subject 8 during a DKB activity with old MCL attachments (green) and new MCL attachments (red). 83
Figure 5-12: Sensitivity analysis on MCL attachment locations during a DKB activity. 84
Figure 5-13: Sensitivity analysis on MCL attachment configuration during a DKB activity. 85
Figure 5-14: Visualizations of posterior capsule of the knee. 87
Figure 5-15: Posterior capsule force for 9 subjects implanted with Attune CR TKA during a DKB activity. 89
Figure 5-16: Sidewall clearance in the Sigma Stabilized + implant. 91
Figure 5-17: Lateral sidewall force for ten subjects implanted with the Sigma Stabilized + during a DKB activity. 91
Figure 5-18: Medial sidewall force for ten subjects implanted with the Sigma Stabilized + during a DKB activity. 92
Figure 5-19: Axial rotation (Low Point) for ten subjects implanted with the Sigma Stabilized + during a DKB activity. 93
Figure 5-20: LAP for ten subjects implanted with the Sigma Stabilized + during a DKB activity. 94
Figure 5-21: MAP for ten subjects implanted with the Sigma Stabilized + during a DKB activity. 95
Figure 5-22: Total knee force for ten subjects implanted with the Sigma Stabilized + during a DKB activity. 96
Figure 5-23: Total quad force for ten subjects implanted with the Sigma Stabilized + during a DKB activity. 97

Figure 5-24: Total patellofemoral force for ten subjects implanted with the Sigma Stabilized + during a DKB activity. 98
Figure 5-25: Patella ligament force for ten subjects implanted with the Sigma Stabilized + during a DKB activity. 99
Figure 5-26: PS cam force (not including side wall forces) for ten subjects implanted with the Sigma Stabilized + during a DKB activity. 100
Figure 5-27: Average FFC AP motion for Sigma UKA during a DKB activity [82]. 103
Figure 5-28: Average FFC motion for Sigma UKA and Preservation UKA during a DKB activity. 103
Figure 5-29: Average medial contact point for Preservation UKA during a DKB activity using modeling and fluoroscopy techniques. 105
Figure 5-30: Average total knee force for Sigma and Preservation UKA during a DKB activity. 107
Figure 5-31: Average quadriceps force for Sigma and Preservation UKA during a DKB activity. 107
Figure 5-32: Average Patellofemoral force on bone and component for Sigma and Preservation UKA during a DKB activity. 108
Figure 5-33: Average ACL force for Sigma and Preservation UKA during a DKB activity. 108
Figure 5-34: ACL force patterns for multiple subjects having a Preservation UKA and Sigma UKA. 109
Figure 5-35: Average PCL force for Sigma and Preservation UKA during a DKB activity. 109
Figure 5-36: AP translation of the medial contact point for a subject implanted with a Preservation UKA with an intact and with a ruptured ACL analyzed in the FSMM. 111

Figure 5-37: A subject implanted with a different UKA analyzed using fluoroscopy with an intact and a ruptured ACL [87]. 111
Figure 5-38: Medial contact point AP motion for a UKA subject performing a step down and DKB activity. 113
Figure 5-39: Lateral contact point AP motion for a UKA subject performing a step down and DKB activity. 114
Figure 5-40: Total knee force for a UKA subject performing a step down and DKB activity. ...115
Figure 5-41: Total quadriceps force for a UKA subject performing a step down and DKB activity. 116
Figure 5-42: Patellofemoral force on the bone for a UKA subject performing a step down and DKB activity. 117
Figure 5-43: Patella ligament force for a UKA subject performing a step down and DKB activity. 118
Figure 5-44: Knee flexion profile during gait activity. 120
Figure 5-45: Axial rotation (top), MAP (left), and LAP (right) during a gait activity. 120
Figure 5-46: Total knee force (top), patella ligament force (left), and patellofemoral force (right) during a gait activity..... 122
Figure 5-47: Average Attune PS contact areas during a DKB activity. 125
Figure 5-48: Average Attune PS contact stress during a DKB activity..... 125
Figure 5-49: Post geometry of Sigma PS (left) and Attune PS (right)..... 127
Figure 5-50: Cam/Post contact area of Sigma PS and Attune PS during a DKB activity..... 127
Figure 5-51: Contact Stress for a Sigma PS and Attune PS TKA during a DKB activity. 128
Figure 5-52: Experimental setup for patellofemoral contact testing. 130

Figure 5-53: Average experimental patellofemoral contact areas. 131

Figure 5-54: Average maximum experimental patellofemoral contact stresses. 131

Figure 5-55: Average experimental patellofemoral contact stress using a TestStarIIm controller. 132

Figure 5-56: Normal patella tracking in the healthy knee (https://www.jaypeedigital.com/book/9789352501670/chapter/ch11) 134

Figure 5-57: Patellofemoral contact area for four activities of daily living. 135

Figure 5-58: Patellofemoral contact stress for four activities of daily living. 135

Chapter 1 Introduction

1.1 Basic Anatomical Definitions

When discussing anatomical structures there are distinct directions and planes that must be established. To describe human movement, three orthogonal planes are utilized: the frontal (coronal), the transverse, and the sagittal planes. Each of these planes bisect a different axis. These axis directions include superior/inferior (SI), medial/lateral (ML), and anterior/posterior (AP) (Figure 1-1). Rotations along the SI axis is considered internal/external rotation of the knee, rotations along the ML axis are flexion/extension of the knee, and rotations about the AP axis are varus/valgus (Figure 1-2).

1.2 Anatomy of the Knee Joint

Since this dissertation involves the modeling of the human knee joint, understanding the anatomy of the knee is critical. First, the knee joint is comprised of three total bones: the femur, the patella, and the tibia (Figure 1-3). Each of these bones share loads and have soft tissue attachments on them. The knee consists of two joints: the femorotibial joint, where the femur contacts the tibia, and the patellofemoral joint, where the patella contacts the femur. These two joints work in tandem to provide function and structure to the knee. The femorotibial joint is responsible for much of the compressive load on the knee since its loads are largely in the vertical direction. The patellofemoral joint is largely responsible for wrapping of the quadriceps and patellar ligament (the extensor mechanism) and allows their forces to be transferred onto the knee [1-3]. Each of these joints may experience load of several times the body weight of the individual and may undergo various translations and rotations during activities [4-8].

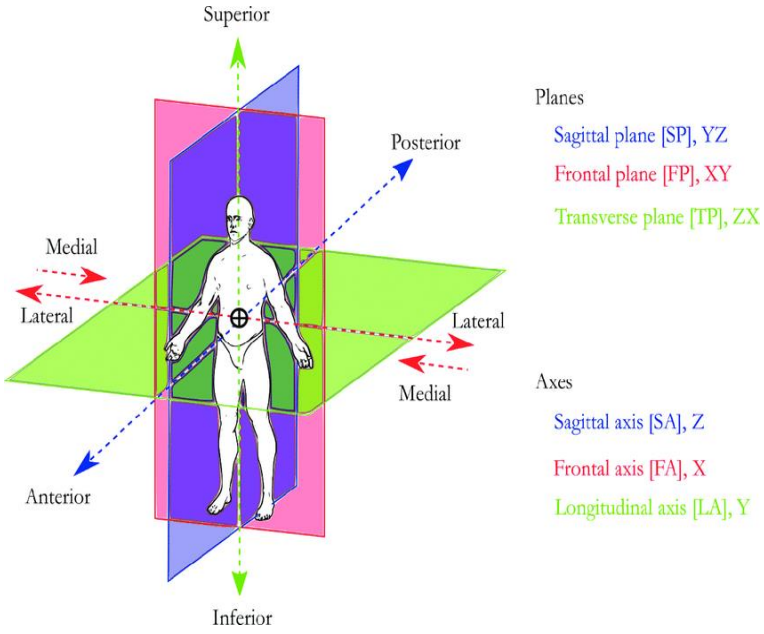


Figure 1-1: Anatomical axes and planes[9]

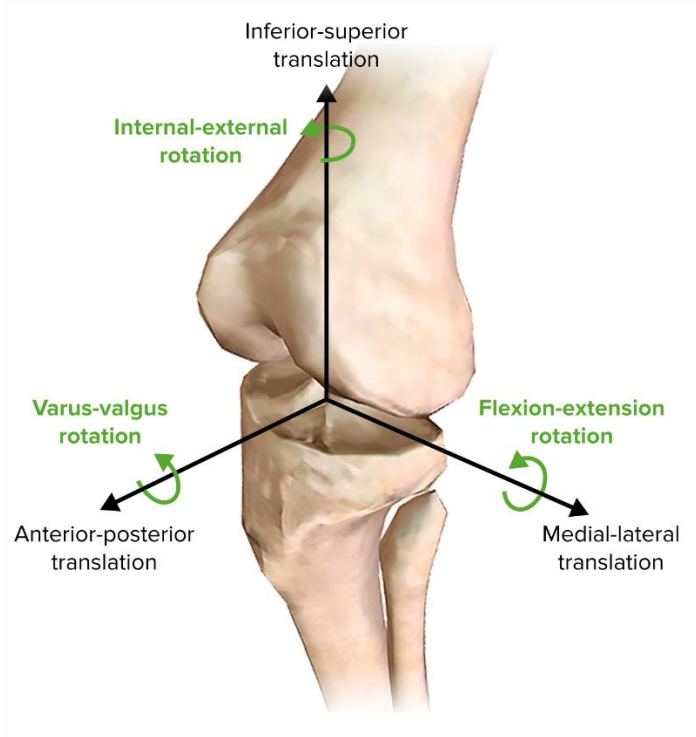


Figure 1-2: Rotational definitions of the knee (mayoclinic.org).

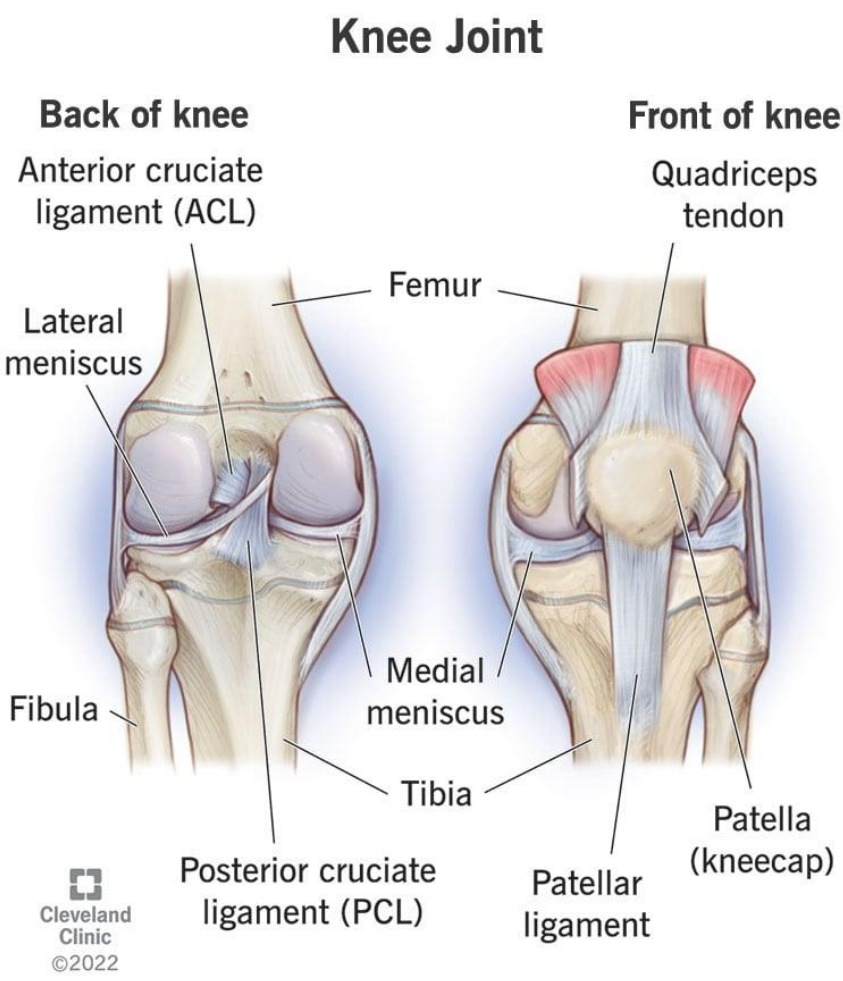


Figure 1-3: Basic anatomy of the knee joint (clevelandclinic.org).

1.2.1 Muscles of the Knee Joint

There are several groups of muscles that surround the knee joint including the quadriceps, the hamstrings, and the gastrocnemius (Figure 1-4,Figure 1-5). The quadriceps act as the extensor mechanism for the knee and is the main active force for most activities. The quadriceps consist of four main bundles: rectus femoris, vastus medialis, vastus lateralis, and vastus intermedius. Each of these four bundles have insertions on the proximal patella. The rectus femoris has attachments on the ilium of the pelvis, while all other bundles attach to the anterior femur. The hamstrings are largely responsible for knee flexion and have four major bundles: the semitendinosus, semimembranosus, bicep femoris long head, and bicep femoris short head. The semitendinosus and semimembranosus originate from ischial tuberosity and insert on the medial tibial condyle, the bicep femoris long head originates from ischial tuberosity and inserts on the lateral side of the fibula, while the bicep femoris short head originates from the posterior side of the femur bone and inserts on the fibula. Finally, the gastrocnemius consists of two major bundles: the lateral head and the medial head. The lateral head originates from the lateral femoral condyle, and the medial head originates from the medial femoral condyle. Both insert on the posterior side of the calcaneus on the back of the foot as the Achilles tendon.

1.2.2Ligaments of the Knee Joint

The four major ligaments of the knee are the anterior cruciate ligament (ACL), posterior cruciate ligament (PCL), medial collateral ligament (MCL), and the lateral collateral ligament (LCL) (Figure 1-6). Unlike muscles, ligaments are not active forces, but work as tensile constraints and prevent abnormal motion [10-12]. The collateral ligaments stabilize the knee when stretched and help to prevent excessive motion.

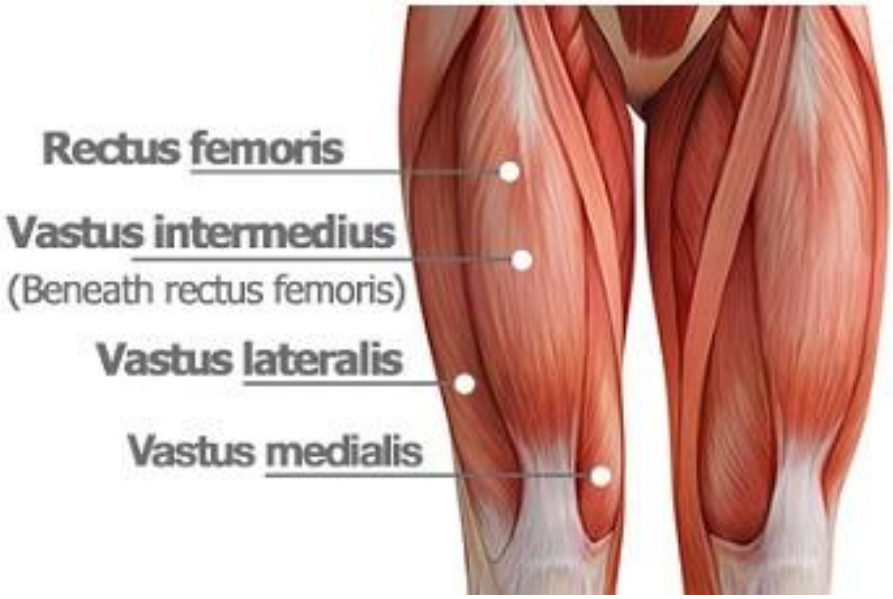


Figure 1-4: Quadriceps muscles of the knee (bodyjunction.co.uk).



Figure 1-5: Hamstrings and gastrocnemius of the knee (physiopedia.com).

The cruciate ligaments work in tandem to largely stabilize the AP motion of the knee[13]. In addition to these main four ligaments of the femorotibial joint, there are several ligaments that help to support the patellofemoral joint as well. The patellar ligament, also often called the patellar tendon, originates from the distal patella and attaches to the tibial tuberosity on the tibia. The patellar ligament transfers much of the extensor force from the quadriceps onto the tibia. This helps to balance the forces on the patella in the SI axis and prevents excessive motion of the patella. There are also several other stabilizing ligaments on the patella including lateral patellofemoral ligament (LPFL), medial patellofemoral ligament (MPFL), and patellomeniscal ligament (Figure 1-7).

1.3 Motion of the Normal Knee

Many surgeons and researchers have documented that the normal knee is the golden standard when it comes to knee kinematics. The kinematics of the normal knee have been well documented over the years [14]. During a deep knee bend activity, the normal knee may often reach an excess of 150˚ of flexion and axial rotation in excess of 20˚ externally (Figure 1-8). Through the use of fluoroscopic studies, it has been observed that lateral rollback may exceed 20 mm, while medial rollback remains minimal, and in some cases may slightly translate anteriorly [15]. One important aspect of normal knee kinematics is the screw-home mechanism. In full extension the normal knee is slightly internally rotated (femoral rotation with respect to the tibia). This allows for the cruciate ligaments to tighten and better stabilize the knee. Since the knee often impacts at flexion near full extension, the screw-home mechanism provides extra stability to the joint and prevents abnormal motion [16].

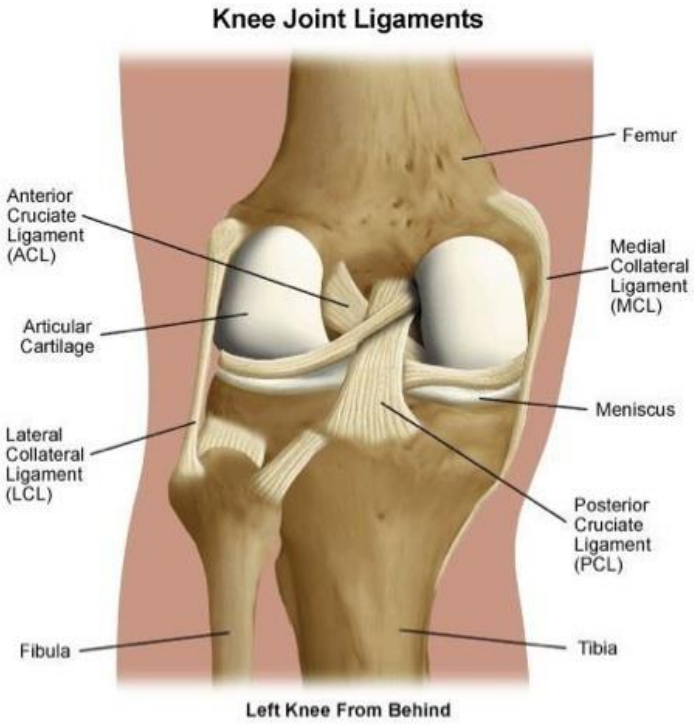


Figure 1-6: Major ligaments of the knee (badamuscle.com).

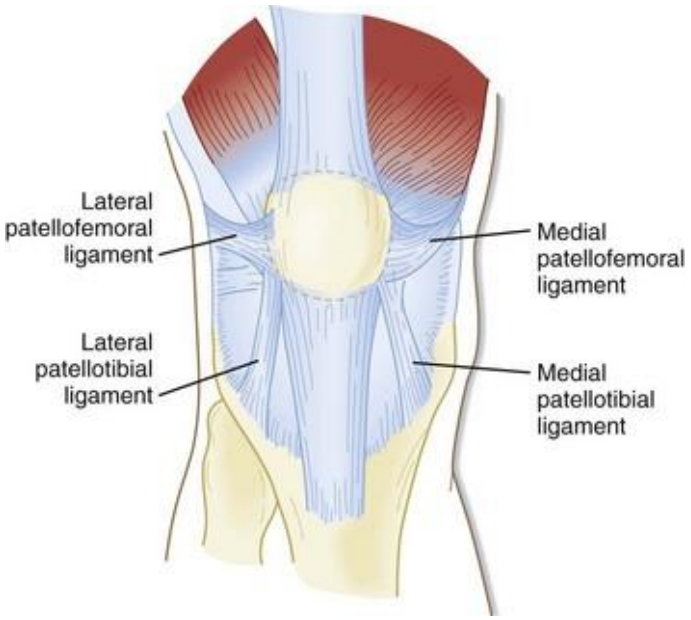


Figure 1-7: Ligaments acting on the patella (badamuscle.com).

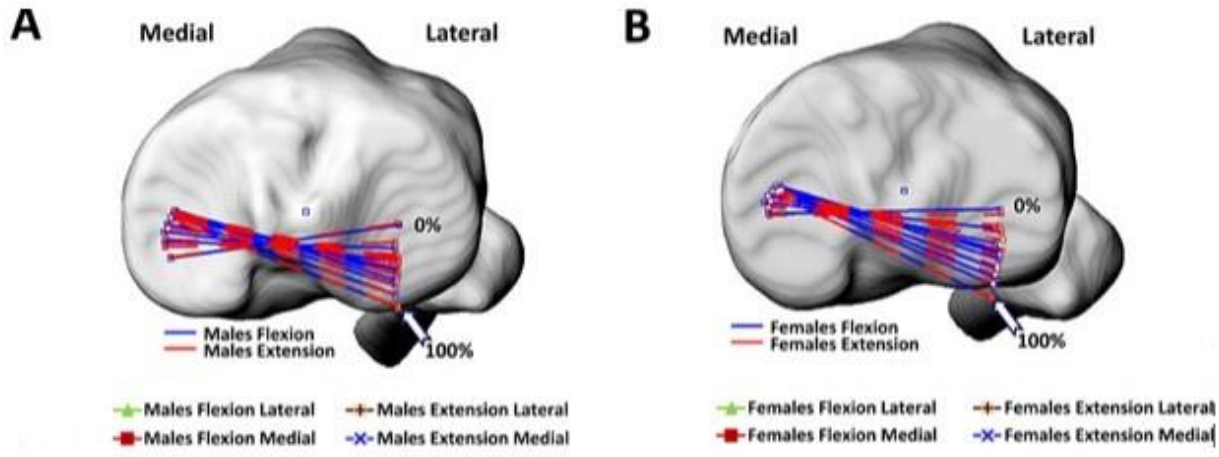


Figure 1-8: Condylar motion of the normal knee [17]

1.4Total Knee Arthroplasty

In cases of severe osteoarthritis, often a total knee arthroplasty (TKA) is utilized to replace the damaged cartilage and bone in order to relieve symptoms of osteoarthritis and reestablish normal-like joint function (Figure 1-9). TKA surgery is often successful, but there remains a subpopulation of recipients who remain unsatisfied with their implant [18, 19]. There are several different types of TKAs which include cruciate retaining (CR), posterior stabilized (PS), bi-cruciate stabilized (BCS), and bi-cruciate retaining (XR). The CR TKA retains the PCL while resecting the ACL, the PS TKA substitutes for the PCL with a cam/post mechanism while resecting the ACL, the BCS substitutes for both the PCL and ACL with both an anterior and posterior cam/post mechanism, while the XR retains both cruciate ligaments. Each of these TKA types have distinct design differences which often lead to different kinematics and kinetics. However, there is still much debate over which implant type is superior.

1.4.1 Common TKA Complications

Although the TKA surgery is considered one of the most successful procedures, there are several common complications that may occur in subjects. The 22 TKA complications and adverse events defined by the Knee Society include bleeding, wound complication, thromboembolic disease, neural deficit, vascular injury, medial collateral ligament injury, instability, malalignment, stiffness, deep joint infection, fracture, extensor mechanism disruption, patellofemoral dislocation, femorotibial dislocation, bearing surface wear, osteolysis, implant loosening, implant fracture/tibial insert dissociation, reoperation, revision, readmission, and death [20]. However, most of these complications are quite rare, and much of the dissatisfaction in TKA subjects is the desire for higher performing implants [21]. Therefore, restoring normal-like function to TKA subjects may lead to higher amounts of satisfied individuals.

Despite this desire being known, the performance of many TKAs remain dissimilar to the normal knee. Especially in CR TKAs, paradoxical motion of the knee is observed (anterior sliding of the femur with increasing flexion) [22]. Range of motion is also consistently less in TKA patients than healthy, nonimplanted patients. It is possible for TKAs to provide better outcomes than currently available. Research efforts and improved designs may help obtain not only better kinematics, but also better patient satisfaction.

1.4.2 TKA Evaluation Techniques

Since TKAs are deemed class II devices by the FDA, they require significant testing and evaluation prior to approval and ultimately being implanted into patients [23]. TKA designs can be evaluated in a number of different ways. One common way TKA designs are evaluated is through the use of wear simulators [24]. These simulators allow for the implant to undergo the physiological conditions of daily living millions of times over a short period of time (Figure 1-10). This allows the device to have its wear patterns analyzed and potential sites of failure to be identified. Since major sources of TKA failure are related to improper wear patterns in the device, this process is an important aspect in TKA design evaluation. Another way to evaluate TKA designs is through the use of mathematical modeling. This evaluation technique is largely done virtually which allows for rapid analysis of various design changes. This technique lowers the cost of physical implant testing since the device can be evaluated without the need for physical manufacturing. Mathematical modeling allows for predictions of kinematics and joint forces, but must be validated to ensure the results are accurate. This is especially significant as patients desire higher performing implants [25]. Results from mathematical models can be gathered in minutes, allowing for many design iterations to be evaluated in a short amount of time.

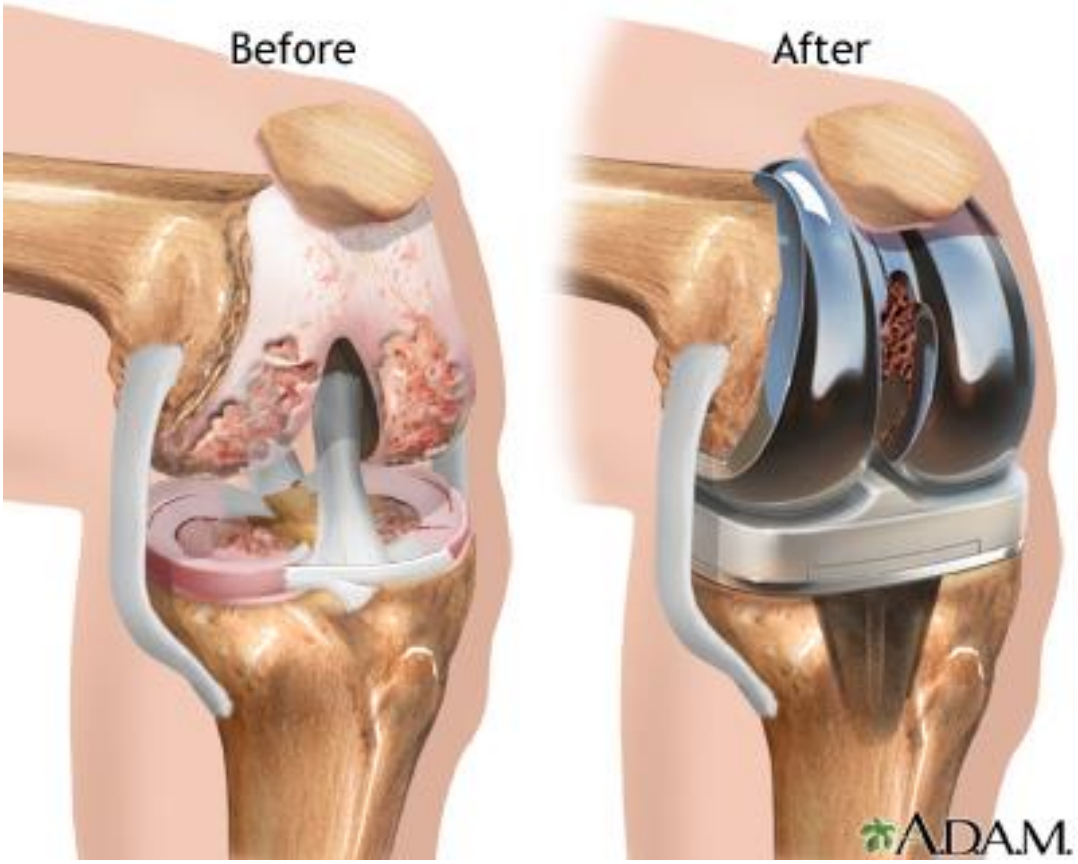


Figure 1-9: Osteoarthritic knee before and after a TKA procedure (ufhealth.com).

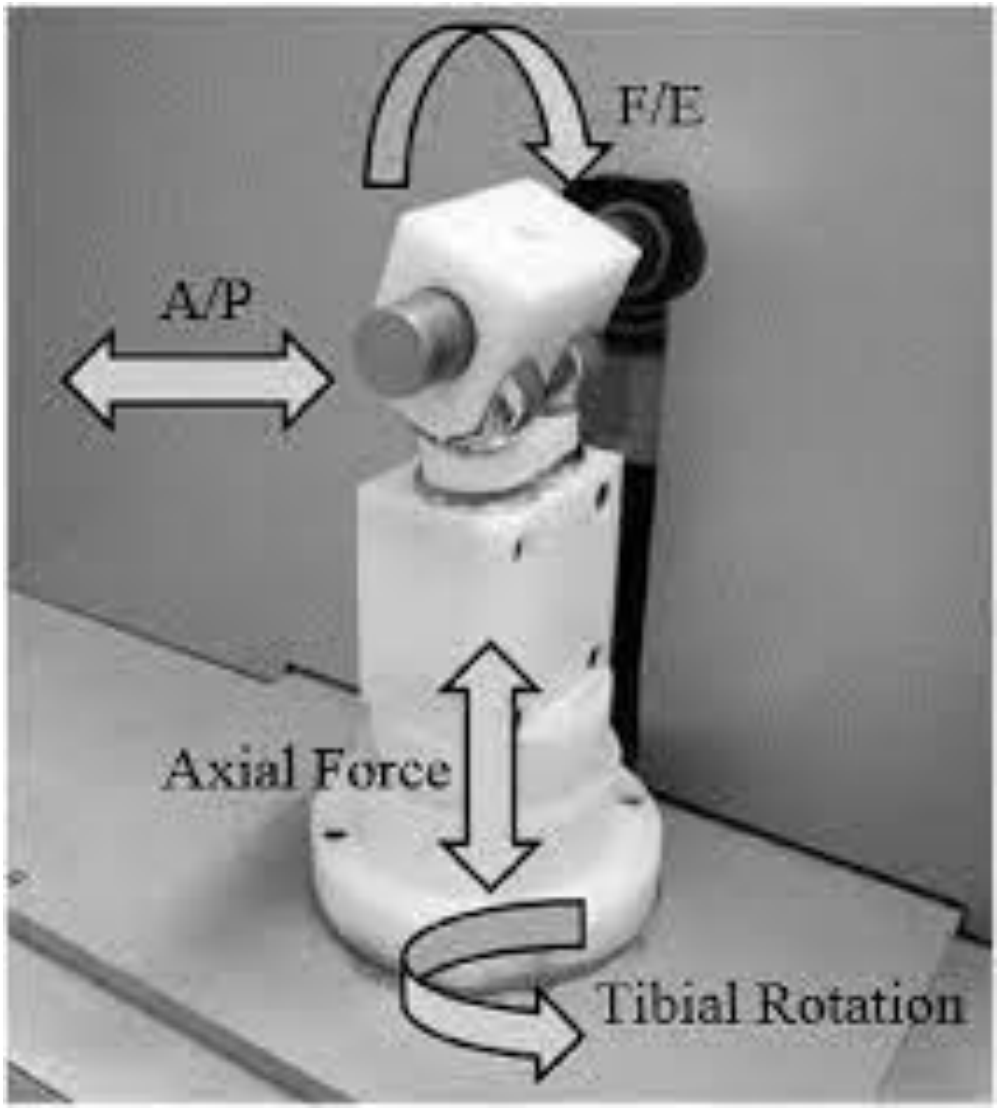


Figure 1-10: Wear simulator applying load to TKA design [26]

There are several different types of mathematical models including forward, inverse, rigid body dynamics, finite element, and others. Each of these model types have their strengths and limitations. For example, inverse mathematical models calculate forces based upon the input of kinematics, while forward mathematical models calculate motion based upon the input of forces[24, 27]. Depending on what information is available, one modeling method may be better than another. To best represent the human body, the model used in this dissertation is a forward model which utilizes rigid body dynamics to simulate the knee. This type of model is very similar to how the human body works, once muscles are activated, they drive the motion of the limb.

A later stage of TKA evaluation is clinical trials. This typically involves the implantation of the device into a limited number of subjects that are closely monitored and assessed [28]. Clinical trials provide valuable feedback from patients and allow the device to be assessed in vivo. While clinical trials provide valuable information, they are often very expensive and may put patients in unnecessary risk through invasive imaging or unknown outcomes, as the device has not been thoroughly tested in a large number of patients. Overall, the process of bringing a new TKA design to market is a long and expensive process. In adherence to the many regulatory requirements, each of the design evaluation types described provide important information which allows for a safer TKA design that optimizes joint performance.

Chapter 2 Background

2.1 Knee Implant Designs

Knee implants of various types have been around for decades. Implant designs have advanced rapidly over the years where now implants are commonly used, with over 800,000 procedures done each year [29]. This increase in procedures is due to a number of reasons including a growing elderly population and overall good outcomes as a result of knee reconstruction surgery. As the number of knee reconstructions continues to increase, it is important to understand the strengths and weaknesses of each implant type in order to inform patients on which implant may best fit their lifestyle.

2.1.1 Fixed Bearing vs Mobile Bearing TKAs

Fixed bearing TKAs are some of the most common types of TKAs. Their design consists of a metal tibial baseplate which is fixated to the tibia typically through cement, although some cementless designs do exist which encourage bone ingrowth for fixation. Typically a polyethylene bearing is attached to the top of the tibial bearing. For fixed bearing designs, this bearing snaps into place and is designed not to move once in position. In theory this limits micromotion and significantly reduces the risk of bearing dislocation [30]. Despite the widespread use of fixed bearing implant types, mobile bearing implants were developed to address the needs of younger patients. This implant type is designed to increase range of motion and reduce wear. A polyethylene bearing is placed on top of the tibial baseplate which is free to rotate. This allows for less sliding between the femoral component and the insert. However, there is sliding between the bearing and tibial baseplate which does not exist in fixed bearing designs (Figure 2-1).

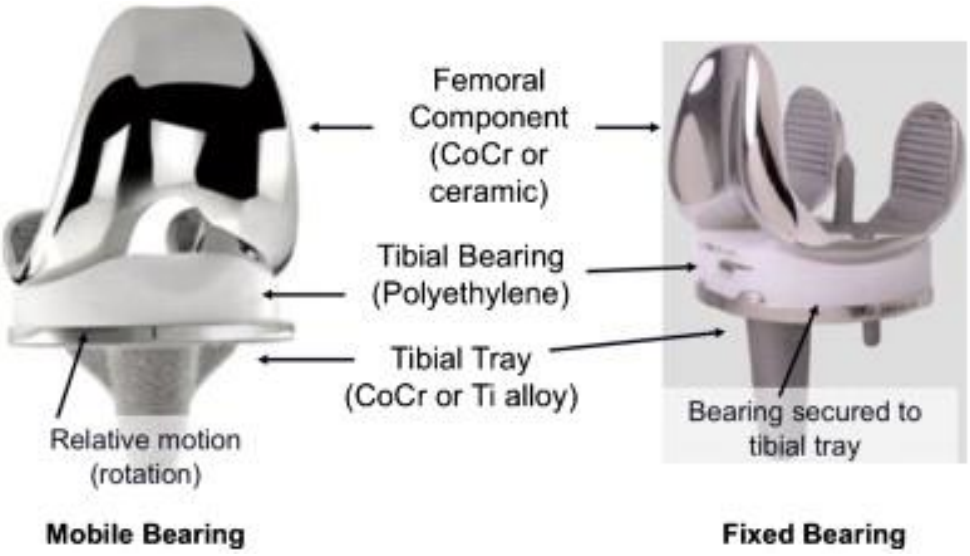
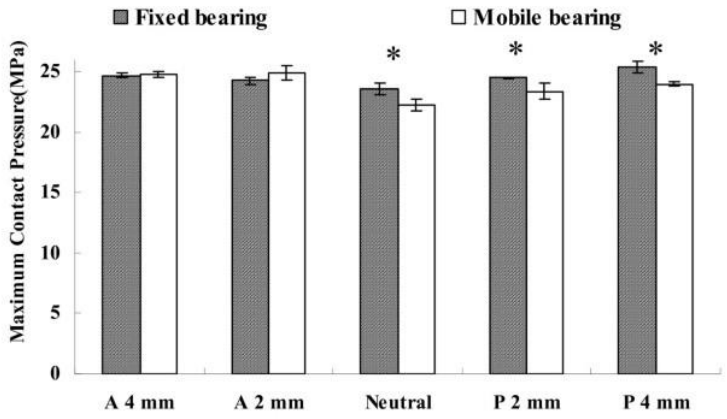


Figure 2-1: Fixed bearing vs mobile bearing TKA designs[31].

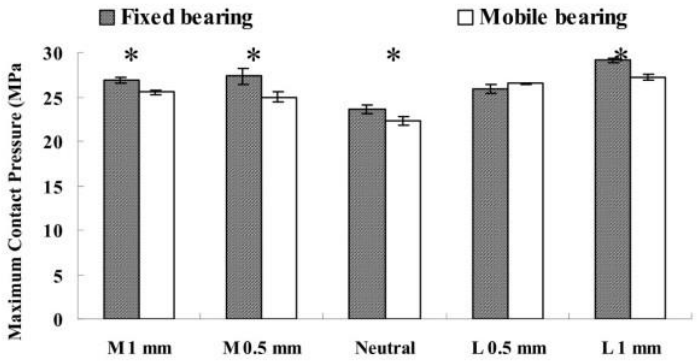
Despite the intent behind mobile bearing designs, the theoretical advantages of mobile bearing TKAs remain controversial[32]. Many studies have looked at the differences in fixed bearing and mobile bearing TKA designs. Ultimately the advantage with the most evidence for mobile bearing designs is that the design can somewhat correct for malalignment during the surgical process[33]. If an implant is malrotated during surgery, the mobile bearing design will account for this by rotating the bearing. Fixed bearing designs are incapable of this accommodation and would likely lead to high wear rates and potentially revision. A sensitivity analysis was done to demonstrate the changes in peak femorotibial contact stress when malalignment occurs in the AP direction, ML direction, and internal/external rotation (Figure 2-2). This confirmed the slightly higher contact stresses in fixed bearing designs for malpositioned components. Despite these slight changes, outcomes for both design types remain consistent. 15 year survivorship for both groups remain close to 90% [34]. Ultimately, the decision for fixed bearing or mobile bearing design comes down to surgeon preference. Since there is no significant difference in outcome or overall performance, the design the surgeons can implant the most accurately should be used.

2.1.2 TKA Designs and Ligament Resection

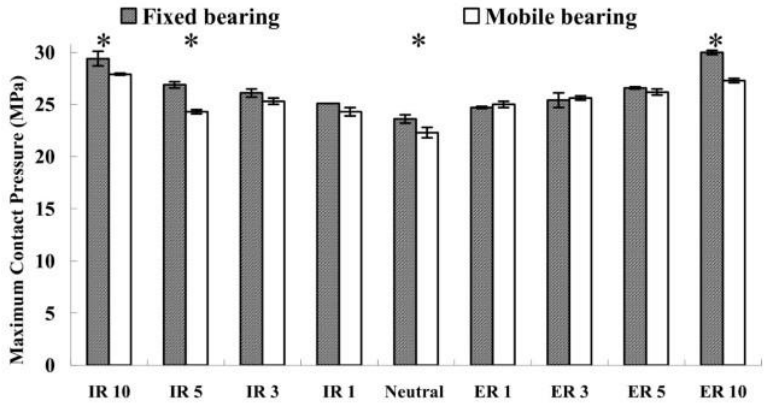
One of the main design choices patients and surgeons have when choosing a TKA is which ligaments will be retained or resected. This decision is often made based upon the integrity of the ligaments, the surgeon's preferred implant type, and the quality of the patient's bone. One of the most commonly used TKA types is the posterior cruciate retaining (CR) TKA. This implant resects the ACL, but retains the PCL. The conformity in the bearing prevents excessive anterior translation of the femur which is typically prevented in the normal knee by the ACL. Another commonly used TKA design is the posterior stabilized (PS) TKA. This design resects both the ACL and PCL, but substitutes the role of the PCL with a cam/post mechanism.



(A)



(B)



(C)

Figure 2-2: Maximum femorotibial contact stress in fixed bearing and mobile bearing designs for a) AP malalignment b) ML malalignment c) rotational malalignment (represent statistically significant differences)[33]*

This results in consistent rollback in deep flexion which is not always achieved in CR designs. However, the cam/post mechanism can experience wear and significant contact forces [35]. The bi-cruciate stabilized (BCS) TKA designs have an anterior and posterior cam/post mechanism to account for the roles of both cruciate ligaments. The anterior cam/post is engaged during early flexion to help prevent excessive anterior motion of the femur [36]. Just like in the PS design, the posterior cam/post promotes rollback of the femur in late flexion. Finally, a new implant type, the bi-cruciate retaining (XR) TKA, which retains both cruciate ligaments has been developed in an attempt to better replicate the mechanics of the normal knee. Since no cruciate ligaments are resected, the design splits the tibial base plate into a lateral and medial part, leaving a bony island intact in the middle of the tibia for ligament attachment sites [37]. This implant type requires a much more precise surgical technique. With the help of robotic surgical assistance, the XR TKA may become more popular in the upcoming years. Each of these different designs are visualized in Figure 2-3 and Figure 2-4.

2.1.3 UKA Designs

Another option for patients experiencing osteoarthritis is undergoing unicompartmental knee arthroplasty (UKA) surgery. This surgery is performed on only one compartment of the knee, typically the medial compartment, but lateral UKAs are also available. The tibial plateau and the femoral condyle on one side of the knee are removed and replaced by a metal femoral component and a metal tibial plate with a polyethylene bearing on top (Figure 2-5). The UKA strives to retain the native anatomy while replacing damaged bone and cartilage. As with TKAs, there are both mobile bearing and fixed bearing UKA designs. Systematic reviews have compared mobile bearing and fixed bearing UKA designs and have shown no significant difference in clinical outcomes data including patient reported outcome measurements, range of motion, and rate of complication [38].

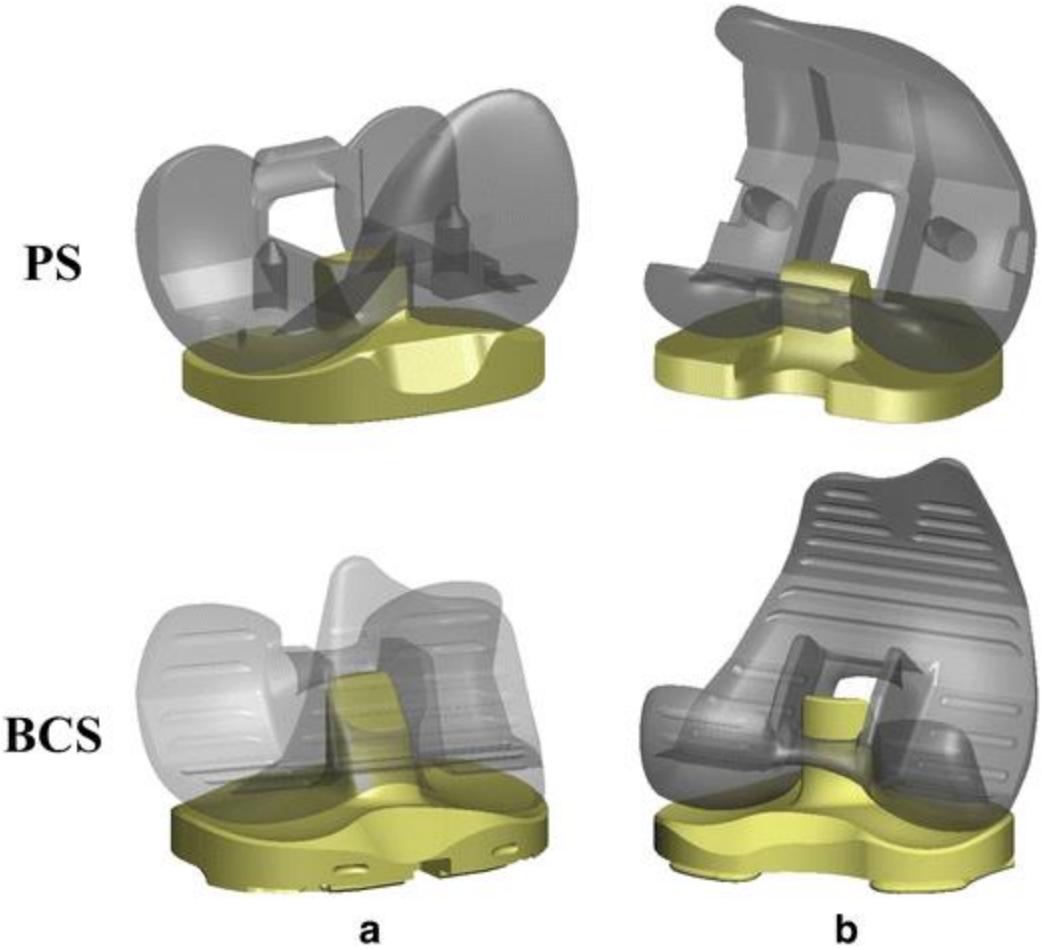


Figure 2-3: Visualization of the PS and BCS TKA designs[39]



Figure 2-4: Visualizations of CR (left) and XR (right) TKA designs[37]

However, Burger et al. showed that mobile bearing UKAs reported higher revision rates than fixed bearing UKA despite having similar outcomes [40]. While there is still some controversy over which UKA type is superior, there is also debate over how UKAs perform in comparison to TKAs. Studies have shown that UKAs have reduced survivorship but demonstrate superior clinical and functional performance [41]. A patient must balance the superior performance of a UKA with the better longevity of a TKA. Depending on the activity level and age of the person, a UKA can be a great option for patients with osteoarthritis limited to one compartment of the knee.

2.2 Mathematical Modeling Techniques

There are many different techniques that can be used to analyze the biomechanics of the human body. Whether they are commercially available software packages, university led research projects, or internal validation models for orthopedic companies, mathematical modeling is a powerful way to both expediate and complement many types of research. In the context of this dissertation, it is important to understand the surrounding landscape in mathematical modeling. Despite the many existing mathematical models, no model has shown the breadth of analysis types and implant specific details that the proposed FSM in this dissertation offers. However, the FSM does build upon many different concepts applied in other mathematical models.

2.2.1 Inverse Solution Modeling

Multibody systems exhibit especially complex behavior often due to a combination of internal and external forces and torques. Reconstructing these internal forces and torques from motion and known external forces is inverse solution modeling. Simply put, inverse solution modeling has inputs of known motion and solves for the forces in the system. This type of modeling is commonly used and can manifest itself in a number of different ways.



Figure 2-5: Fixed bearing and mobile bearing UKA designs.

One common field inverse solution modeling is used in is robotics. Inverse dynamics algorithms are used to solve for the required torques needed to move the tip of a robotic arm to a desired position. This inverse dynamics problem was first solved by Eduardo Bayo in 1987 [42]. His solution solved how each of the many motors in a robotic arm must apply torque into the system. To build upon this work, Bayo applied frequency-domain methods to solve for the inverse dynamics of a single link robotic arm [42]. This work was the foundation to prove the efficacy of the inverse dynamics method as this was the first time research had been done on determining the exact motion of the motor needed to produce the desired motion of a robotic arm. This inverse dynamics approach yielded a very stable tracking that controls for both single-link and multi-link robotics.

Since internal forces are often difficult to measure, the inverse dynamics technique is commonly used in biomechanics research. However, the motion of the system must be known before an accurate estimation of the forces can be completed. Motion can be measured in a number of ways including fluoroscopy, 3D motion markers, and goniometers. Each of these methods have drawbacks. Fluoroscopy exposes individuals to radiation and struggles with motion blur in fast moving activities [43]. 3D motion marks are attached to the skin and can often be inaccurate since the marker attachments are not on the bone [44]. Finally, goniometers are difficult to attach to the subject and may not capture all directions of motion [45]. Once the known motion profile is gathered, an equation of system dynamics, typically using Newtonian-Euler methods, can be produced (Figure 2-6). With the existing knowledge of the system's bodies' masses and their motion, the forces and torques can be solved for.

Several inverse solution models have been developed to analyze knee joint mechanics. One such model utilized measured ground reaction forces, kinematics of the joint, distance from the force

vector to the mass center and moments of inertia about the mass center during gait to calculate the torque around the center of the knee [46]. However, this model is limited as loading not only around the joint center is important, but also the medial and lateral compartment of the knee. Other more advanced models incorporate more complicated models of the knee joint. Separating medial and lateral joint contact forces as separate forces, as well as patellofemoral contact [47]. However, as these models account for more detailed outputs, the inputs must become more detailed as well. Overall, inverse models have both strengths and weaknesses. Capturing accurate motion can prove challenging and may not be possible in early stages of device design.

2.2.2 Forward Solution Modeling

In contrast with inverse solution modeling, forward solution modeling inputs forces and torques to produce the motion in the system (Figure 2-7). One of the greatest strengths of the forward solution modeling methodology is that it is capable of predicting motion for implants or devices which have not yet been implanted into subjects. This makes forward solution models ideal for the design phase of products and can be a useful tool in investigating the effects of various ligament changes, muscle profile changes, and implant design changes. One challenge of forward solution modeling is measuring the force profile inputs necessary to solve the system. Often times assumptions must be made as muscle forces, for example, may not be available in detail for a variety of patients. While EMG data can prove valuable in this, there are some accuracy concerns regarding EMG [48]. Additionally, in order to measure deep muscle activation, intramuscular wires are needed. These are often painful and uncomfortable for the subject and it is difficult to measure specific muscular bundles. Other methodologies to gather the input force data include PID controllers and inverse dynamic derived forces.

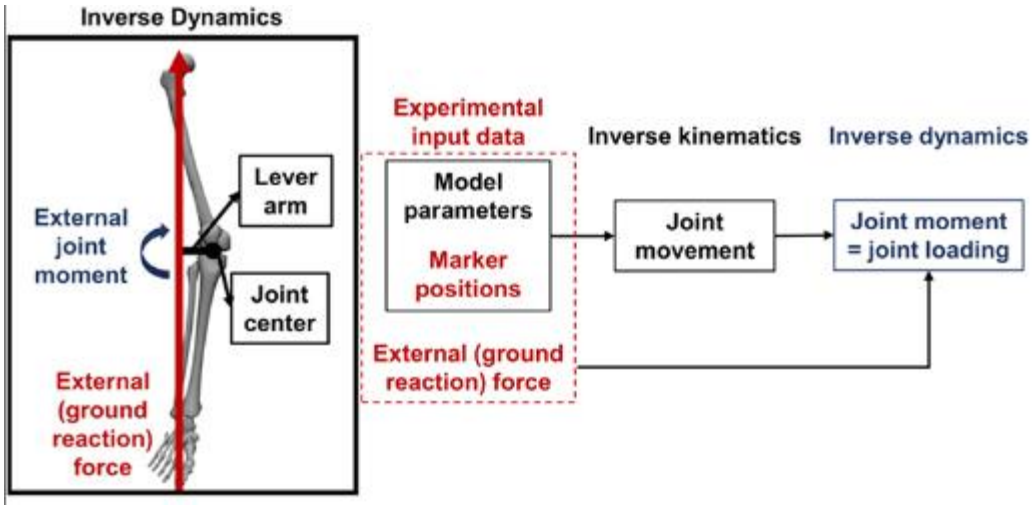


Figure 2-6: Inverse solution dynamics modeling overview[49]

Due to its strengths in theoretical modeling, forward solution dynamics models have been investigated for a number of uses. Thelen and Anderson [50] demonstrated a forward dynamic model of a gait activity which incorporates computed muscle control algorithms, which showed increased mathematical efficiency. In this model, 92 Hill-type muscle/tendon units were input into the system. An optimized feedback loop was used to produce desired kinematics of gait. This model generated kinematics that generally matched within 1° of rotational experimental data and within 10mm or less of translational experimental data. The muscle profiles produced in this model closely match that of existing EMG profiles. This model is an example of a successful forward solution dynamics model, but is limited to gait analysis.

2.2.3 Rigid Body Dynamics

Mathematical models must also define the properties of the bodies in the system. One way to do this is to assume rigid bodies. This means that the bodies will not deform when under force. In the knee, there is not a significant amount of deformity in the bodies (femur, tibia, patella, etc), so this assumption can allow for the simplification of the system. Rigid bodies reduce the needed parameters that describe the system to the translation and rotation. This also allows for reference frames to be attached to each body [51]. While simplifying the system, assuming rigid bodies may cause the model to be slightly less accurate. If the system's bodies undergo deformation in real life, the simulation may report inaccurate results. This may limit the application of rigid body models in detailed analyses of soft tissue structures, like cartilage or meniscus, which are often deformable. Rigid body dynamics models do well representing the larger system. One such example of this is a model developed by Dhaher et al [52] which used a rigid body model to investigate the effects of quad forces on patellofemoral forces.

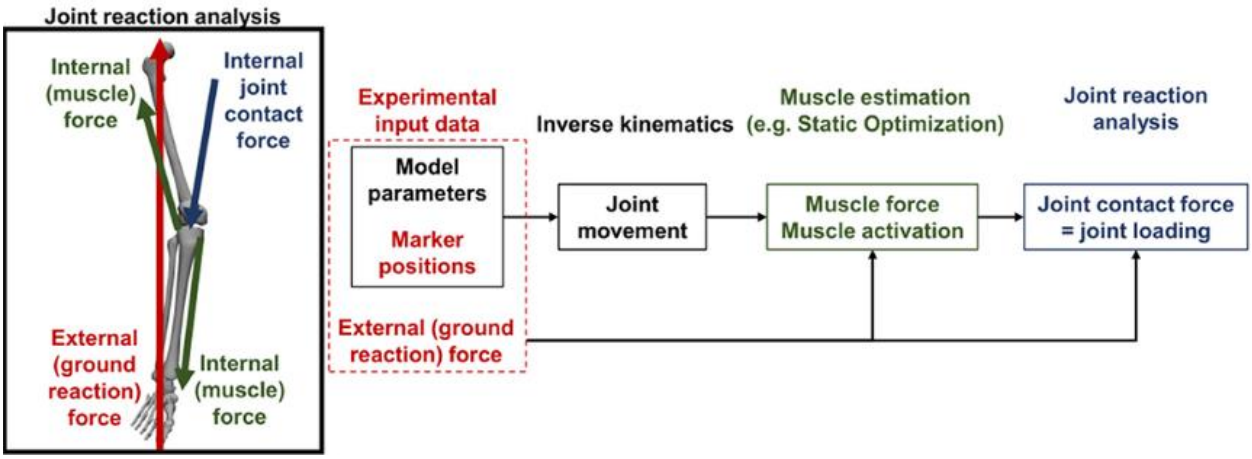


Figure 2-7: Forward solution dynamics modeling overview[49]

By varying the relative force generation ratios of the quadriceps heads, the patellofemoral contact forces were estimated. A systematic investigation of various quad force ratios was used to find the ratios that cause a reduction or an increase of lateral contact forces, often the cause of patellofemoral pain. This study found that increased contact forces are more dependent on combinations of muscle forces than solely on muscle weakness. Simulation data showed that the contact force levels are also highly dependent on the knee flexion angle. Rigid body models have shown promise in various situations but should only be considered in situations where the lack of deformity will not greatly affect the results in the system's outputs.

2.2.4 Finite Element Analysis

One modeling method that does account for deformation of bodies is the finite element method. This method separates the entire body into many smaller parts called finite elements (Figure 2-8). Each element has its associated elemental equations of motion solved and then by combining all elemental equations, a global system of equations can be evaluated. This modeling method is especially useful in identifying details of contact mechanics, including contact stresses and contact areas. This method is also very useful in modeling deformable bodies or viscoelastic materials. However, finite element analysis is often very computationally expensive and requires well defined boundary conditions and material properties to accurately provide results. In vivo material properties can be difficult to assess, and incorrect assumptions could compromise the accuracy of the overall analysis. Also determining the number of necessary elements can be difficult as a balance of accuracy and efficiency must be struck.

A finite element model of the knee joint was developed by Kiapour et al [53] which analyzed the mechanism of injury for ACL tears. This model analyzed a wide variety of loading conditions. The model was validated against tibiofemoral kinematics, ligaments strain/force, and articular cartilage

pressure data measured directly from static, quasi-static, and dynamic cadaveric experiments. Finite element predictions showed low deviations (root-mean-square (RMS) error) from average experimental data under all modes of static and quasi-static loading, falling within 2.5 deg of tibiofemoral rotation, 1% of anterior cruciate ligament (ACL) and medial collateral ligament (MCL) strains, 17 N of ACL load, and 1 mm of tibiofemoral center of pressure. This model performed well in producing accurate ligament forces in a range of loading conditions. However, this model does not provide contact force results and has unreported simulation times.

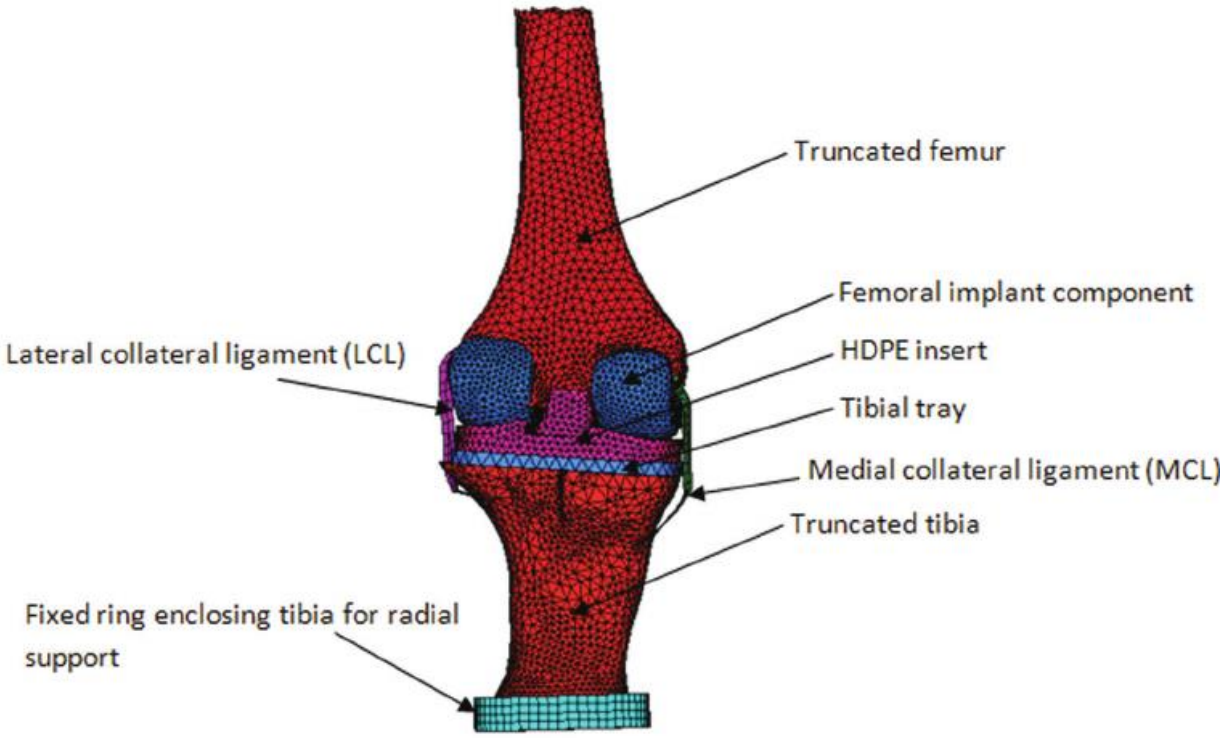


Figure 2-8: Finite element representation of the knee [54]

Chapter 3 Objectives and Contributions

3.1 Dissertation Objectives

The emergence of mathematical modeling has led to orthopedic analyses which are more efficient, allow for quicker, more in depth, and larger subject size analyses. Also, theoretical analyses don't require the inclusion of live subjects which is easier to conduct, not requiring IRB approval, in comparison to live subject analyses that take significantly more time to complete. Accurately assessing in vivo soft tissue forces, contact forces, and contact mechanics has proven to be extremely difficult without the use of mathematical modeling. These parameters, along with many others, can provide vital information to clinicians, researchers, and implant design engineers. Thus, an accurate and adaptable mathematical model of the knee can provide potential information about outcomes for clinicians that could be used to implement implant design changes which may lead to better implants and solutions for patients for years to come. Despite significant advances in mathematical modeling over the past few decades, further improvements can still be made.

The mathematical model of the knee that is being advanced in this dissertation provides an unrivaled level of versatility including ten subjects with subject-specific bones and soft tissue information, several different TKA and UKA designs, and seven different activities of daily activities, including gait and deep flexion activities like DKB. This model is capable of providing both detailed kinematic and detailed kinetic results.

Overall, this mathematical model of the knee provides value to a number of different fields and remains an important tool for knee arthroplasty analysis. The main goals of this dissertation are to incorporate a more sophisticated patellar tracking system, provide more detailed in vivo contact mechanics information including contact areas and stresses, develop new boundary conditions and

modeling algorithms to assess additional activities including gait, incorporate new implant types including the Sigma Stabilized + and UKA in such a way that key design features can be assessed, and the inclusion of a posterior capsule of the knee into the model along with more precise ligament attachment sites. This has been accomplished by completing the following objectives:

- Create a patellofemoral contact detection system which allows for a medial/lateral contact area split in deep flexion, while preventing improper contact being calculated in the intercondylar space.
- Develop a contact mapping algorithm which can utilize modeling results to calculate contact areas and contact stresses.
- Incorporate a gait activity into the model which assesses kinetics and kinematics during the stance phase of gait.
- Include highly constrained implants (Sigma Stabilized + TKA) and medial fixed-bearing UKA implants in the model and modify the contact detection system to properly account for implant specific features.
- Develop a method to model the posterior capsule of the knee to provide increased stability at full extension.
- Consult with orthopedic surgeons to identify correct ligament attachment sites that were implemented in the model.

3.2 Dissertation Contributions

Although there are several existing mathematical models of the knee, many of them do not have the required detail for sufficient analysis of the knee or focus mainly on one aspect of biomechanical analysis.

While they may provide value in one area of analysis or for one subject, these models are often unable to provide accurate information to drive clinical decisions or implant design changes, particularly with respect to patellar tracking, contact mechanics, soft tissue contributions, and versatility in terms of subject numbers, implant types, and activity types. In order to advance this model and accomplish the goals of this dissertation, the following contributions were made:

- A new patellofemoral contact detection system is developed to allow for a smooth transition of the patella from full extension to deep flexion.
    - Advancements include a polynomial surface mapped to the patella, a point cloud of the trochlear groove utilized for contact detection, and the medial/lateral split of forces to better quantify the location of the contact.
    - Unlike previous iterations, no contact is calculated in the intercondylar space which allows for more accurate patellofemoral contact information in deep flexion.
- A contact mapping tool is created in order to calculate contact areas and contact stresses for the following contact types: femorotibial, patellofemoral, cam/post, and sidewall .
    - This algorithm also animates the contact patch onto a component to help visualize the contact patterns occurring during a simulation.
    - A deformation factor is included to help simulate the change in shape of components under high loads.
- A gait activity is incorporated into the model to analyze the kinematics and kinetics of the stance phase of gait.
    - Significant changes to boundary conditions, soft tissue force profiles, model inputs, and GUI components are made.

    - This activity produces results consistent with other publications including the presence of an M-curve for total knee force, a hallmark of gait.
- The ability to analyze UKA subjects is added into the model.
    - This incorporates contact detection on both the native bone and implant components.
    - Patellofemoral forces on the bone and component can be assessed separately to further investigate patellar tracking and the transition between native bone and implant components.
    - By controlling cruciate ligament properties, the roles of these ligaments in UKA mechanics can be further investigated.
- The Sigma Stabilized + TKA is included in the model.
    - A novel sidewall contact detection system is developed in order to investigate the rotational constraints of revision TKAs.
- The posterior capsule is included into the model to further stabilize the knee in early flexion.
    - Wrapping of the posterior capsule around the posterior aspect of the femoral condyles is included.

Chapter 4 Methods

4.1 General Mathematical Modeling Methods

As stated in the previous section of this dissertation project, advancements were made pertaining to the forward mathematical model of the knee joint that accurately assesses joint kinematics, kinetics, and contact mechanics for a number of implants performing several different activities. Previous work has been done to create a mathematical model of the knee which has achieved very promising results. This model produced kinematic results including medial condyle anteroposterior motion (MAP), lateral condyle anteroposterior motion (LAP), and axial rotation of the femur with respect to the tibia for ten subjects virtually implanted with FB CR, FB PS, and MB PS TKAs. This model is also capable of producing kinetic results including femorotibial contact forces, patellofemoral force, and cam/post contact force. Validation has been done for TKA kinematics through the use of fluoroscopy and telemetric TKA implants for kinetics[55]. This work builds on the foundation of this model in this dissertation and contains much of the same basic methodology. The model is made up of three parts: a Matlab user interface to provide initial conditions and geometric information, an Autolev code to produce equations of motion via Kane's dynamics, and a C++ code to solve the differential equations of motion and to generate outputs data (Figure 4-1).

There are two major types of mathematical models: (1) inverse and (2) forward solution. Inverse models utilize kinematic information as inputs to produce kinetic results. These models are especially useful in cases where detailed information on the system's motion is available [56]. Forward solution models utilize estimated forces as inputs to produce the motion of the system. The work discussed in this dissertation pertains to a forward mathematical model. This means that

the output motion is unknown, while the input forces and torques are determined through the use of contact detection algorithms and muscle PID controllers. Generally, forward solution mathematical models are best at predicting the behavior of a system with unknown kinematic results [57]. In this case, the input parameters and boundary conditions of the activities analyzed in the model (DKB, DKB and rise, rise, step up, step down, chair rise, and gait) are known. This makes utilizing a forward mathematical model a good choice since many of the goals of this dissertation are to analyze new implants or activities where detailed kinematic data is not available.

4.1.1 Modeling Techniques to Analyze the Lower Leg

As mentioned previously, Autolev, a symbolic manipulation algorithm developed by Professor Thomas Kane, is utilized to produce the system's equations of motions through the use of Kane's dynamics. Autolev is an interactive multibody dynamics program which is capable of formulating equations of motion for complex systems with various constraints and outputs. Autolev provides a process for formulating equations of motion which is unencumbered by the computer memory limitations, leading to faster run times [58]. In the Autolev code developed for the mathematical model described in this dissertation, the bodies in the system are defined. Each body has its weight defined as a percentage of the total body weight based upon previously established literature [59] (Figure 4-2). Important points, ligament and muscle attachment sites, and spatial relationships between bodies are also defined. Interactive forces at both the patellofemoral and femorotibial joints are also calculated and applied to the system. This model is a 12 degree of freedom model with 6 degrees of freedom (x, y, and z translational freedom and x, y, and z rotational freedom) at both the patellofemoral joint and femorotibial joint. Other bodies like the foot and pelvis have constraints put on them to restrict their motion based upon the boundary conditions input into the system.

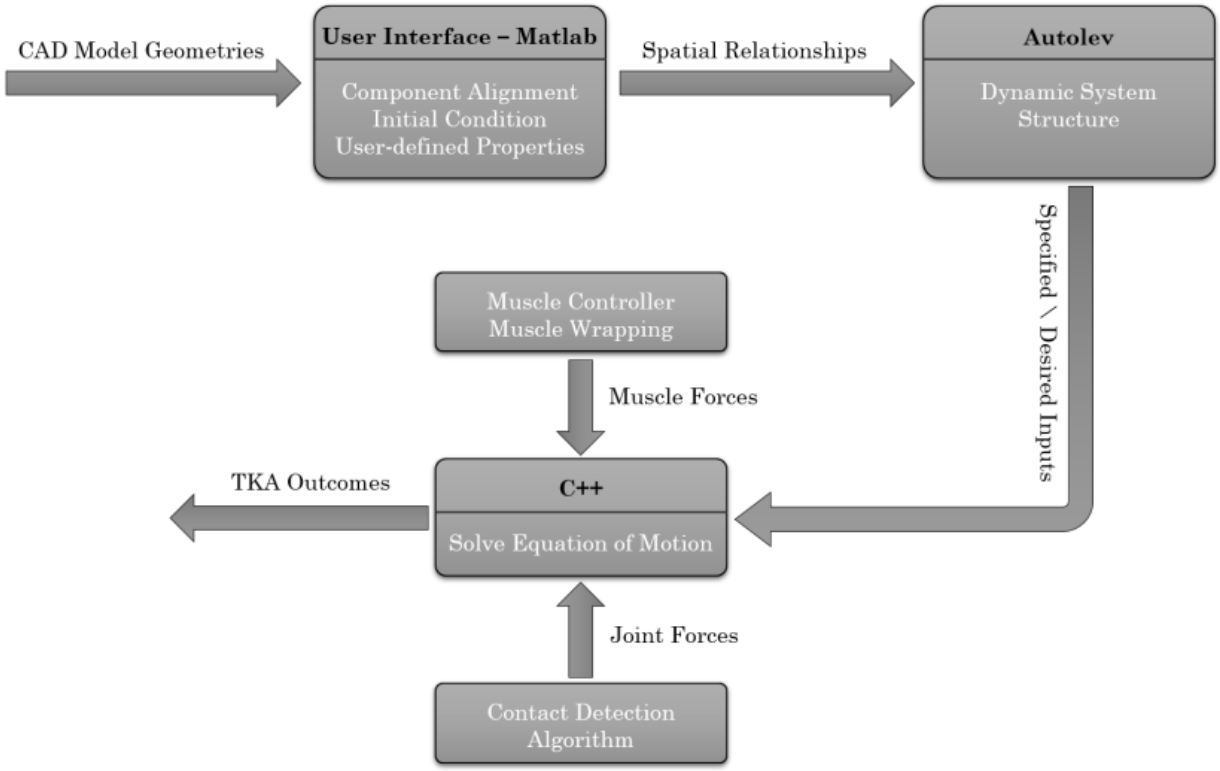


Figure 4-1: Process of the forward solution mathematical model of the knee.

For example, the foot is fixed to the ground during a DKB activity, so it will not translate. Thus that body's translations do not need to be solved for in the equations of motions. These constraints allow for the system to be determinant, allowing for the number of unknowns that are being solved to be equal to the number of equations of motion. After the Autolev code has run, a C++ file is created which can be further modified to include more complex algorithms and definitions. This is why it is necessary to develop both an Autolev code and a C++ code.

4.2 Modeling Human Anatomy

In the described knee model, the human anatomy is separated into three main categories: bones, muscles, and ligaments. Each of these structures are modeled using different techniques, and each structure is vitally important to the system. The bones in the human body provide strength and structure and are considered interactive active forces. They also provide a place for soft tissues to attach. Bones are modeled as rigid bodies, and when in contact with other bones or components produce a contact force which is calculated and applied into the system. Muscles drive the motion of the body and are classified as either active or stabilizing muscles in the model and therefore, are the active forces in the system driving motion. Active muscles, driving the motion, are modeled with PID controllers to produce a desired motion in an activity, while stabilized muscles are modeled as non-linear springs. Ligaments, modeled as tensile constraint forces, provide translational and rotational constraints in the human body and are modeled as non-linear springs, with ligament properties being defined within the input parameters of the model. Each of these three major aspects of modeling the human anatomy will be further discussed in further detail in the following sections.

Bodies	Body-weight Percentage
Foot	1.4%
Tibia	4.9%
Femur	11%
Patella	0.5%
Torso	32.1%
Bearing Insert	0.05%

Figure 4-2: Selected bodies and their weight percentages.

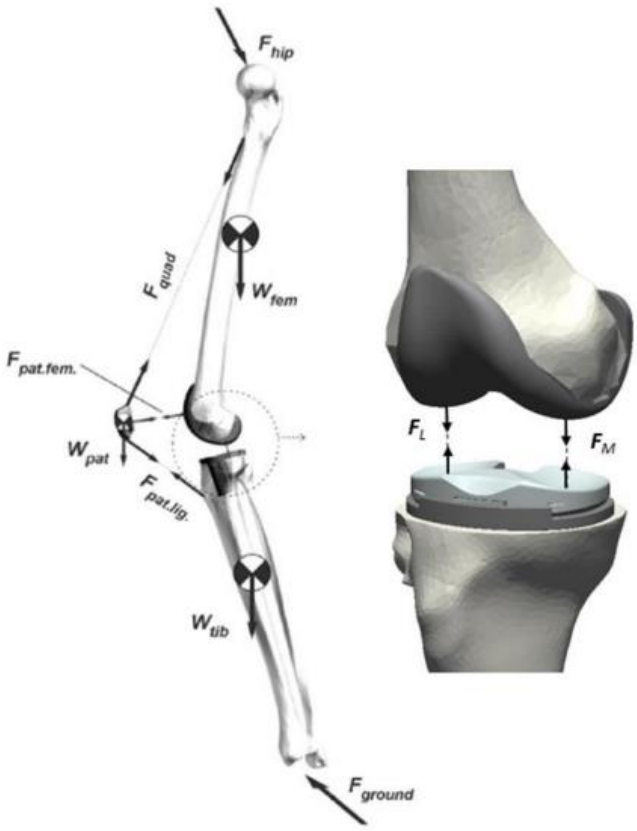


Figure 4-3: Forces at the patellofemoral and femorotibial joint

4.2.1 Modeling Bones

This model includes the pelvis, femur, patella, tibia, and foot bones (Figure 4-4). The contralateral leg is accounted for via a contralateral leg force located at the contralateral hip socket. In the model there are ten unique subjects whose bone models were created through the use of CT imagery and segmentation techniques[57]. These 3D bone models are able to recreate the exact geometries of the subjects' bones with good accuracy. Specific traits like leg length, native varus/valgus knee alignment, and native tibial slope can be gathered from these models. This allows for implants to be virtually implanted onto these bones more accurately, while providing variability to assess how different implants may perform in different subjects. Since this model is a rigid body model, the bones are not deformable. While real bone may have some level of deformation in vivo, the amount of deformation is quite low [60], leading this assumption to be a reasonable one and a good way to simplify the system.

4.2.2 Modeling Muscles

Muscles generate forces that produce motion and specific force patterns for each muscle can produce different activities within the model. Each muscle modeled has attachment points on the respective bones. Each muscle group is made of several bundles, and those bundles are made of several fibers. Thus, the attachments of a single muscle group will be spread across an area of the bone, just as it is in the human body. In this model, there are two major types of muscles and they are modeled in very different ways. First, is the actively controlled muscles in the system. These muscles, typically the quadriceps, are controlled via a PID controller to maintain proper knee flexion/extension. A desired flexion profile of the knee is input into the controller and may vary depending on the activity type. At each time step, the difference between the actual and desired flexion is calculated.

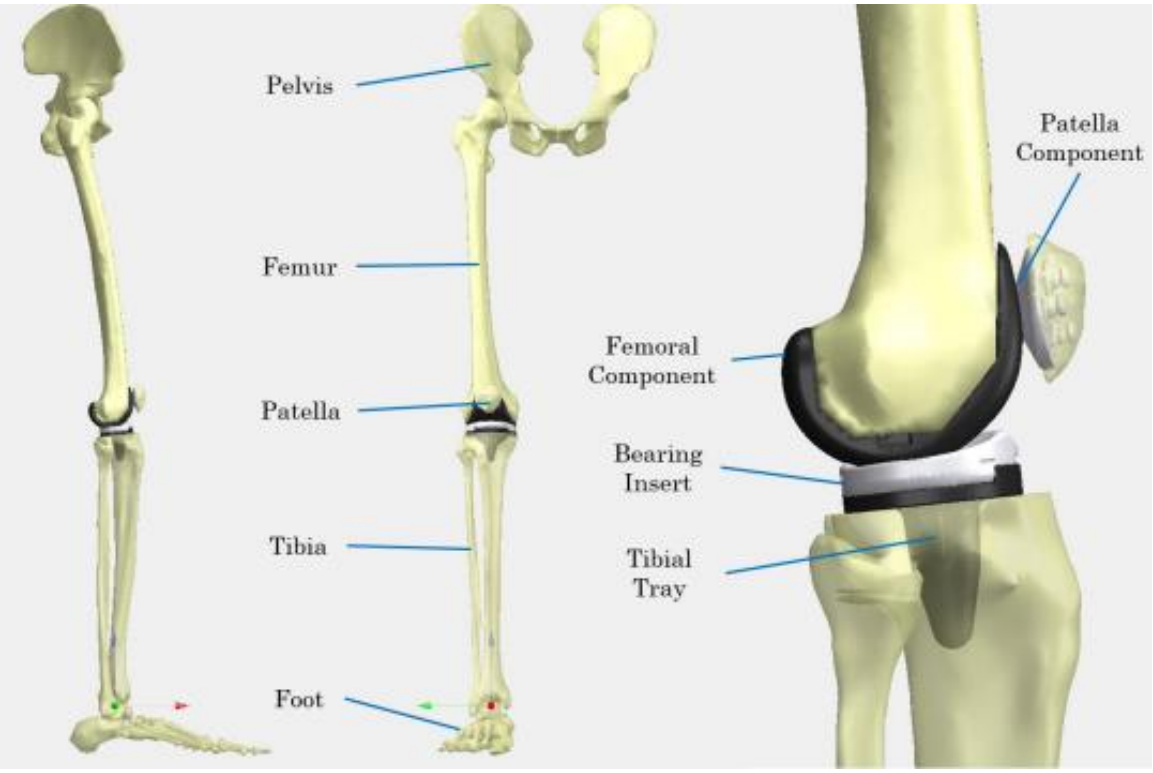


Figure 4-4: Bones and components included in the model.

This value, as well as its integral and derivative, are then utilized to calculate the change in force of the muscle. The gains for each of the proportional, integral, and derivative terms are tuned to minimize the error between the desired and actual flexion profiles. Other muscles in the model are stabilizers. They help to stabilize the leg and distribute loads across the leg. These stabilizing muscles utilize the Hill type model for muscles [61] which incorporates contractile and elastic elements to best represent in vivo muscle response. Figure 4-5 shows major muscles included in the model and a list of their insertion and origin locations.

One important aspect of muscles in this model is the ability to wrap around bone and components. This allows for the line of action of the muscle to change, depending on the positioning of the leg. Rather than the muscle simply being a line between two points, the automatic wrapping algorithm prevents the muscles from going through bone or implant components which would lead to improper force calculations (Figure 4-6). This is especially important in the quadriceps which often would unrealistically go through bones if this tool was not in place. The line of action of the muscles being correct not only affects the resultant contact forces at the joints, but also the torques which are applied to the system (Figure 4-7).

4.2.3 Modeling Ligaments

Ligaments play a very important role in providing both translational and rotational constraints for the knee joint. The presence or absence of ligaments are often important differences between TKA types, while ligament forces and profiles are important results to evaluate TKA performance. In this model, ligaments are modeled as non-linear springs and have multiple bundles to account for the thickness of the ligaments. In this ligament force equation (Figure 4-8), the following are used as inputs: L, the current ligament length; L_0, the ligament slack length; ε_1, the reference strain; and ε, the current ligament strain.

Muscle Group	Muscle	Insertion	Origin
Quadriceps	RF	Proximal patella	Illium – pelvis
	VL	Proximal patella	Anterior femur
	VM	Proximal patella	Anterior femur
	VI	Proximal patella	Anterior femur
Hamstring	BFS	Lateral tibial condyle	Posterior femur
	BFL	Lateral tibial condyle	Ischial tuberosity – pelvis
	SMB	Medial tibial condyle	Ischial tuberosity – pelvis
	SMT	Medial tibial condyle	Ischial tuberosity – pelvis
Gastrocnemius	GL	Calcaneus on foot	Lateral femoral condyle
	GM	Calcaneus on foot	Medial femoral condyle

Figure 4-5: Muscle insertions and origins.

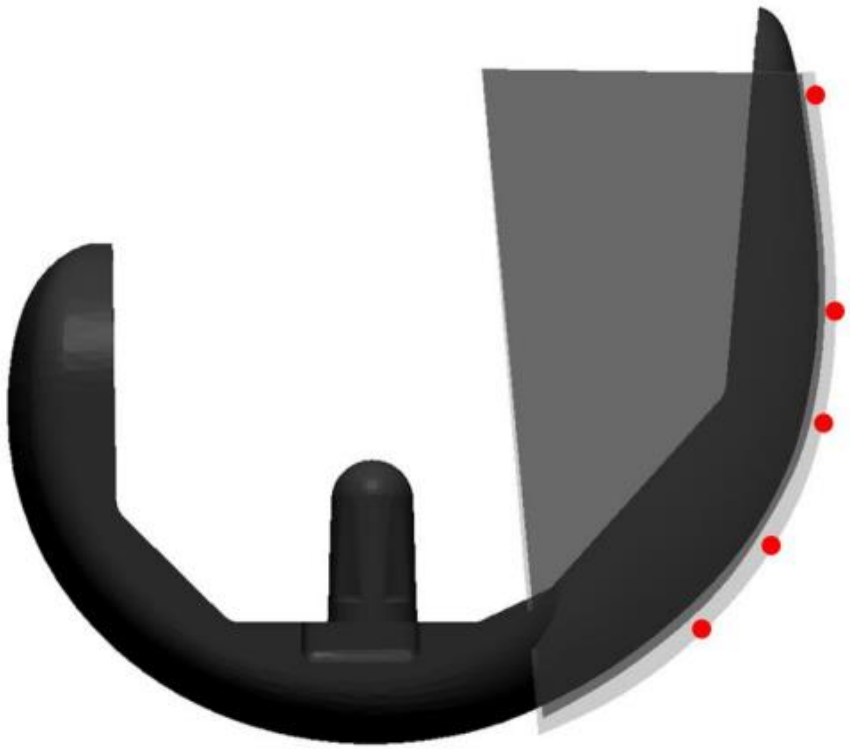


Figure 4-6: Wrapping points on the femoral component.

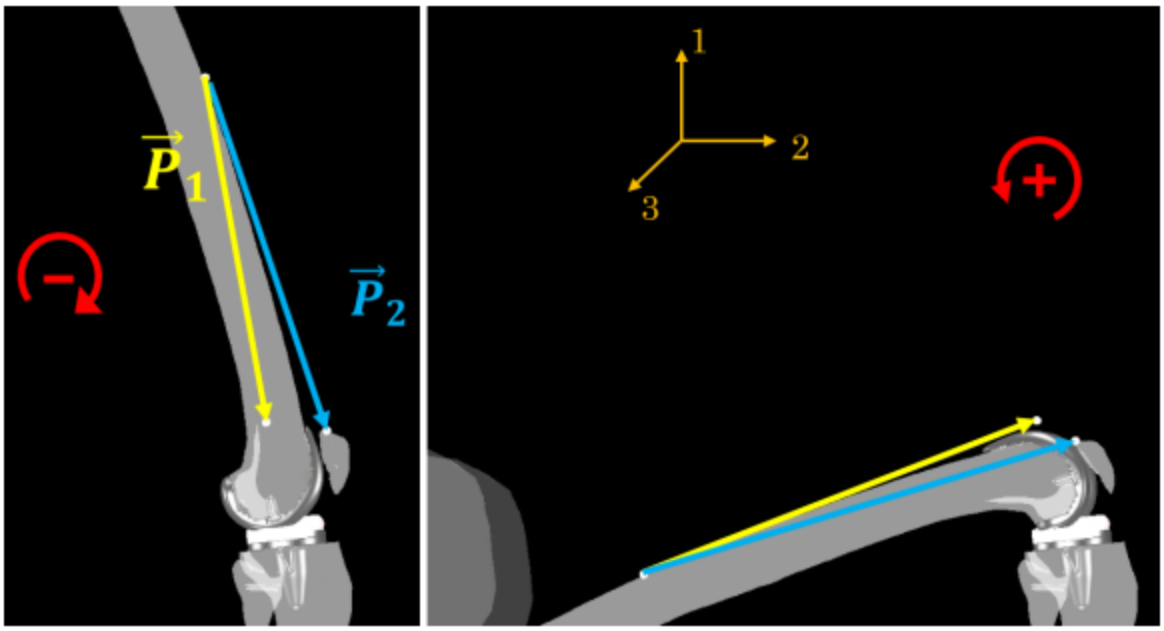


Figure 4-7: Choosing a wrapping point based upon the muscle angle.

Included in the model are the following ligaments: anterior cruciate ligament (ACL), posterior cruciate ligament (PCL), medial collateral ligament (MCL), lateral collateral ligament (LCL), patellar ligament, lateral patellofemoral ligament (LPFL), medial patellofemoral ligament (MPFL), and medial patellomeniscal ligament (MPML) (Figure 4-9). Attachment sites for each of these ligaments were determined based upon bony landmarks and literature. In addition to the ligaments listed, the posterior capsule of the knee was theoretically included in the model as well. To incorporate the posterior capsule into the model, two lateral and two medial bundles were utilized to represent the posterior capsule. These bundles attach to above the femoral condyles, wrap around the posterior aspect of the femoral condyles and attach to the posterior aspect of the tibia. The posterior capsule forces were calculated with similar methods to other ligaments. All these ligaments provide important constraints in the knee and help drive proper femorotibial and patellofemoral motion.

4.3 Contact Detection and Contact Mapping

4.3.1 General Contact Detection

The contact detection algorithm in this model is used to calculate the contact forces between bodies and is used for several different contact types including femorotibial contact, patellofemoral contact, cam/post contact, and sidewall contact. In order to calculate contact forces, one body is represented as a point cloud, while a polynomial surface is mapped onto the other body (Figure 4-10). Since the polynomial surface only needs to be defined where the contact can occur, a convex hull is established, using a 2D bounding polygon that contains all the points used to create the original polynomial surface [62]. The convex hull allows for points outside of the convex hull to be excluded from contact detection calculations, making the overall algorithm more efficient.

$$F = \begin{cases} 0 & \varepsilon \leq 0 \\ k/_2 (L - L_0) & 0 \leq \varepsilon \leq 2\varepsilon_1 \\ k[L - (1 + \varepsilon_1) l_0] & 2\varepsilon_1 \leq \varepsilon \end{cases} \qquad \varepsilon = \frac{L - L_0}{L_0}$$

Figure 4-8: Ligament force equations utilized in model.

Ligament	No. of Bundles	Bundles	Stiffness (N/mm)
ACL	2	Posterolateral (PL)	108
		Anteromedial (AM)	108
LCL	1	-	180
MCL	3	Deep	72.2
		Anterior	27.9
		Oblique	21.1
PCL	2	Anterolateral (AL)	90
		Posteromedial (PM)	50
LPFL	1	-	5.4
MPFL	1	-	20.4
MPML	1	-	20.4
Patellar Ligament	2	Lateral	400
		Medial	400

Figure 4-9: List of modeled ligaments and ligament properties.

Once the convex hull is established, the point cloud is transformed into the other body's coordinate system utilizing the transformation matrices between the two bodies. The height of the polynomial surface is calculated from the polynomial coefficient values used to define that surface and the coordinates at which the height is being calculated. For each point represented in the point cloud, within the convex hull, a polynomial height is calculated. The difference between the point in the point cloud and its corresponding polynomial height is defined as penetration. Contact forces are calculated using a spring-damper system based upon the stiffness of the articulating surface and a damping coefficient. Friction forces are calculated based upon the velocities of the contacting points. Frictional coefficients based upon the component material are used to calculate a friction force applied in the opposite direction of the point's motion. Contact is calculated in one direction, this direction changes depending on the contact type. Femorotibial contact is calculated in the SI direction, patellofemoral and cam/post contact is calculated in the AP direction, and sidewall contact is calculated in the ML direction.

4.3.2Contact Mapping

As discussed previously, the contact detection algorithm is a unique feature of this mathematical model. It allows for contact forces to be calculated between bodies, but this algorithm does not calculate the area which is in contact. In order to accomplish this, a new contact mapping algorithm had to be developed. This contact mapping algorithm went through several iterations with some of them visualized in Figure 4-11. The first step of this algorithm is to determine which points are in contact. This can be done similarly to the contact detection algorithm, by identifying points which penetrate the polynomial surface of the other body. Once these points are identified, the points are triangulated using Delaunay triangulation methods [63].

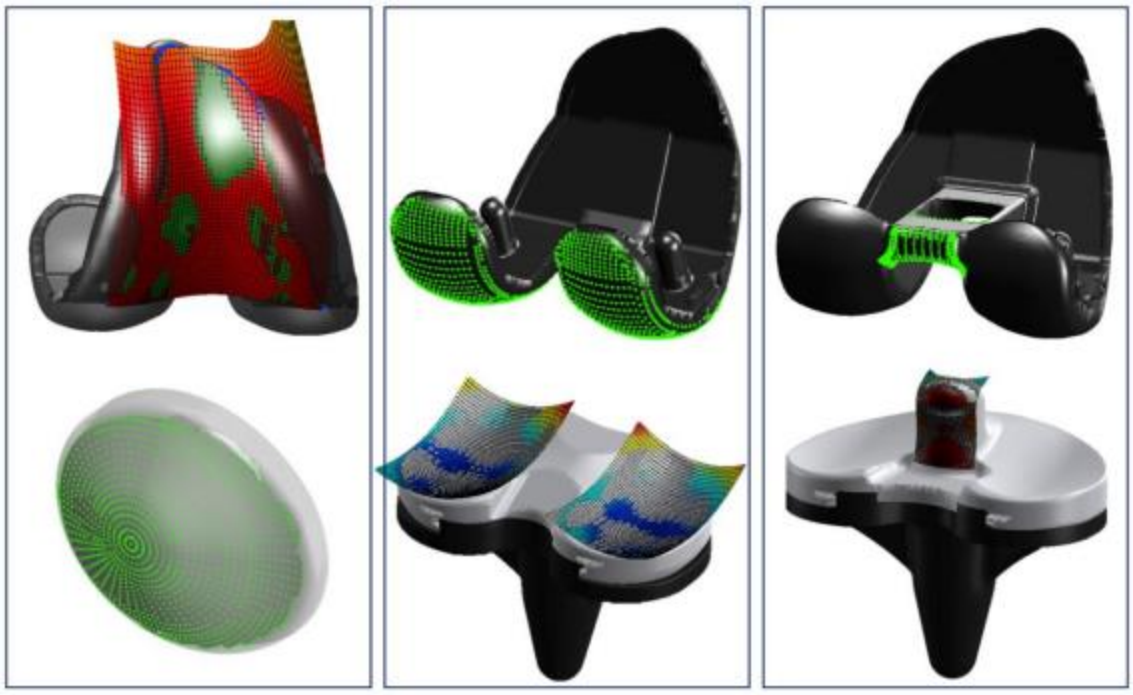


Figure 4-10: Polynomial surfaces and point clouds utilized in patellofemoral, femorotibial, and cam/post contact types.

This triangulation method maximizes the minimum angle of triangles in the mesh, but does not necessarily minimize the length of edges. This allows for more consistent face sizing and connectivity between points. The determination of connectivity in this group of points allows for a patch object to be created and visualized. The area of this patch object can then be determined with the polyarea function in Matlab. This function calculates the area of the best fit polygon which encircles the contact patch.

While the model assumes rigid body mechanics for bones and implant components, the contact mapping algorithm does account for some deformation of polyethylene components. To better understand the material properties of polyethylene, material testing was done by engineers at DePuy-Synthes, a Johnson and Johnson Company, utilizing a modified Oxford rig of the knee, simulating a DKB activity. The strain in the bearing component during this activity was calculated experimentally and the data showed a relationship between axial load and strain of the bearing component (Figure 4-12). However, when doing this material testing, the changing shape and radius of the femoral component was not considered.

A changing radius leads to a changing contact area, so the stress in the material changes not only based upon the axial force applied, but also the contact area between the femoral component and poly. Thus, a deformation factor was calculated based upon the relationship between stress in the material and the strain of the material, rather than the axial load being applied. This method is more accurate because it is not merely the force which causes deformation, but utilizes the stress within the material. This stress-strain relationship was used to calculate the amount of deformation in the poly at each time step, utilizing the stress in the material at the previous time step (Figure 4-13). This deformation factor was added to the contact threshold value, the amount of penetration required for a point to be considered in contact.

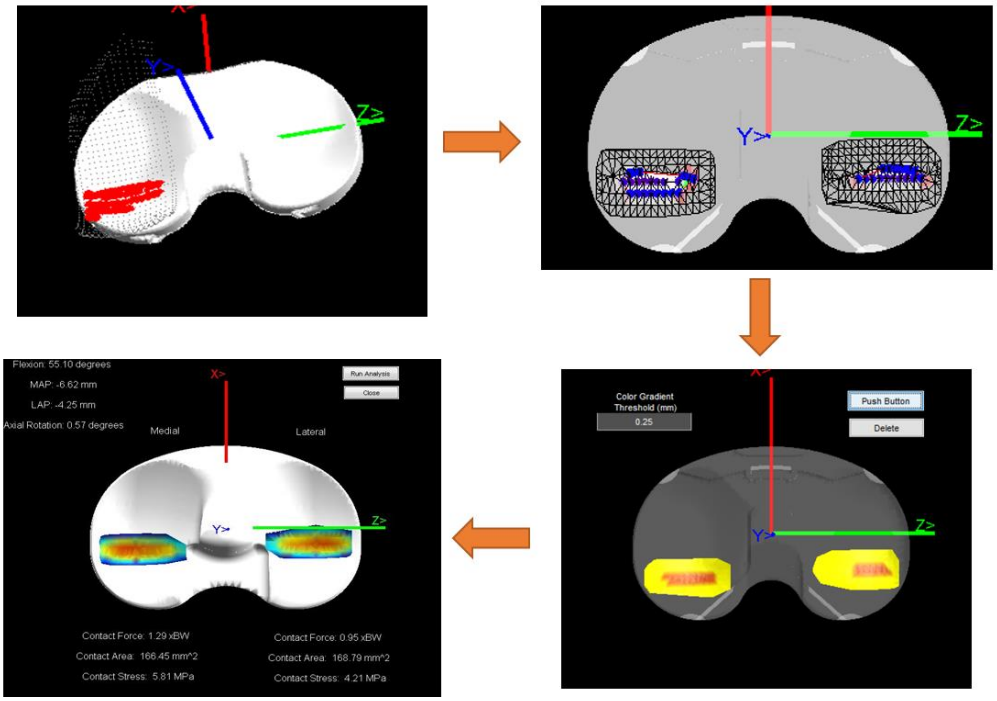


Figure 4-11: Iterations of the femorotibial contact mapping tool.

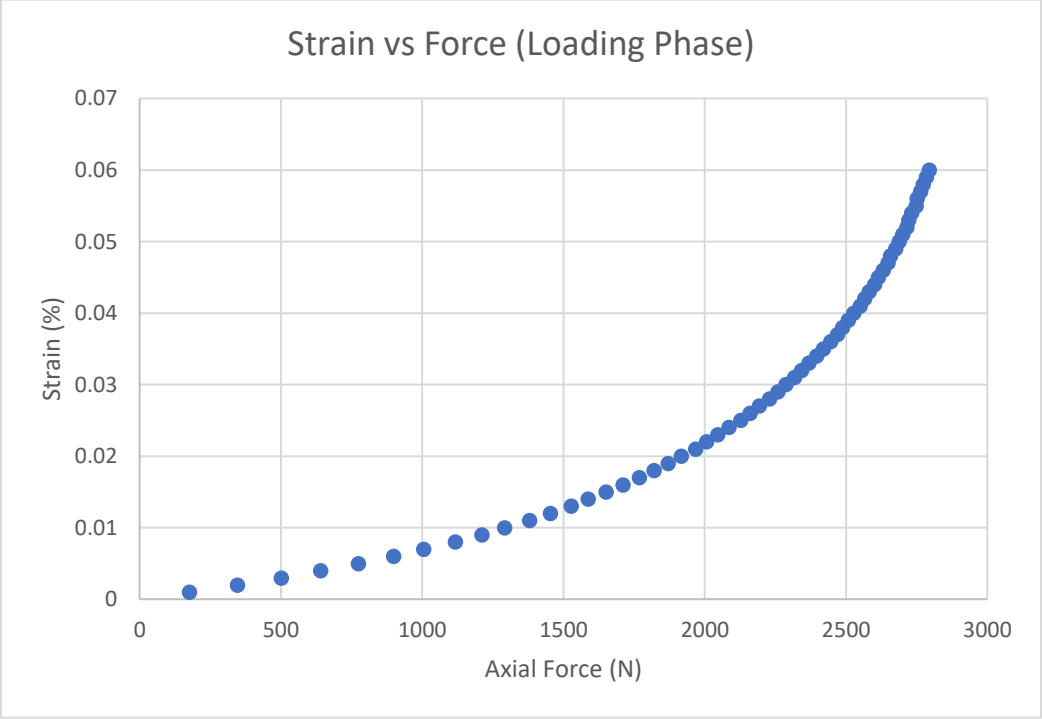


Figure 4-12: Strain vs axial load for polyethylene component.

Thus, the more positive contact threshold leads to more points being deemed in contact to help simulate the increased contact areas which would be seen if deformation was occurring in the polyethylene component. This method is based upon the contact mechanics of elastic solids [64]. An elastic surface will conform its shape to that of the object being pressed into it (Figure 4-14). This phenomenon occurs between two spheres of different radii, which is what the femoral condyle and bearing surfaces can be simplified as. As the deformation of the polyethylene component increases, the contact area increases as well. The methodology discussed allows for the contact area to be calculated, while contact force values can be obtained from the simulation result data. Since contact area and contact force are both known, an average contact stress can be calculated using the following equation: $\sigma=F/A$. The average contact stress, σ, the force for that contact type, F, the contact area, A. Contact areas, forces, and stresses can be further split based upon location if needed. This is done in the patellofemoral contact type to provide more detailed information on patellar tracking and force locations. The methodology of this is discussed in further detail in the following section. To improve user friendliness, the areas of the contact patch with higher penetration were colored red, while areas with lower penetration were colored blue. At each time step of the simulation, this algorithm updates the positions and number of points in contact, and then updates the visualization and area calculation at that point in time.

4.3.3Patellofemoral Contact Mapping Improvements

To improve the patellofemoral contact mapping calculations, it was necessary to modify the patellofemoral contact detection algorithm to allow for improved patellar tracking in late flexion, as well as more detailed information regarding the location of patellofemoral contact.

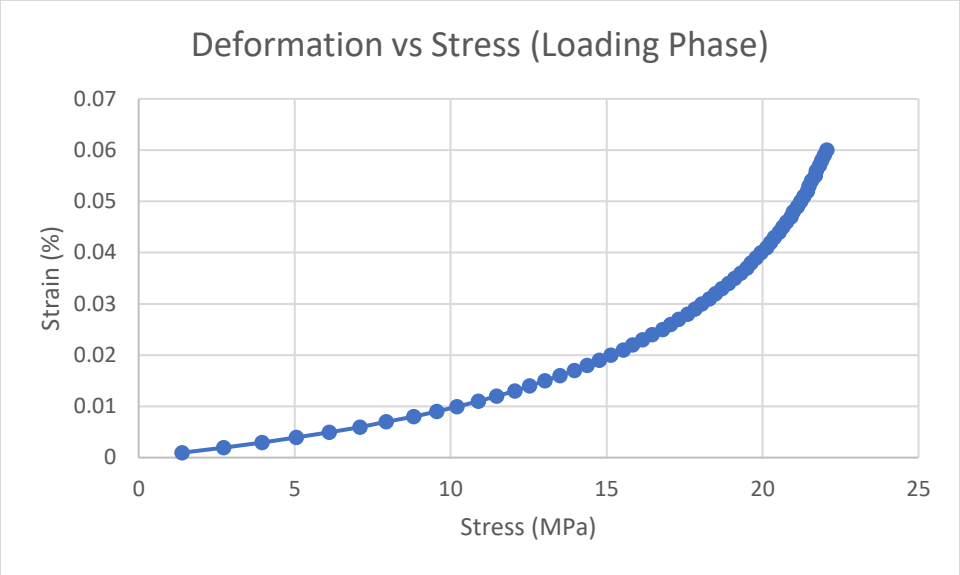


Figure 4-13: Deformation and Stress relationship of polyethylene.

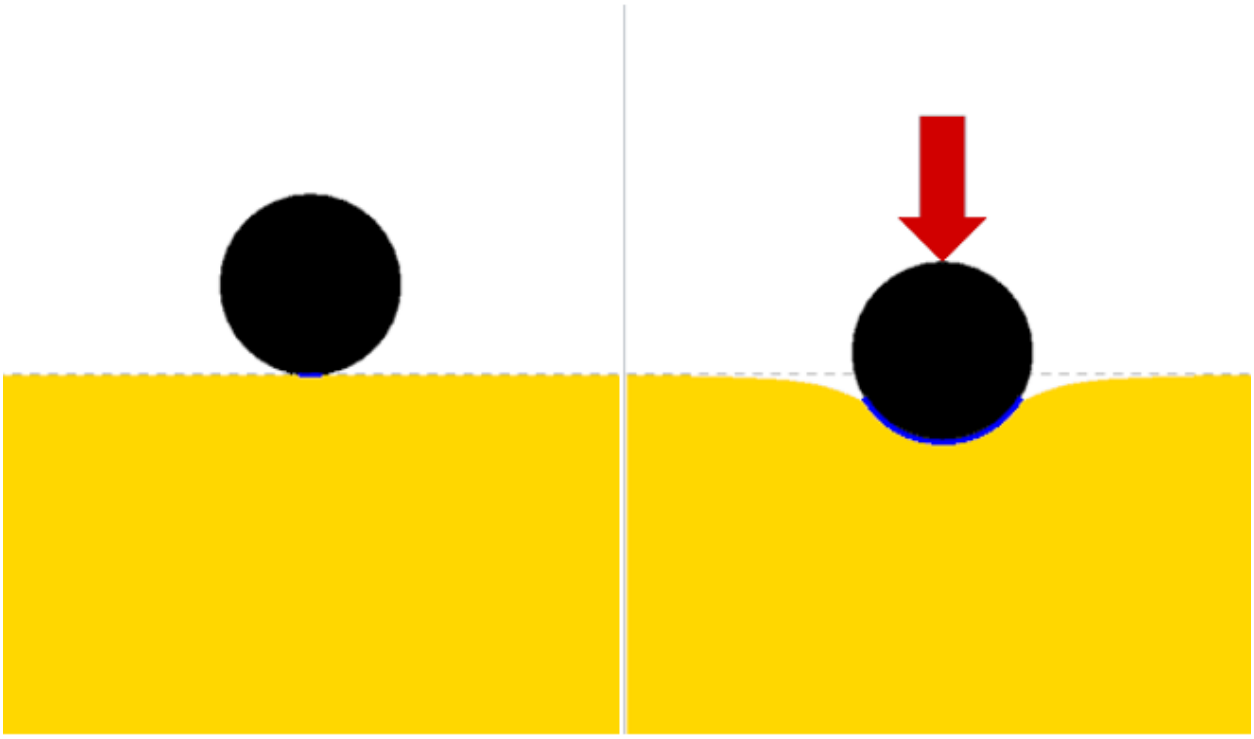


Figure 4-14: Visualization of increasing contact area with increased surface deformation.

In previous iterations, a polynomial surface was mapped onto the trochlear groove of the femur (Figure 4-15), while changes were made in the new iteration to map the polynomial surface to the patella and a point cloud for the trochlear groove was used (Figure 4-16).

In addition to simply changing the bodies of the surface and point cloud several changes were made to the code. A new surface mapping tool had to be created to map the patella surface and establish the surface's coefficients and convex hull information. New transformation matrices were also utilized in the contact detection codes to now transform the trochlear groove points into the patella's coordinate frame. Changes also had to be made to calculate penetration in the positive AP direction rather than the negative AP direction. Meaning if trochlear points are more anterior of the patella's surface there is contact. Additionally, the patellofemoral force was separated into medial and lateral patellofemoral forces based upon the location of the point in contact. If the point is more lateral of the femoral component's midline, the force contribution from that point is added to the lateral patellofemoral force. Likewise, the points medial of the femoral component midline had their force contributions added to the medial patellofemoral force. So, this contact detection tool calculates medial, lateral, and total patellofemoral force. Overall, these changes allow for more detailed patellofemoral contact information to be obtained, while providing more accurate contact information in deep flexion. Within the contact mapping tool that is utilized, the contact area was calculated by triangulating the points deemed to be in contact and then taking the area of that patch. This concept works well in cases where there is one contact patch, but advancements were required to calculate a splitting contact patch which occurs in late flexion in the patellofemoral contact mapping tool. Rather than determining which points in the point cloud were in contact and triangulating them, it was determined which faces have vertices in contact. Since the connectivity of the points is already known, the faces with at least one vertex in contact can be identified.

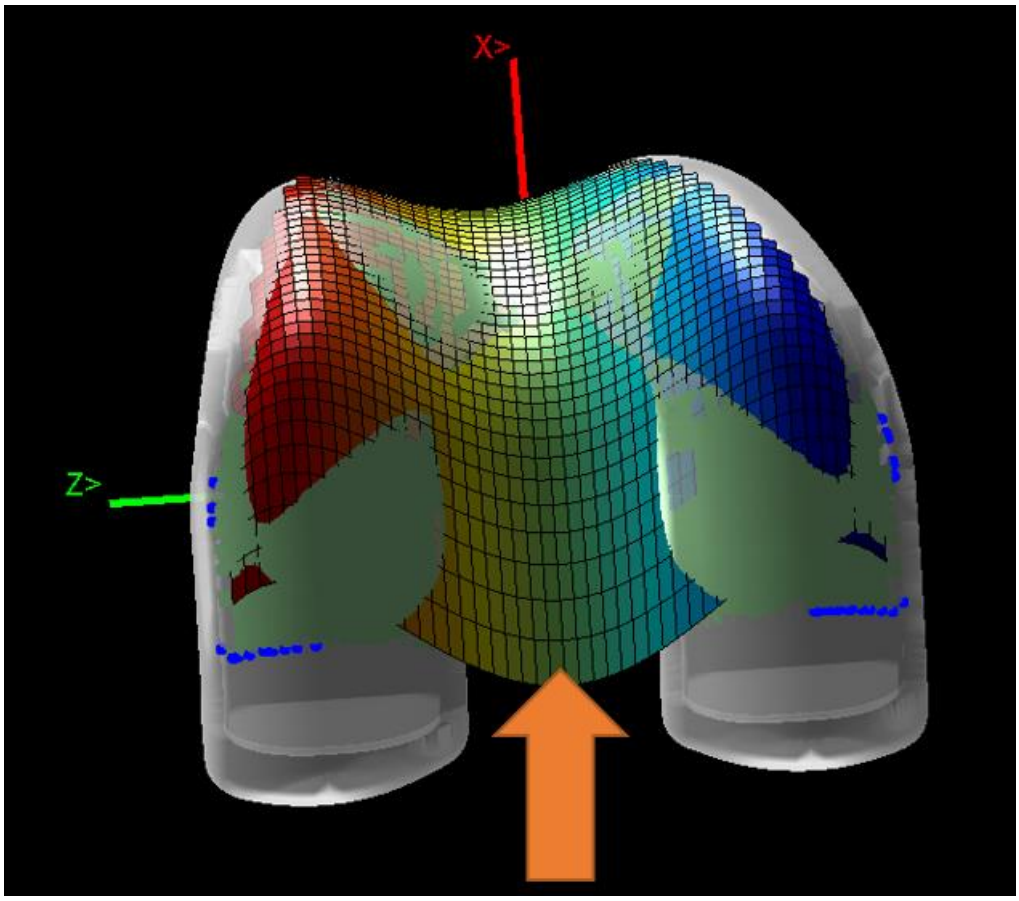


Figure 4-15: Previously used polynomial surface on the trochlear groove.

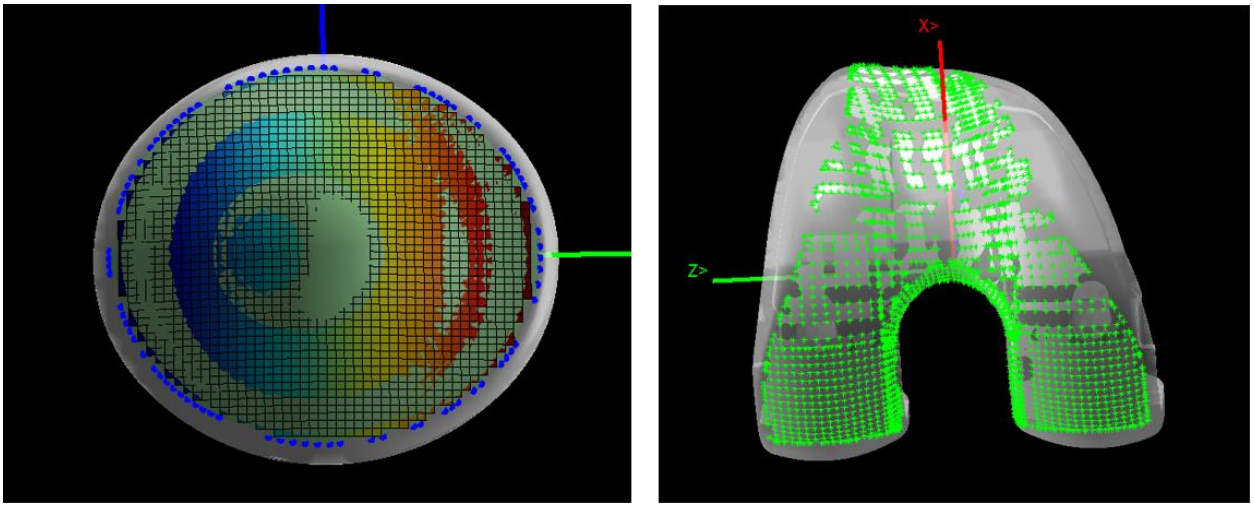


Figure 4-16: Updated polynomial surface on the patella and point cloud on the trochlear groove.

Utilizing this information, if all three vertices had contact, that face is fully in contact and the entire area of that face is added to the contact area calculation. If only two of the three vertices were in contact, then two thirds of the face's area was added into the contact area calculation. Similarly, one third of the face's area was added into the contact area calculation if one vertex was in contact. The total area of a face was calculated by utilizing the area of a triangle formula: ($Area = \frac{1}{2} b * h$), where b is the length of the base of the triangle and h is the height of the triangle. Using this method, no retriangulation is required, thus no new contact patch is required. This simply allows for faces in contact to be colored while faces not in contact remain transparent. The contact area visualization can now be split into multiple parts while still accurately calculating the contact area (Figure 4-17). This contact area can also be split into medial and lateral patellofemoral contact areas. If the midpoint of the face is lateral of the femoral component's midline, then that face's area is added to the lateral patellofemoral area. Similarly, if the face's midpoint is medial of the femoral component's midline, then that face's area is added to the medial patellofemoral area. The medial and lateral patellofemoral areas can be added together to calculate the total patellofemoral contact area. The contact forces utilized in the contact mapping tool are retrieved from the model's contact detection algorithm which provide total, medial, and lateral patellofemoral force. So, this contact mapping tool is capable of providing medial patellofemoral stress, which is calculated utilizing the medial patellofemoral contact area and the medial patellofemoral contact force, lateral patellofemoral stress which is calculated utilizing the lateral patellofemoral contact area and the lateral patellofemoral contact force, and the total patellofemoral stress, which is calculated utilizing the total patellofemoral contact area and the total patellofemoral contact force. These more detailed results can help identify trends in implant design or the effects of different surgical alignments.

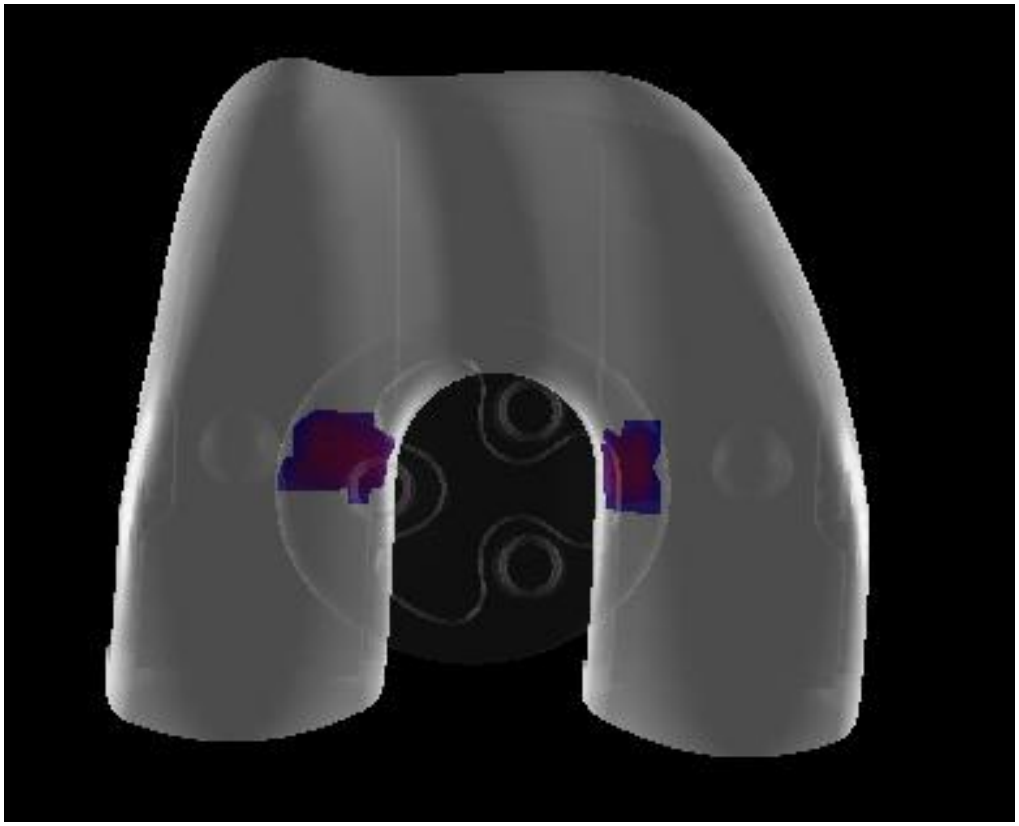


Figure 4-17: Patellofemoral contact area split into two parts in late flexion.

4.4 Developing Solutions for New Implants

In this model, there are several different knee implant types that were included, which can be analyzed. Therefore, the model is more robust than previous versions, but each implant type offers a unique challenge in how they are to be modeled. Previous iterations of the model have included CR, PS, Medial Pivot, and ASTKA designs. Each of these implants retain or resect different ligaments and some of these designs include unique features to substitute for these ligaments and lead to more normal-like mechanics. To further improve the model's versatility, two new implant types were added into the model: Sigma Stabilized + and fixed bearing medial UKA. The Sigma Stabilized + implant is similar to a PS implant but has a wider cam/post mechanism which is used to further stabilize the knee and restrict excessive rotation. The FB medial UKA resurfaces only the medial compartment of the knee, leaving the native lateral side and patella. This implant retains all native ligaments but offers the challenge of incorporating both native and implanted geometries into a single simulation.

4.4.1 Sigma Stabilized +

Although primary TKA's and surgeries are often successful, revision surgeries and implants may be utilized to alleviate continued symptoms of osteoarthritis and improve overall joint performance. One common reason for TKA revision surgery is varus/valgus instability. Increased varus/valgus instability can lead to excessive forces in the collateral ligaments, potentially leading to rupture of the ligaments. It may also lead to abnormal kinematics including paradoxical sliding and mid-flexion instability [65]. The Sigma Stabilized + TKA is often used as a revisionary TKA to provide increased varus/valgus stability to the knee. To accomplish this, the Sigma Stabilized + TKA increases the width of its posterior post/cam mechanism compared with the traditional Sigma PS. The shape of this post is also flat rather the rounded posts seen in other implant types (Figure

4-18). Since the clearance between the femoral sidewalls and the post at 0° and 90° flexion is 0.2 mm, it is significantly less than the traditional Sigma PS which has 0.75 mm of clearance and required modifications in the algorithm. Due to the lower amount of clearance in the Sigma Stabilized + TKA design, additional contact is likely to occur between the sidewall of the femur and the side of the posterior post. Understanding how this sidewall contact force contributes to kinematics and kinetics of the overall TKA would assess the design goals of increased varus/valgus stability and restricted rotational motion (Figure 4-19).The side wall mechanism used in this FSM is very similar to other contact detection methods already used in the model to determine femorotibial contact forces as well as posterior stabilized (PS) and anterior stabilized (AS) cam/post forces. The main difference for this sidewall mechanism is that the contact is calculated in the medial/lateral direction. The sidewall of the femur is modeled as a polynomial surface, while the side of the post is modeled as a point cloud (Figure 4-20, Figure 4-21). Utilizing the transformation matrices between the two bodies, the points of the post are transformed into the femoral component's reference frame. Each point within the convex hull of the sidewall's surface has its height (ML coordinate) compared with the height of the polynomial surface. For the medial sidewall, if the point is more medial than the polynomial height, then that point is determined to be in contact. In the lateral sidewall, the points must be more lateral of the polynomial height to be considered in contact. When a point is determined to be in contact, the penetration value, the difference between the polynomial height and the ML coordinate of the point, is utilized to calculate the contact force contributed by that point. The larger the penetration value, the larger the resulting force will be. Based upon this penetration value, three different components of the contact force are calculated: normal force, frictional force, and damping force.



Figure 4-18: Post shape comparison between the Sigma Stabilized + (left) and the Attune PS (right).



Figure 4-19: Sidewall clearance for Sigma Stabilized +.

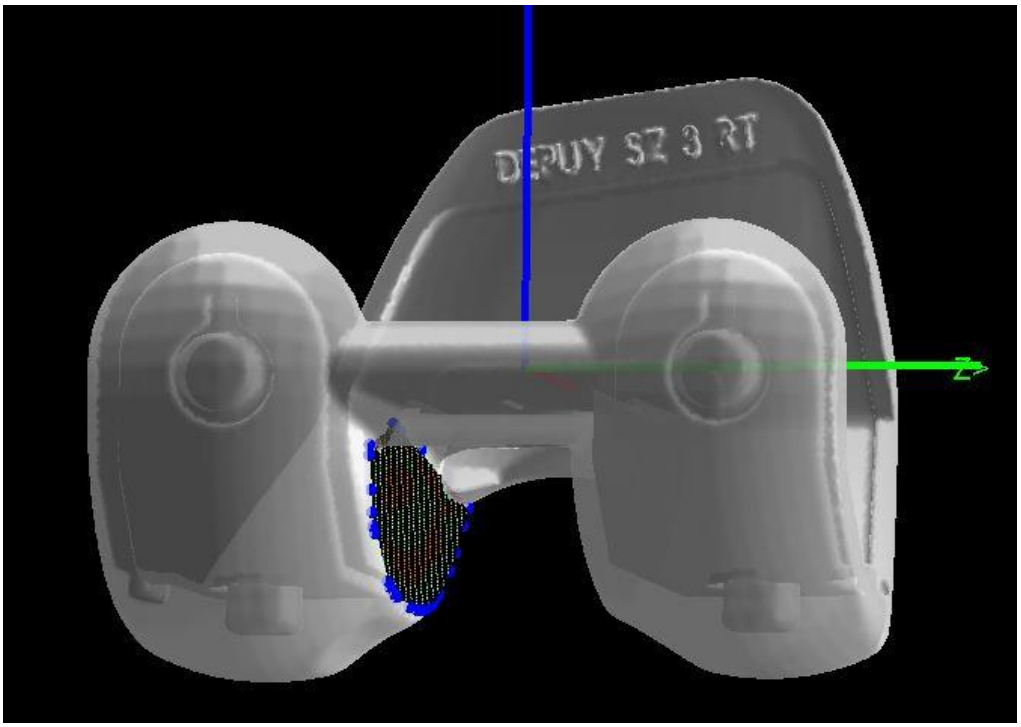


Figure 4-20: Medial femoral sidewall polynomial surface for the Sigma Stabilized +.

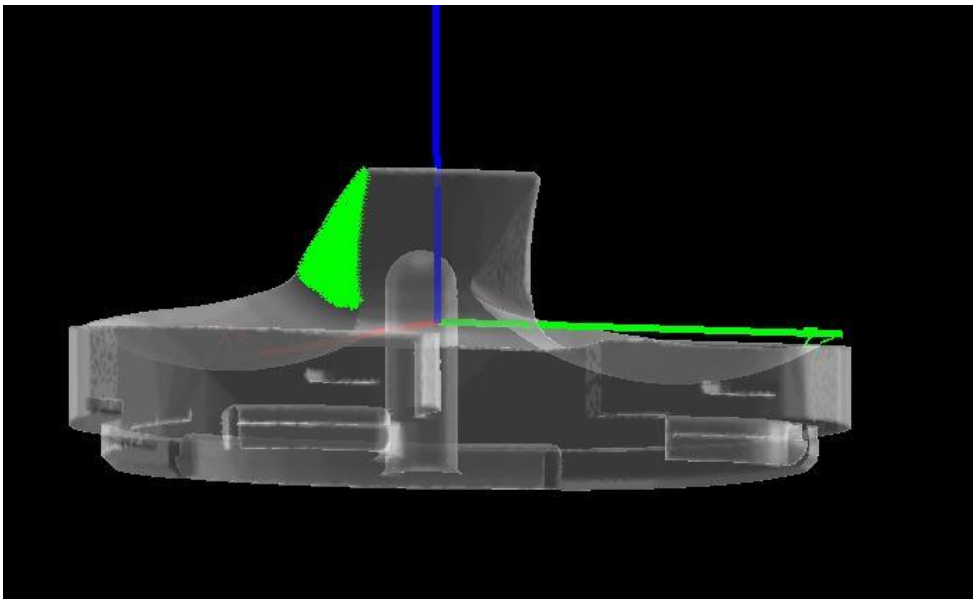


Figure 4-21: The medial side post point cloud for the Sigma Stabilized + implant.

```
xnormforce=-xgrad*(K*pen[n])/pow((pow(xgrad,2)+pow(zgrad,2)+1) ,0.5);
ynormforce=(K*pen[n])/pow((pow(xgrad,2)+pow(zgrad,2)+1) ,0.5);
if (penold[n]>10000 || T < 0.0002){
    dampforce=0;}
else{dampforce=(DAMP*(pen[n]-penold[n])/TSTEP)/pow((pow(xgrad,2)+pow(zgrad,2)+1) ,0.5);}
ynormforce=ynormforce+dampforce;
znormforce=-zgrad*(K*pen[n])/pow((pow(xgrad,2)+pow(zgrad,2)+1) ,0.5);
totnormforce=pow((pow(xnormforce,2)+pow(ynormforce,2)+pow(znormforce,2)) ,0.5);
```

```
frictionforce[0]=-vx/vtot*MU*totnormforce+frictionforce[0];
frictionforce[1]=-vy/vtot*MU*totnormforce+frictionforce[1];
frictionforce[2]=-vz/vtot*MU*totnormforce+frictionforce[2];
```

Figure 4-22: Equations for normal, damping, and friction forces in FSM contact detection.

The equations for each of these three calculations are shown below (Figure 4-22). If the point does not penetrate the surface, all three force values are set to zero.

4.4.2 Unicompartmental Knee Arthroplasty

An alternative, and viable option for patients inflicted with single compartment arthritis, most commonly occurring on the medial side, is a unicompartmental knee arthroplasty (UKA). Although it has been documented that this is a good alternative, many surgeons still believe that a TKA remains the best option for their patients [66, 67]. Implantation of a UKA does conserve bone at the time of surgery, allowing for a TKA to be used at the time of revision, if required. UKA does also seem to be a good option for younger patients where the anterior cruciate ligament can be spared [60]. Although there are ample studies documenting the kinematic and functional results for a TKA, there aren't as many in vivo studies evaluating the kinematics of UKA and thus, there isn't ample data to support UKA kinematics being more normal-like in pattern and magnitude. By adding the UKA into the model, it further increases the versatility of the model and allows for analyses to be conducted upon an often used, but relatively understudied implant type. The simulation control in the model allows for clinically relevant analyses to be conducted including UKA alignment comparisons, analysis of the roles of the cruciate ligaments, and comparison between different UKA types.

To accommodate the UKA implant type, advancement and modification were required and needed to be implement for the Autolev, C++, and Matlab codes. One of the main changes was the incorporation of the native bone structures on the patella and non-implanted side. This resulted in the removal of the patella button body throughout the code and relying on the patella bone model for the contact surface. Similarly for the non-implanted side, the native femoral condyle and native

tibial plateau of the bone models were identified to create point clouds and polynomial surfaces utilized in the contact detection algorithm. Since the bone models were made from CT information, no cartilage was present. In order to account for this, and make the contact between the native surface less irregular, the native surfaces and point cloud were smoothed and the native surfaces were raised off the bone approximately 2-3 mm to account for cartilage thickness. This allows for the joint line to remain consistent with the preoperative conditions. The contact detection methods on the native side remain consistent with how it is done on the implanted side.

In addition to changes with femorotibial contact detection surfaces, points of interest including muscle wrapping points and ligament attachment points were defined. Since no previous implant in the model retained the ACL, ACL attachment points were located with bony landmarks and information gathered from literature [65]. The flexion facet center (FFC) of the implanted side was also identified. The FFC is the center point of a circle fitted to the posterior aspect of the femoral condyle (Figure 4-23). This point is often utilized to track the motion of the condyle. By including this point in the model, the motion of the FFC can be compared directly to other literature.

In this model two different UKA types were analyzed: (1) the Sigma UKA and (2) the Preservation UKA. For each of these implant types, a fixed bearing medial UKA was utilized in the model, as this is the most commonly used UKA. The positioning of the femoral component was determined by best matching the femoral implant surface with the native condyle's surface. CAD software was utilized to visualize the components and bones. Bone cuts were then made along the cut lines of the properly positioned implant (Figure 4-24). A similar technique was utilized for the positioning of the tibia.

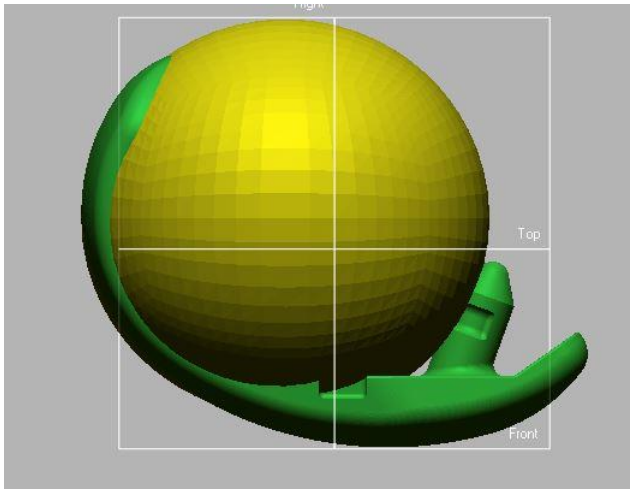


Figure 4-23: Circle fitted to femoral condyle to identify FFC location.



Figure 4-24: Implanted components are placed on the bones to best recreate the native surfaces.

The tibia component with the polyethylene bearing fitted on top was virtually positioned to best match the native tibial plateau. Once this position was identified, the medial tibia bone was cut to match the inferior aspect of the tibial tray.

Another important aspect of the UKA module is the interaction between the native trochlear groove and the implanted femoral component. In order for the patella to smoothly transition between both non-implanted and implanted geometries, two trochlear groove surfaces are used, with one on the native bone and one on the anterior aspect of the femoral component (Figure 4-25), as well as a point cloud on the articulating surface of the patella. Throughout an activity contact can be detected when the patella's point cloud penetrates either the polynomial surface on the native trochlear groove or anterior aspect of the femoral condyle. Therefore, the patellofemoral forces on the bone, patellofemoral forces on the implant, and total patellofemoral forces can be reported.

4.5 Developing New Activities

4.5.1 Gait

In previous attempts to include gait as an available activity in the model, it has proved to be very challenging and previous attempts were failures. This is largely due to the fact that the gait activity is vastly different from any other activities in the model because the direction of rotation changes from flexion to extension throughout the motion cycle. Therefore, previous activities in the model were mostly variations of flexion or extension of the knee, but not both. If the motion cycle only rotates in one direction, the model can utilize the quadriceps muscles to control the rotation of the knee and drive the activity in one direction.

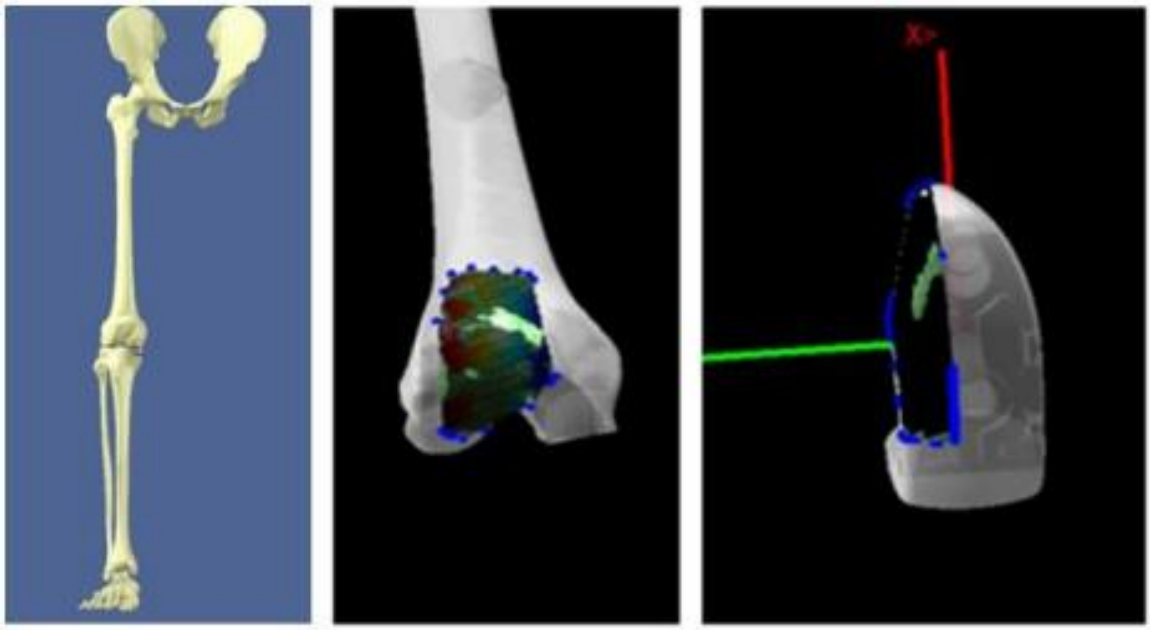


Figure 4-25: Surfaces on the bone and femoral implant to assess patellofemoral contact.

The gait activity begins at heel strike, with the knee slightly flexed. As the activity continues, the knee further flexes as the leg accepts more weight. During midstance the knee begins to extend again, and ultimately flexes again at toe off. The knee flexion profile used during the gait activity can be seen in Figure 4-26.

Due to the vast differences in the gait activity and previously modeled activities, the code for gait needed to be started from scratch. The resulting model is an eleven degree of freedom model, with the patella remaining completely free (3 rotations and 3 translations) and the femur remaining free except for flexion (2 rotations and 3 translations). Other bodies like the tibia, pelvis, and foot have their motion specified based upon literature and data from a validated hip model which previously analyzed gait [68]. Some important changes in the gait code include specified muscle forces for major muscles like the quadriceps, hamstrings, and gastrocnemius. Although modified slightly to better fit the subject used in the model, the muscle profiles were found in literature and based upon EMG data gathered from subjects [69]. These profiles can be seen in Figure 4-27. Unlike in previously modeled activities where the quadriceps were controlled via a PID controller, the quadriceps muscle profile is gathered from EMG data and the flexion of the femur is specified. This allows for a more stable simulation which can switch between knee flexion and extension without the inefficiencies that often accompany PID controller response times. This gait model has more constraints that previous activities in the model since flexion of the femur is specified, but this allows subject specific profiles to be input into the model with information like step length, walking speed, and knee flexion to be precisely controlled. A filmstrip of the gait activity can be found in Figure 4-28.

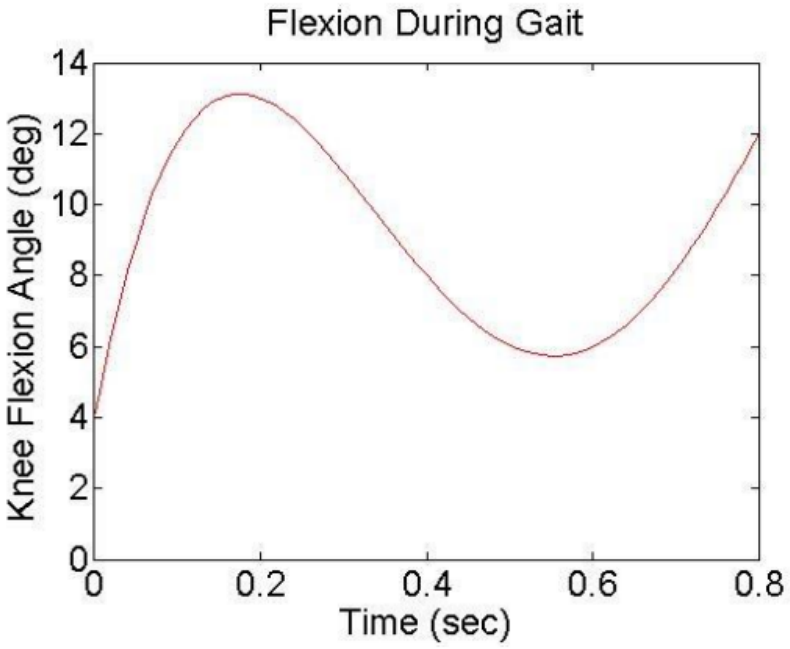


Figure 4-26: Knee flexion profile during gait activity.

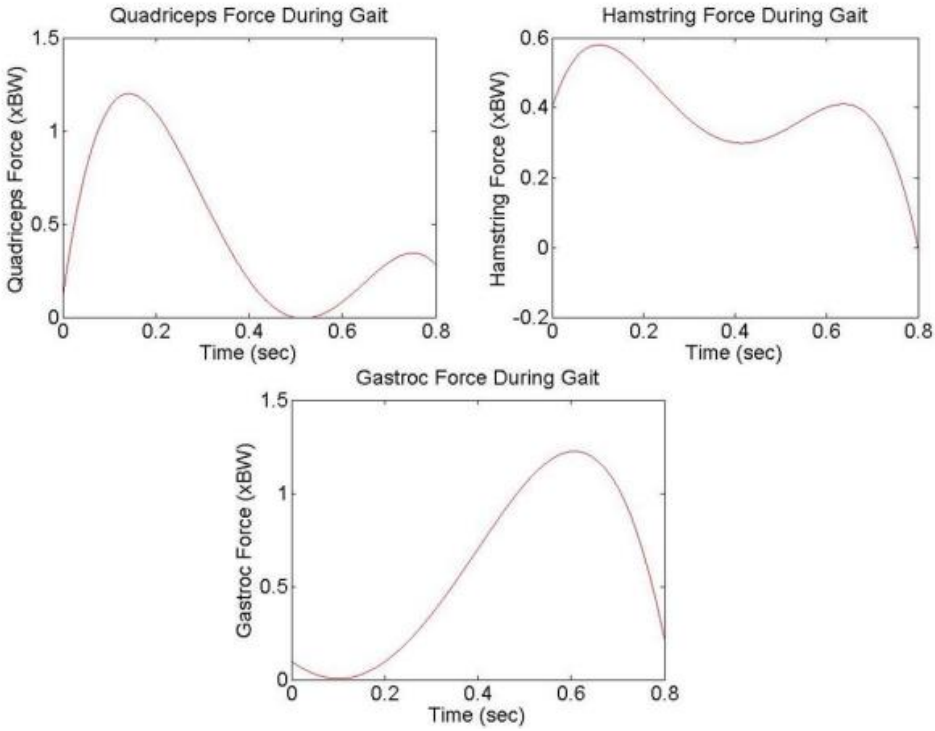


Figure 4-27: Muscle force profiles utilized in gait activity.

One of the main challenges of gait was incorporation of motion at the first time-step of the activity. Since gait is a continuous activity, at the beginning of stance phase the leg has velocities and accelerations in the first time-step. All other activities in the model begin at rest, so starting the activity in motion was a significant hurdle to navigate. First, the motion profiles of some bones (foot, tibia, pelvis) are known, so taking the first derivative of these profiles gives the velocities and the second derivative gives the acceleration. The flexion profile of the femur is also known, which is the most significant motion of the femur observed in gait. At heel strike there is minimal rotational motion along the AP and SI axes of the femur [70] so these rotational velocities were assumed to be 0. These factors along with proper initial boundary conditions allow for the activity to start at heel strike with the leg in motion, thus simulating the stance phase of a continuous gait activity.

Another aspect of the gait model is the inclusion of ground reaction forces which are applied on the foot. The profiles of these ground reaction forces in all three directions were found in literature [71]. The most significant GRF contributor, the SI ground reaction forces, can reach up to 1.2 xBW. Throughout the gait activity, the location of where this GRF is applied on the foot changes as the contact between the foot to the ground moves from the back of the heel to the big toe. From heel strike to toe-off, the location of the GRF translates anteriorly and slightly medially when approaching toe-off (Figure 4-29). Overall, significant changes to the model were made to account for activity specific challenges in gait. The resulting model is slightly more constrained than other activities in the model but provides ample information regarding the kinematic and kinetic results during one of the most common activities of daily life.

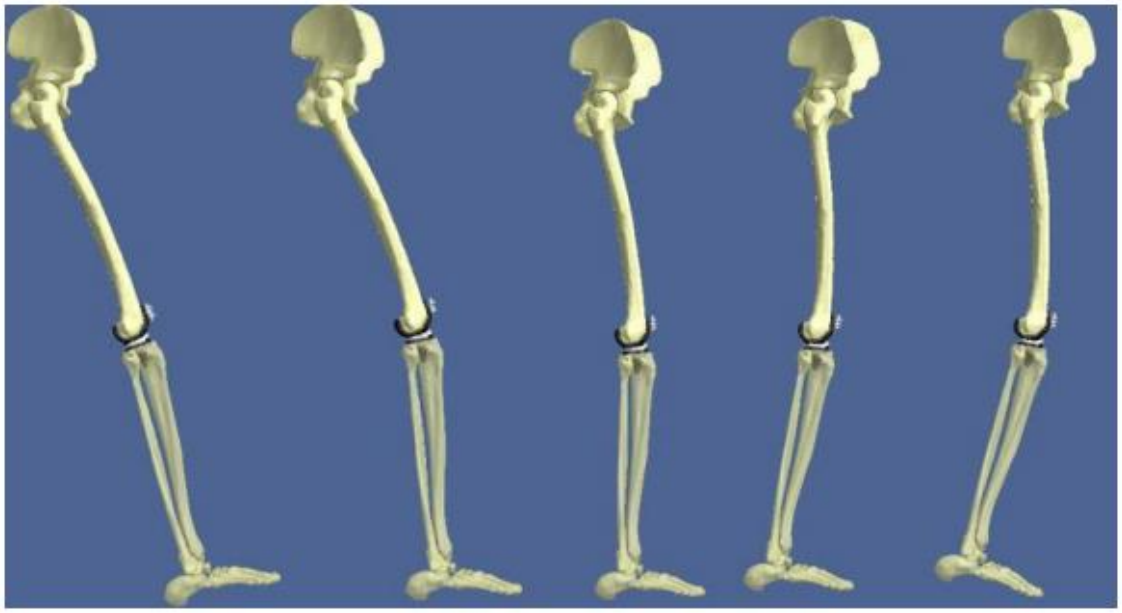


Figure 4-28: Filmstrip of gait activity.

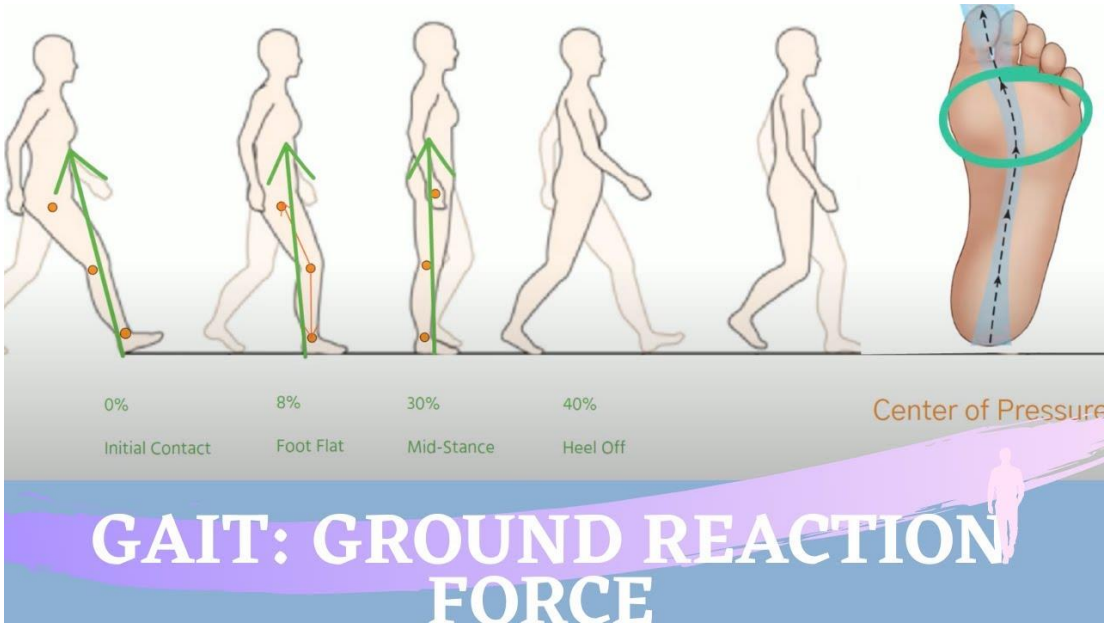


Figure 4-29: Visualization of the GRF location and direction during the stance phase of gait.

4.6 Graphical User Interface

To interact with the model and visualize results, a graphical user interface (GUI) was created in Matlab (Figure 4-30). This GUI allows for the user to select an implant, subject, and activity, and further adjust the initial positioning of the components and other key simulation variables including ligament properties, PID controller gains, and soft tissue attachment points. After a simulation has run, the user has the option to load in the results from that simulation into the GUI. At this point the user can visualize many results including relevant kinematic results, kinetic results, and other simulation specific results. The GUI is consistently modified in order to incorporate advancements that are being developed in the algorithm. For example, as the contact mapping tool was developed, a contact mapping module was incorporated into the GUI to help visualize contact mapping results and allow the user to select analysis parameters like contact type and color mapping details. New implant types and activities are also added to the GUI as they become available for analysis. The GUI also contains several analysis tools including femorotibial animations, patellofemoral animations, and total leg animations. These tools allow for more in depth analysis as well as the ability to contextualize results by visualizing them.

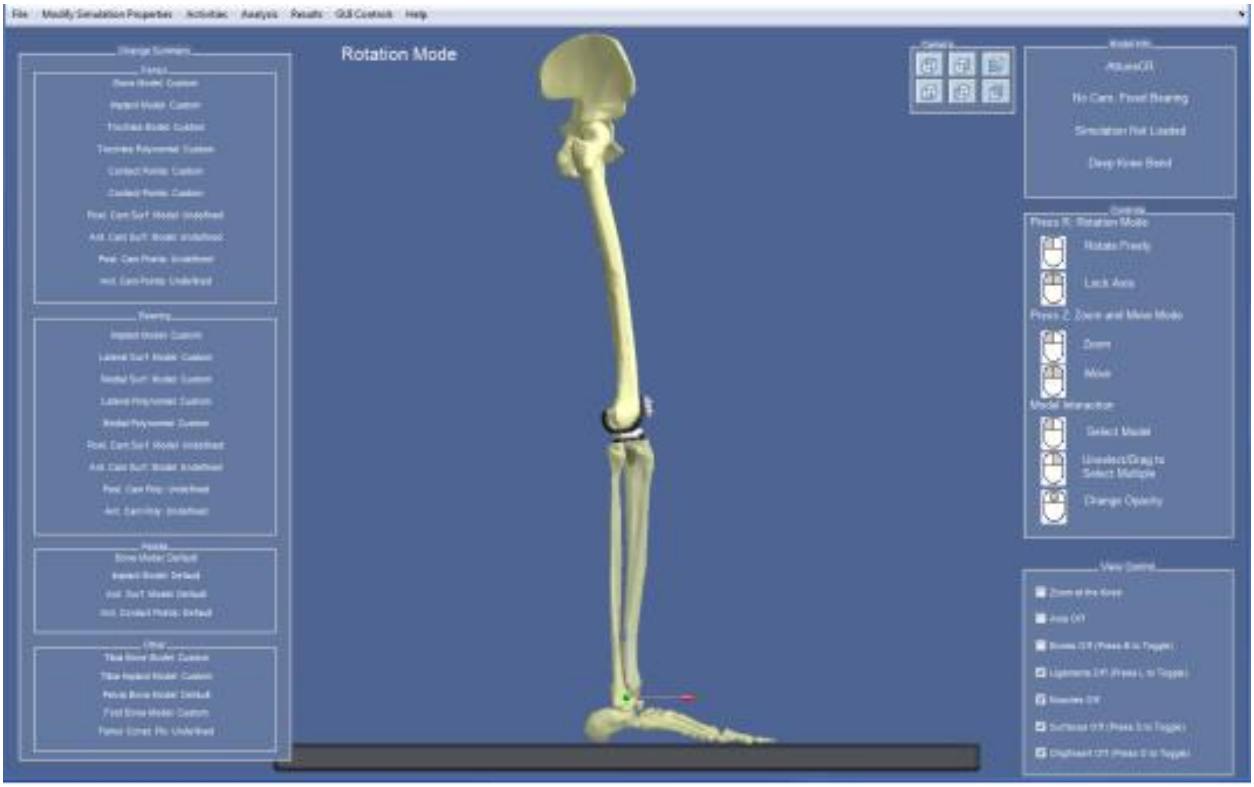


Figure 4-30: Visualization of the knee model GUI in Matlab.

Chapter 5 Results and Discussion

5.1 Improving Soft Tissue Representations

5.1.1 Modifying MCL Attachments

In the model, the MCL consists of 3 bundles with two fibers each. Both the superficial MCL (2 bundles) and deep MCL are included in the model. Generally, the MCL provides valgus stability and greatly influences medial condylar motion [72]. The MCL attaches slightly proximal and posterior of the medial epicondyle on the femur in a triangular shaped pattern. On the tibia, the MCL attachments span a greater area of the bone and attach on the proximal tibia. The deep MCL inserts directly onto the tibial plateau, while the superficial MCL has a broad insertion of about 60 mm distal to the tibial joint line (Figure 5-1). This increased attachment area is why two bundles are used to represent the superficial MCL, rather than one.

To allow for a more accurate representation of soft tissue forces, the ligament attachments sites of the MCL were optimized. The model is very sensitive to the location of the MCL attachment sites on both the femur and tibia. To ensure accurate placement of landmarks, an orthopedic surgeon was consulted in locating the proper attachment sites for the MCL in these outlier subjects. Often it can be difficult to ascertain the exact location of MCL attachments based upon MRI images due to poor imaging quality or scarring around the knee (Figure 5-2). In this model, soft tissue attachments are defined based upon bony landmarks. MCL origins were modified to demonstrate their effects on force profiles. Below are shown the new MCL attachment sites in these subjects, where the two lighter blue spheres represent the two superficial MCL attachments and the darker blue sphere represents the deep MCL (Figure 5-3 - Figure 5-7).

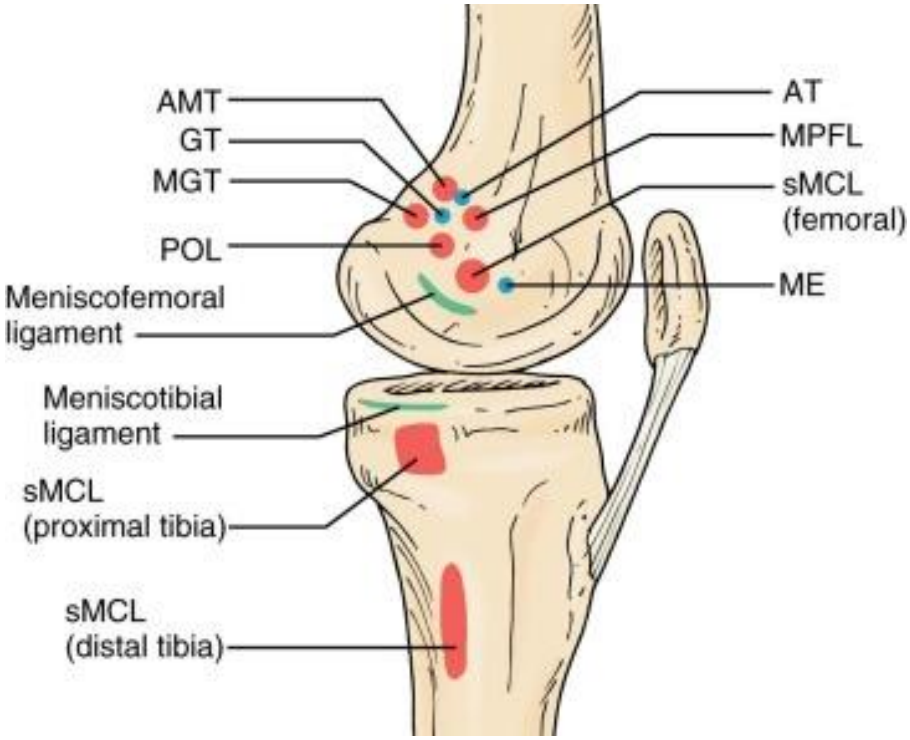


Figure 5-1: Medial knee soft tissue attachment sites.



Figure 5-2: MRI image showing MCL attachments on femur and tibia [73].

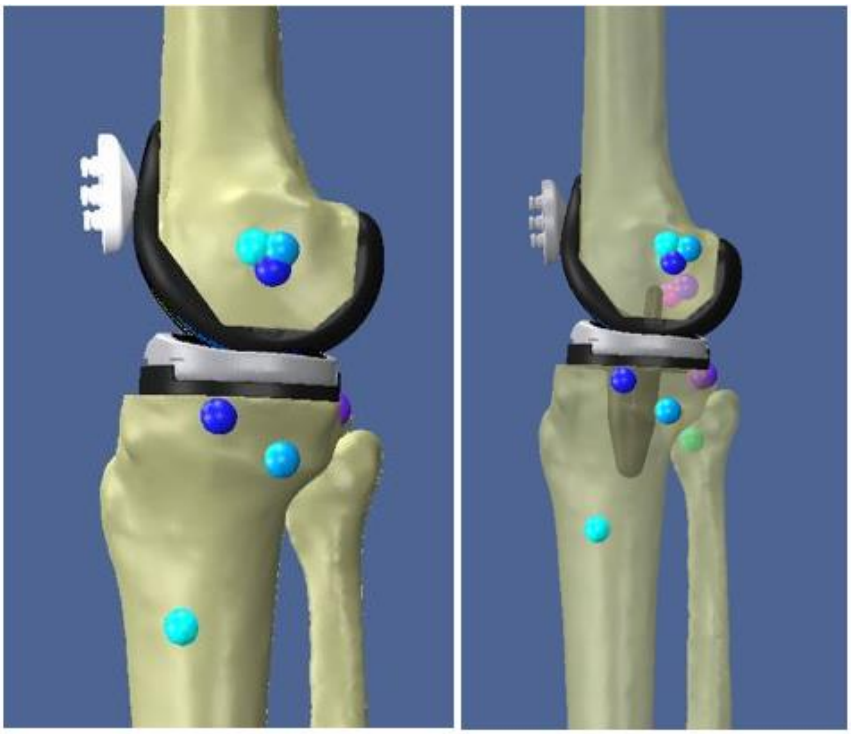


Figure 5-3: New MCL origins (left) and old MCL origins (right) for Subject 4.

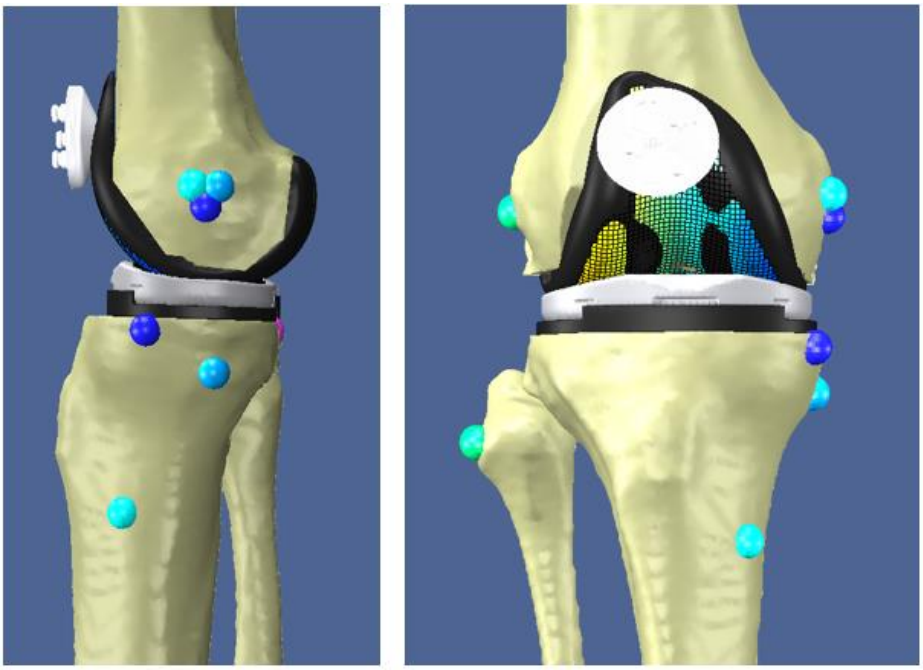


Figure 5-4: Subject 5 updated MCL attachments.

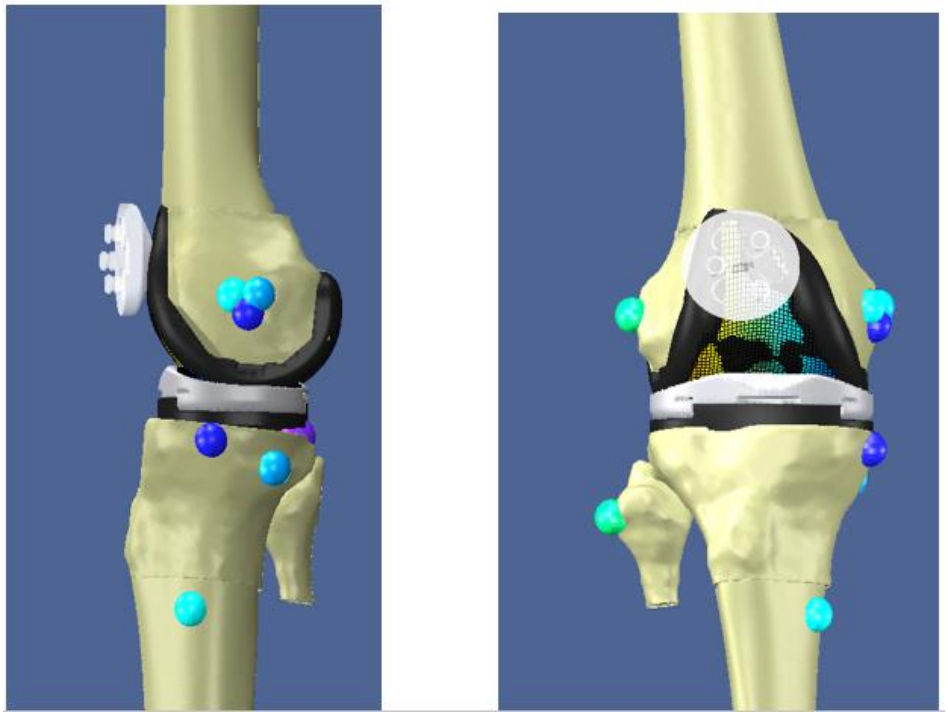


Figure 5-5: Subject 6 updated MCL attachments.

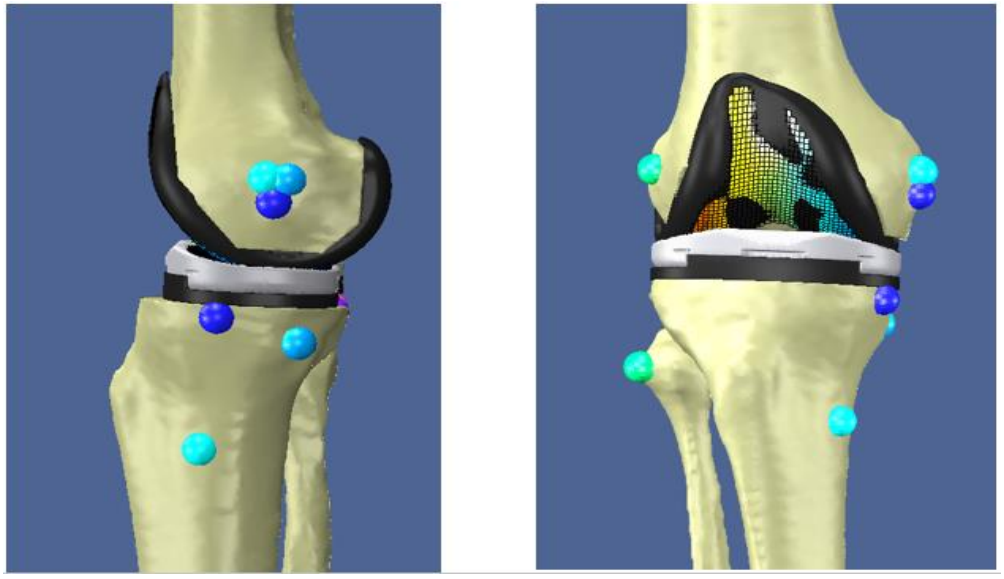


Figure 5-6: Subject 7 updated MCL attachments.

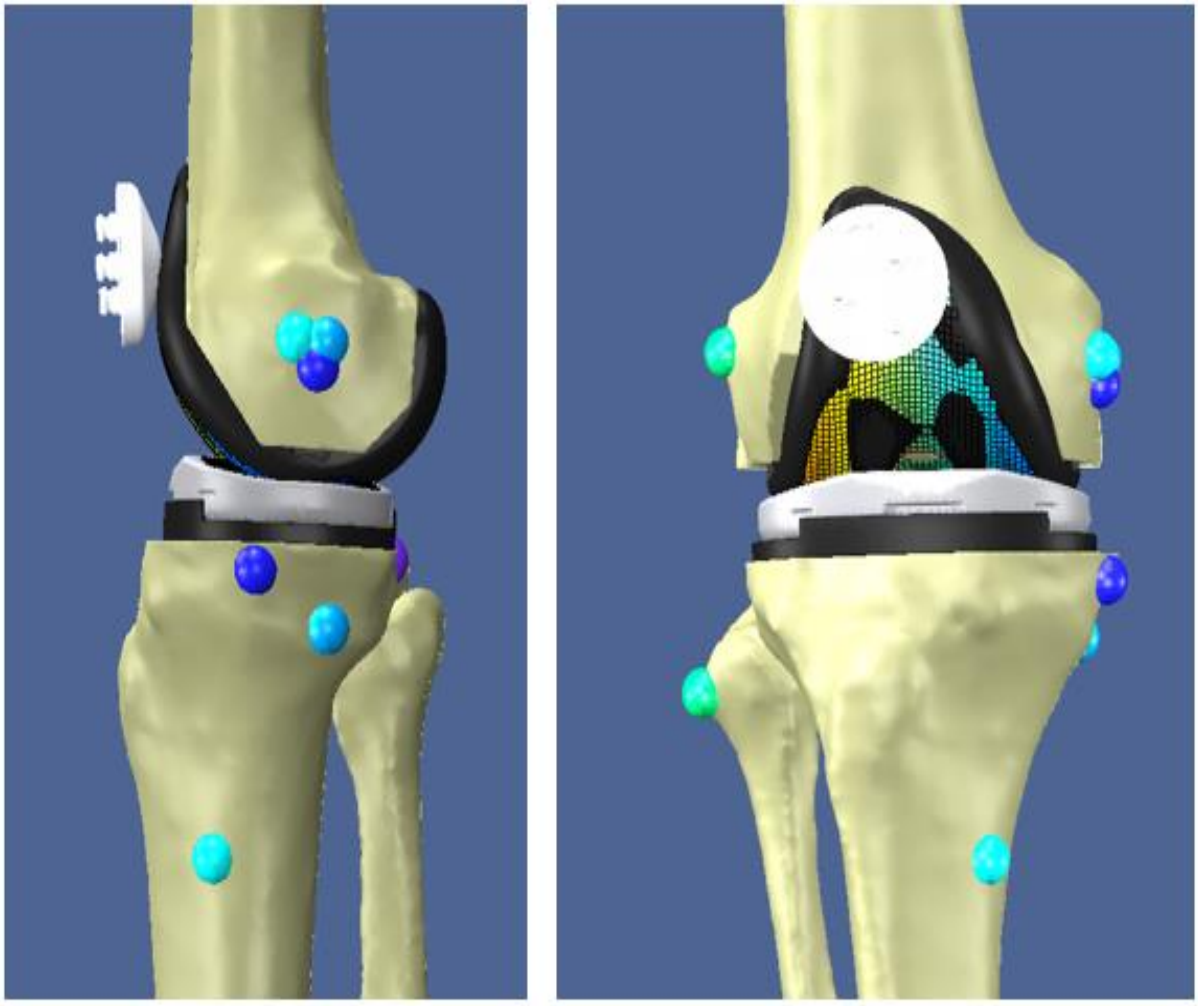


Figure 5-7: Subject 8 updated MCL attachments.

With the new MCL attachments in place, new MCL force profiles for the modified subjects were available (Figure 5-9 - Figure 5-11). Previous MCL positioning had the MCL going slack during later flexion in the deep knee bend activity, which is not seen in vivo or consistent with literature (Figure 5-8). Proper MCL profiles increase with flexion and may level off in deeper flexion (80˚ - 120˚) [74]. In addition to the modified MCL attachment sites for the selected subjects, some sensitivity analyses were conducted in order to further understand how the positioning of the attachment sites affect the resulting MCL force profiles. The first sensitivity analysis conducted was focused upon the location of the attachment sites. The movement of each of the MCL attachments were modified 1 mm in four directions: superior, inferior, anterior, and posterior. Moving the attachments superior leads to elevated MCL forces in early flexion, while moving attachments inferior leads to decreased MCL forces in early flexion. Moving the attachments anterior leads to elevated MCL forces in late flexion, while moving the attachments posterior leads to decreased MCL forces in late flexion (Figure 5-12). The second sensitivity analysis done was on widening or narrowing of the triangular shaped of the attachments on the femur by 1 mm. Imagining the attachments as the points of an equilateral triangle, the widening of the attachments increases the sides of this triangle by 1mm, while the narrowing of the attachments decreases the sides' lengths. Narrowing this triangle leads to lower MCL forces in early flexion and higher MCL forces in late flexion, while widening this triangle has the opposite effect (Figure 5-13). Although medial condylar motion of the knee can often be less in magnitude than that of the lateral side, the MCL acts as the primary constraint against anterior tibial tilt [75]. One distinct advantage of the modeling techniques in this model is the ability to precisely control the attachment point of each bundle of the ligament. This allows for a better ability to match the anatomical shape of the MCL.

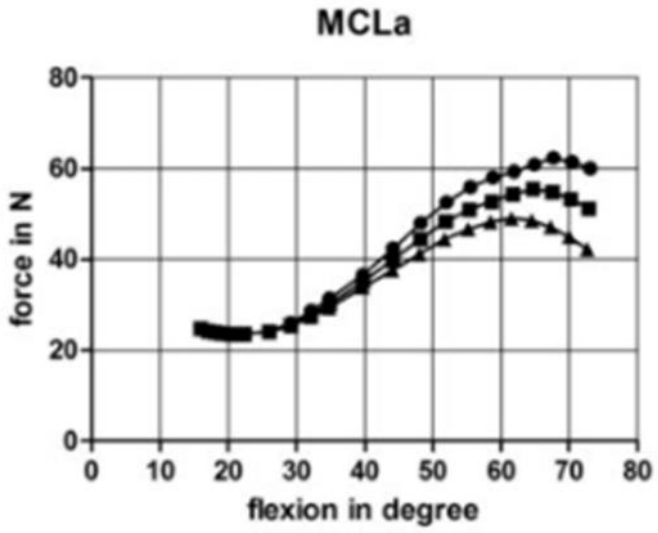


Figure 5-8: MCL force in a CR TKA during a DKB activity[74].Each line representing a EMG measurement.

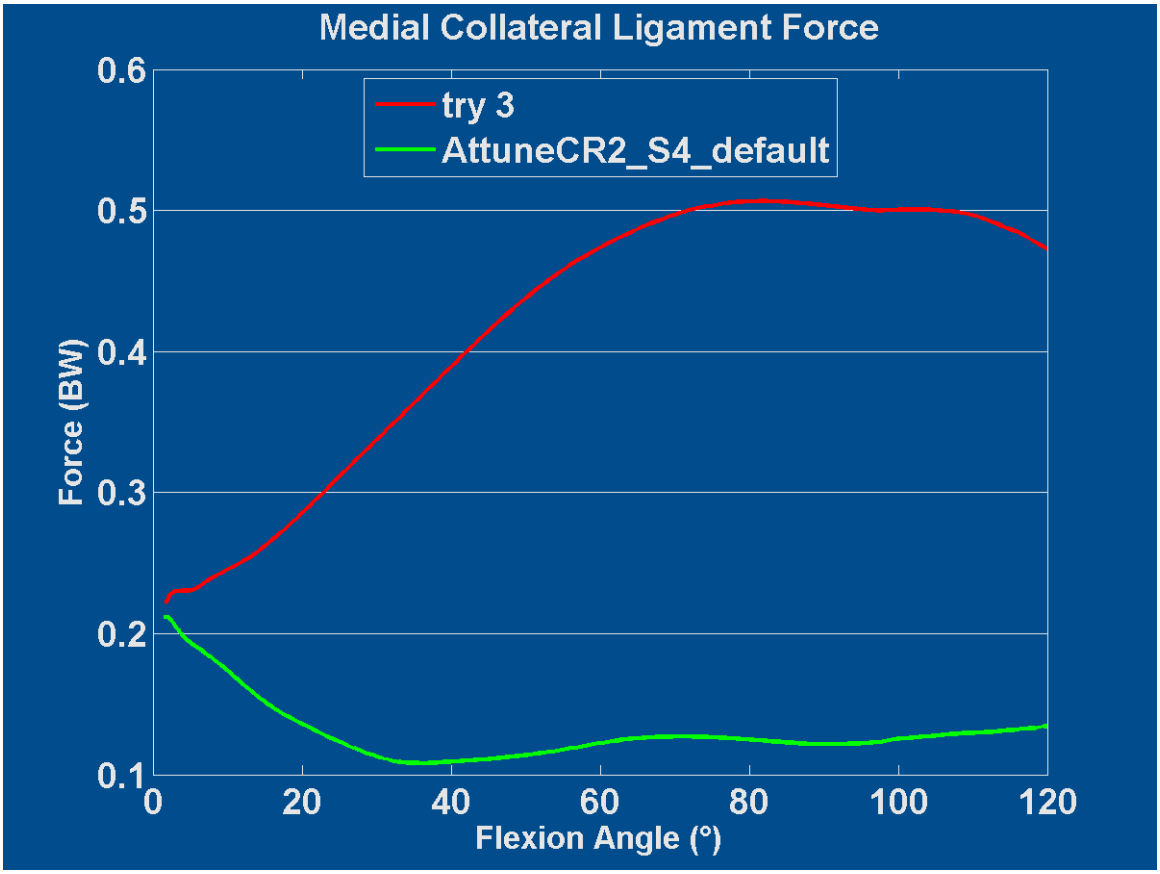


Figure 5-9: MCL force profiles for Subject 4 during a DKB activity with old MCL attachments (green) and new MCL attachments (red).

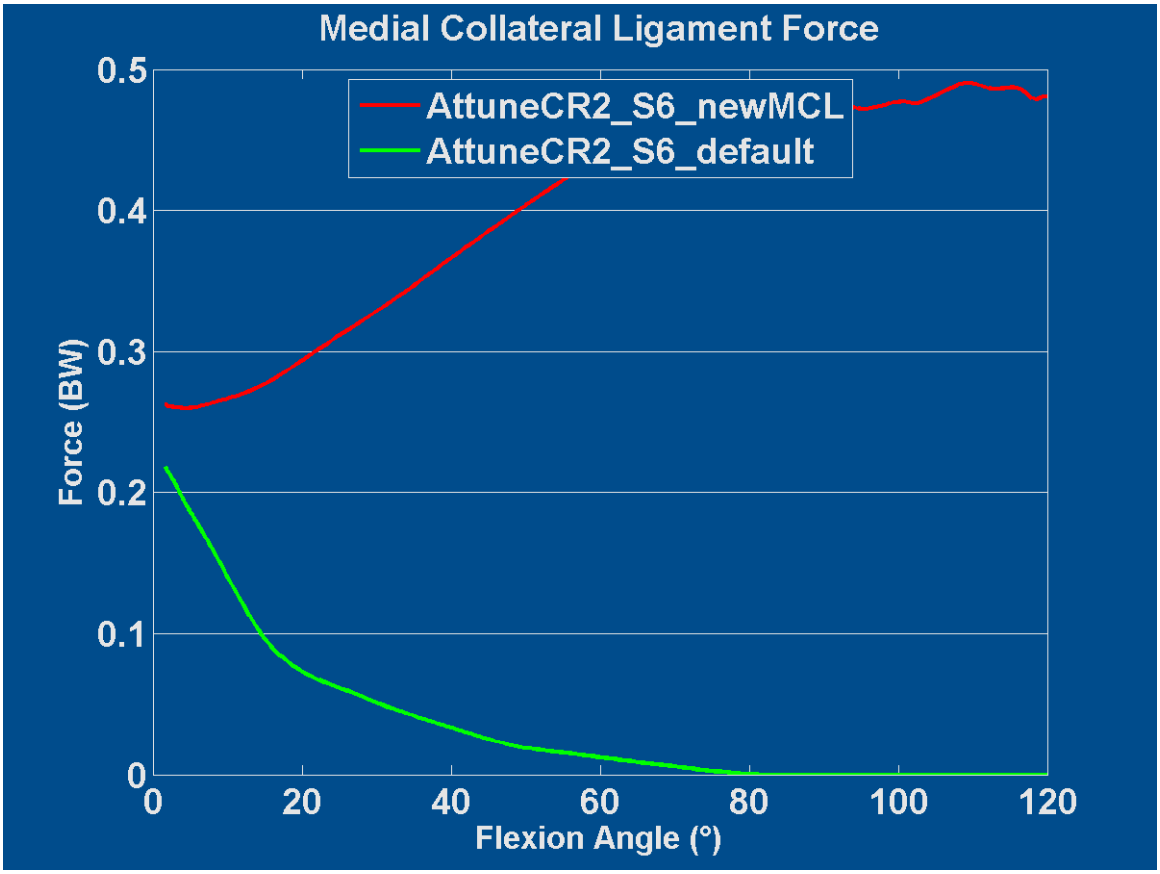


Figure 5-10: MCL force profiles for Subject 6 during a DKB activity with old MCL attachments (green) and new MCL attachments (red).

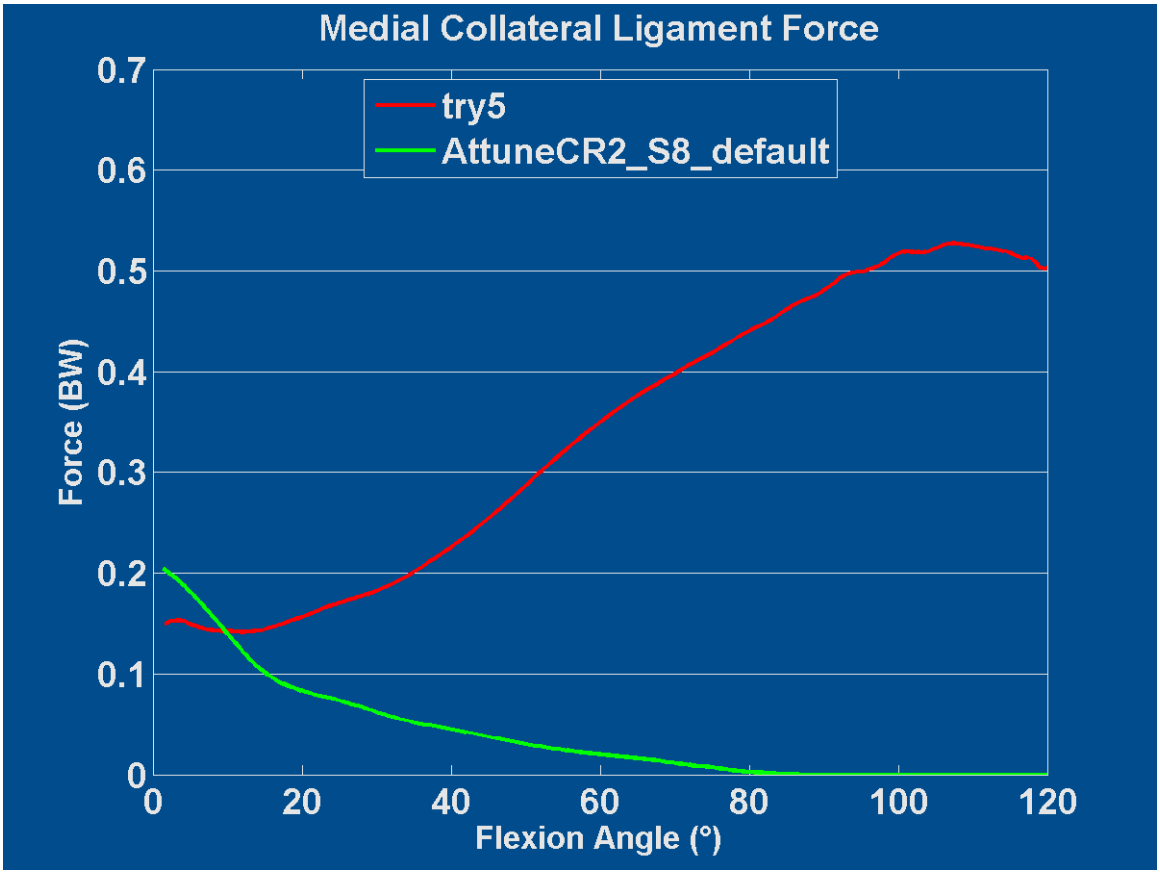


Figure 5-11: MCL force profiles for Subject 8 during a DKB activity with old MCL attachments (green) and new MCL attachments (red).

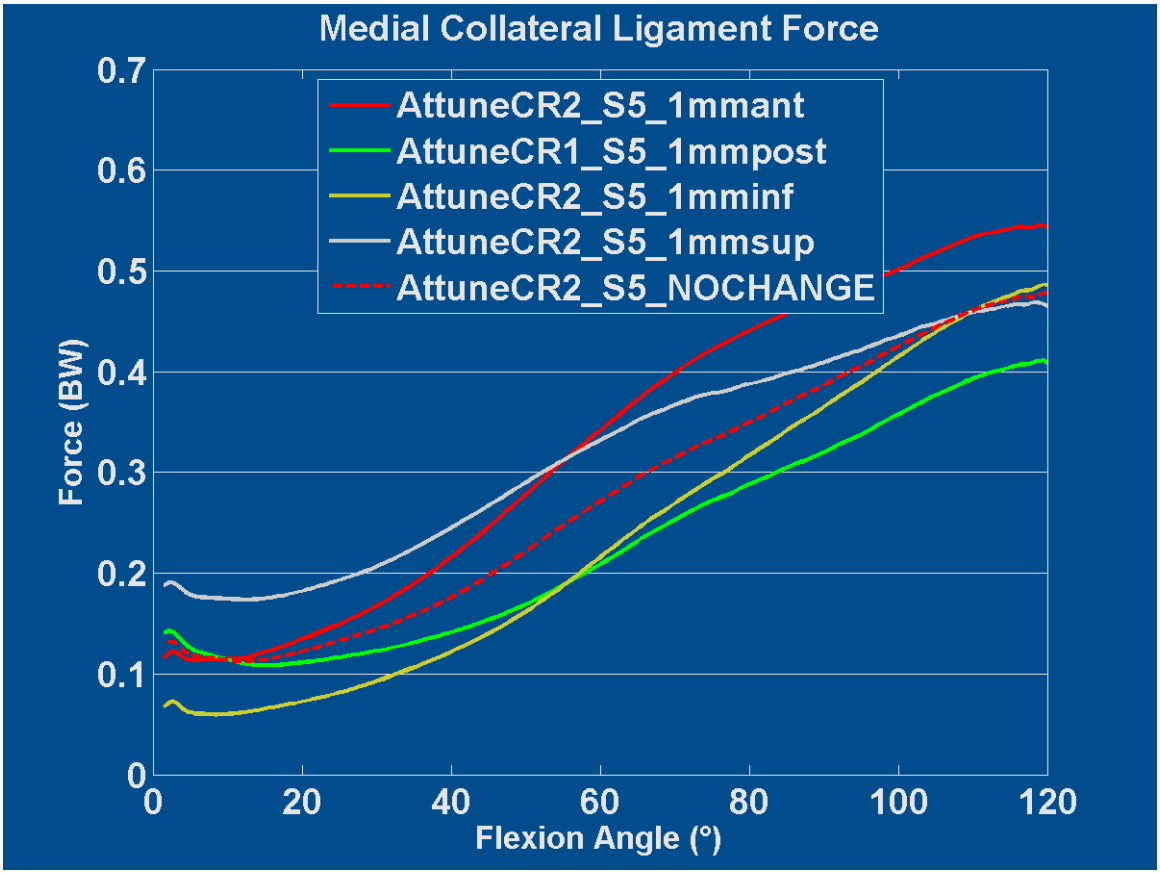


Figure 5-12: Sensitivity analysis on MCL attachment locations during a DKB activity.

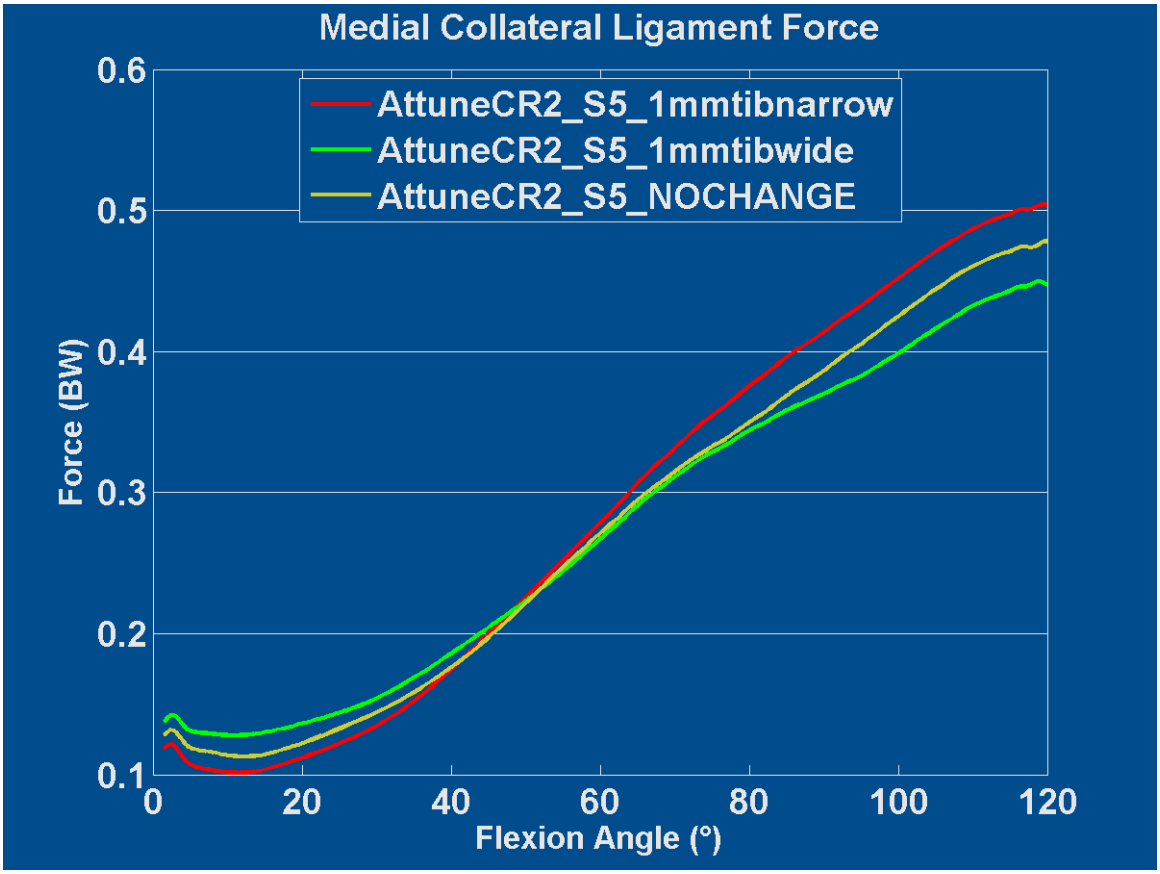


Figure 5-13: Sensitivity analysis on MCL attachment configuration during a DKB activity.

In other musculoskeletal models of the knee, the lack of this capability leads to a representation of the MCL which is the same width as the LCL and thus equally constraining [76, 77]. This may lead to a larger range of varus-valgus motion in some cases where the proper width of the MCL is not being accounted for. As previously demonstrated in the sensitivity analysis plots, the width of the MCL attachment points is an important aspect of its function and will directly affect the resulting ligament force's magnitude and direction.

An important contribution this model makes is providing force profile data that continues into deep flexion (>100˚). This is often an understudied area in other mathematical models of the knee as it can prove challenging to keep the system stable as forces increase. However, providing information throughout the full range of motion is a valuable distinction for the model discussed in this dissertation. TKA subjects typically have reduced range of motion in comparison to healthy, non-operated knees, but it is not uncommon for TKA subjects to reach deep flexion in excess of 100 ˚ [78]. Overall, the MCL changes made have led to more anatomically correct ligament attachment sites, resulting in ligament force profiles which remain consistent with trends found in other literature. The sensitivity analyses done on ligament attachment site positioning allows for a better understanding of the importance of attachment site width and location. This may ultimately guide surgical decisions such as potential MCL releases and provide more information on MCL forces during active squatting (deep knee bend) activities.

5.1.2 Incorporating the Posterior Capsule

The posterior capsule consists of a complex mesh of fibrous tissue that encapsulates the posterior aspect of the knee. Its main function is to help stabilize the knee, especially near full extension. The posterior capsule helps to prevent hyper extension of the knee and to limit malrotation of the knee.

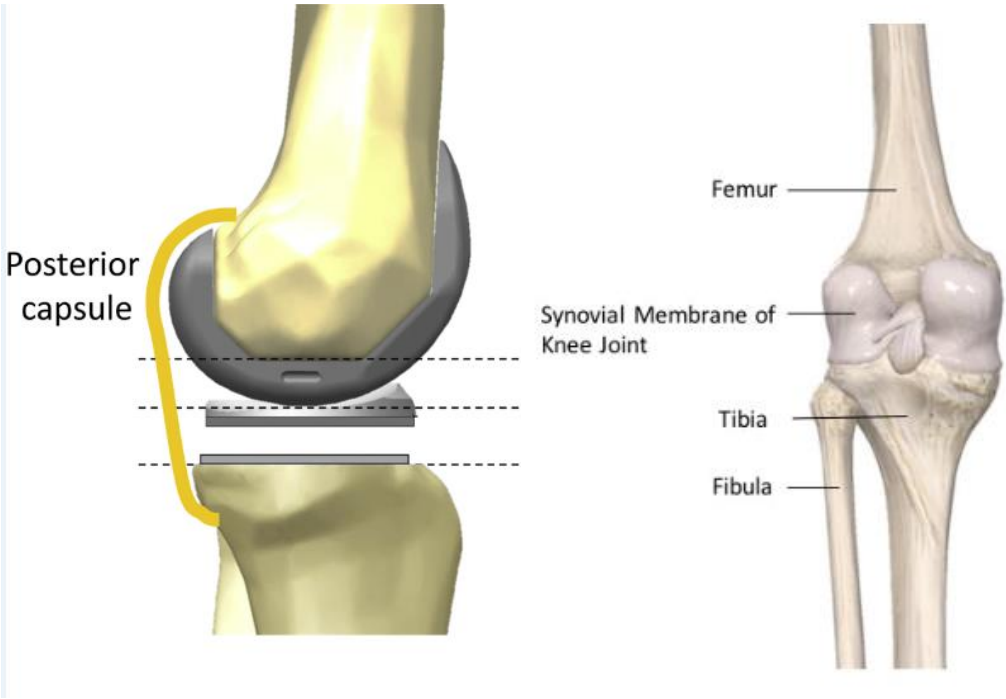


Figure 5-14: Visualizations of posterior capsule of the knee.

When modeling the posterior capsule, it was split into two main parts: the medial posterior capsule and the lateral posterior capsule. Each of these structures was further broken down into two ligaments with one more medial and one more lateral. In total, the posterior capsule was broken down into four ligamentous structures (referred to as ligaments for brevity). The posterior capsule ligament origins on the femur were place superior of the femoral condyles, while the ligament insertions on the tibia were placed inferior of the tibial plateau (Figure 5-14). Wrapping points on the femoral condyles were also included. Posterior capsule forces began between 0.225 xBW and 0.275 xBW for all subjects and steadily decreased until slack at approximately 35˚ flexion for all subjects (Figure 5-15). Since the posterior capsules forces are low (<0.3 x BW) and only active in the first 35º, the addition of the posterior capsule did not significantly affect the other results in the model. Despite not significantly changing the simulation results, the posterior capsule does further advance this mathematical model. The posterior capsule of the knee largely acts as a constraint against excessive varus/valgus motion. While none of the current activities in the mathematical model achieve sufficient varus/valgus stress, future work to stress the knee in different ways will illuminate the role that this structure plays in overall knee function. Another mathematical model of the knee which incorporated the posterior capsule showed some decrease in MCL, LCL, and ACL forces and an increase in PCL forces in comparison to other mathematical models [79]. Further investigation is required to fully understand how the posterior capsule may affect the other ligaments surrounding the knee. Although it is hypothesized that the inclusion of the posterior capsule may take some of the load on of the ACL in early flexion, as the posterior capsule aids in preventing hypermotion at full extension.

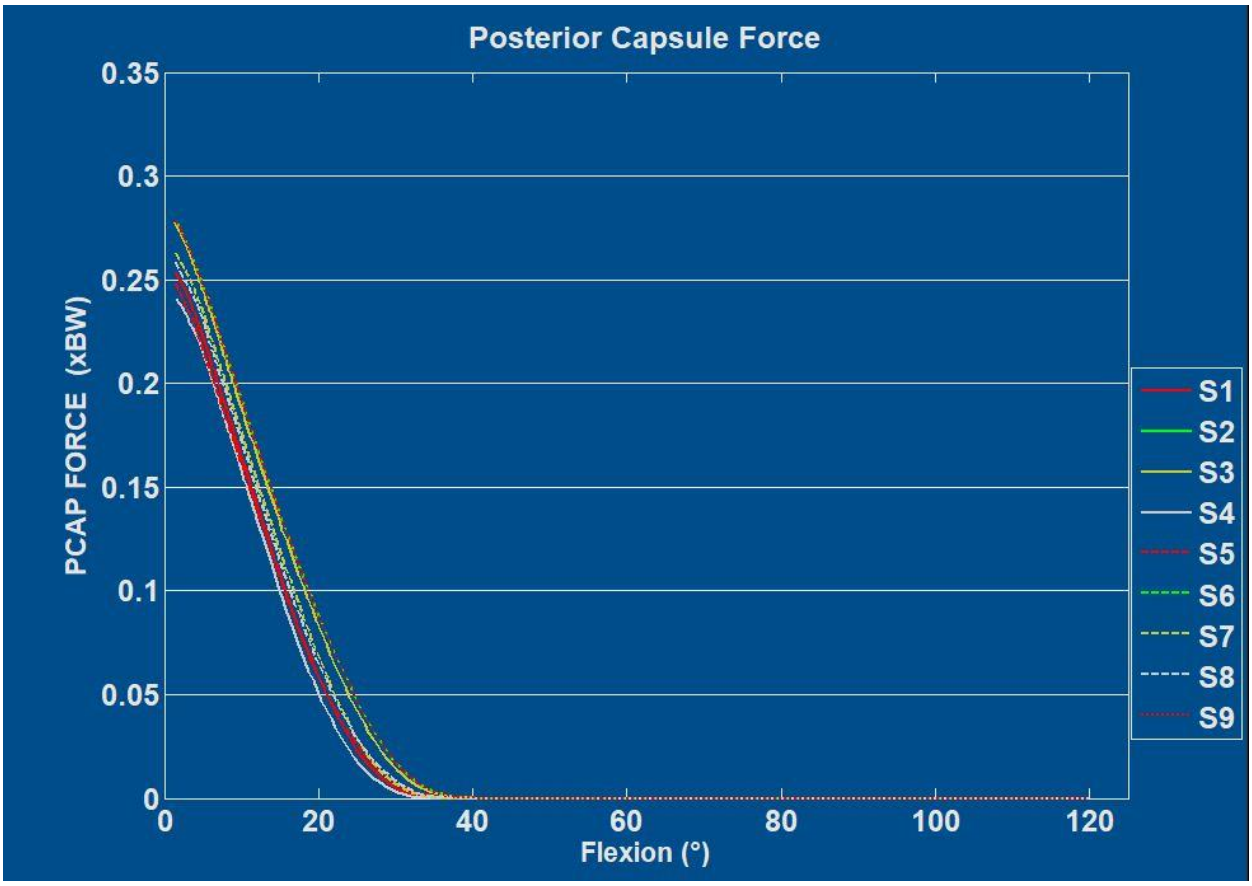


Figure 5-15: Posterior capsule force for 9 subjects implanted with Attune CR TKA during a DKB activity.

5.2 Incorporating New Implant Types

5.2.1 Sigma Stabilized +

The Sigma Stabilized + TKA is often used as a revisionary TKA in order to provide increased stability to the knee. In order to accomplish this, amongst other design changes, the Sigma Stabilized + TKA increases the width of its posterior post/cam mechanism compared with the traditional Sigma PS. This allows for a greater contact area for the posterior post, which results in lower contact stresses. This TKA type is especially useful in cases where the patient needs additional stability because this design reduces the clearance between the sidewall of the femur and the side of the posterior post. The clearance between the femur sidewall and post at 0° and 90° flexion is 0.2 mm (Figure 5-16). This is significantly less than the traditional Sigma PS which has 0.75 mm of clearance. Due to the lower amount of clearance seen in the Sigma Stabilized + TKA design, contact is expected between the sidewall of the femur and the side of the posterior post. This contact should reduce the amount of rotational freedom in the implant, thus limiting the excessive condylar motion as well. Understanding how this sidewall contact force contributes to kinematics and kinetics of the overall TKA is critical to the implant's performance. A DKB activity was analyzed in the FSM to assess the overall performance of the Sigma Stabilized +. When analyzing the results of the Sigma Stabilized +, the sidewall forces are one of the most significant results. Overall, the sidewall forces were quite low throughout the activity. Although not every subject demonstrated a lateral sidewall force, the overall forces were very low when it did occur. The medial side wall does not engage significantly until later flexion but has a larger magnitude than the lateral sidewall force. Other major results include axial rotation, LAP, MAP, total knee force, total quad force, patellofemoral force, patella ligament force, and PS cam force (Figure 5-17 - Figure 5-26)



Figure 5-16: Sidewall clearance in the Sigma Stabilized + implant.

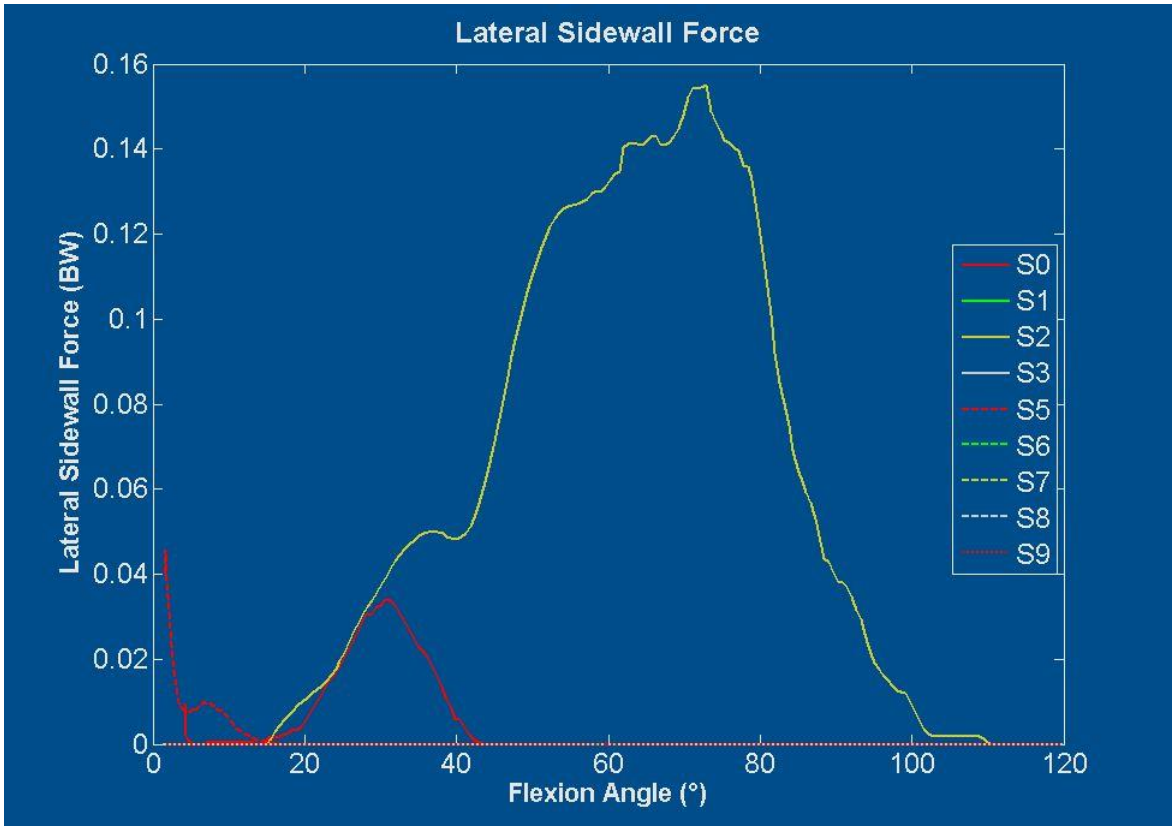


Figure 5-17: Lateral sidewall force for ten subjects implanted with the Sigma Stabilized + during a DKB activity.

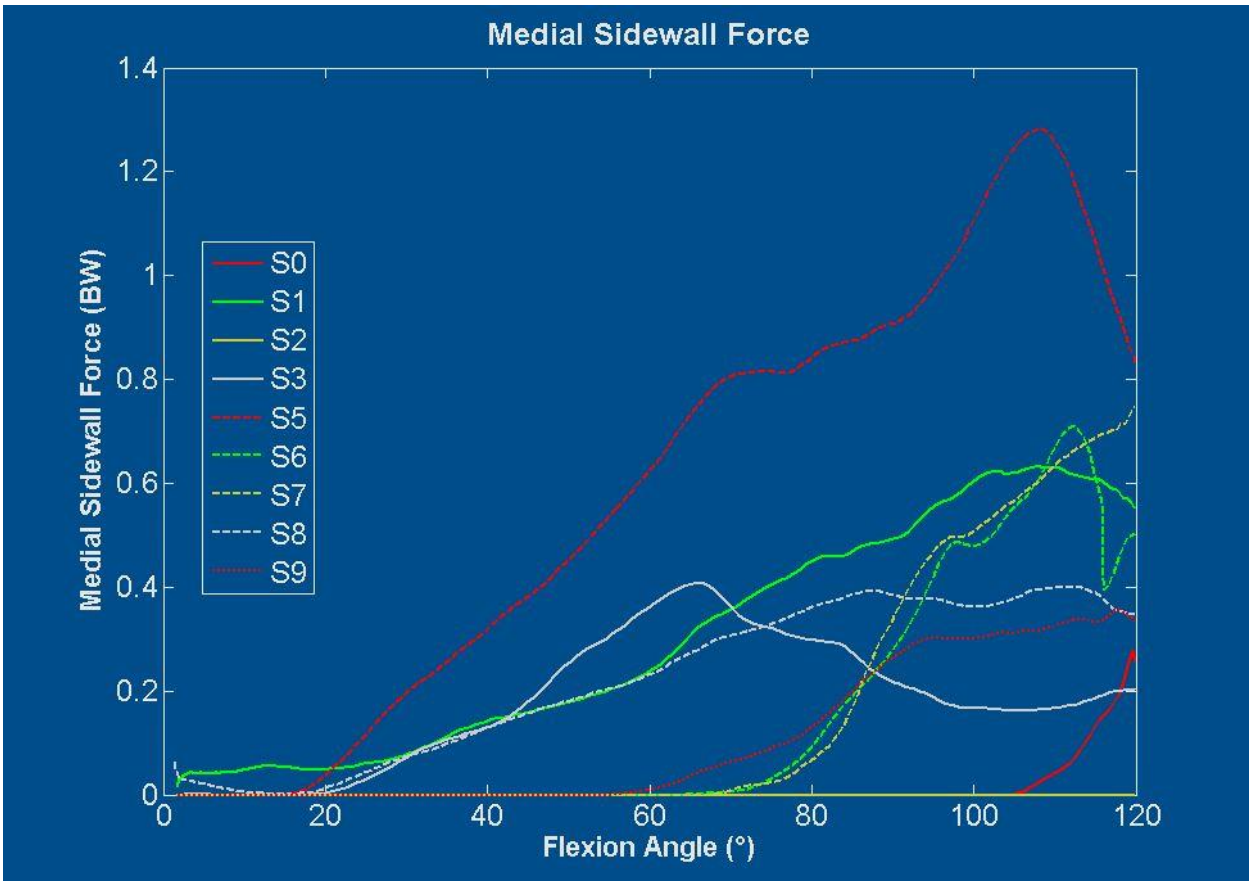


Figure 5-18: Medial sidewall force for ten subjects implanted with the Sigma Stabilized + during a DKB activity.

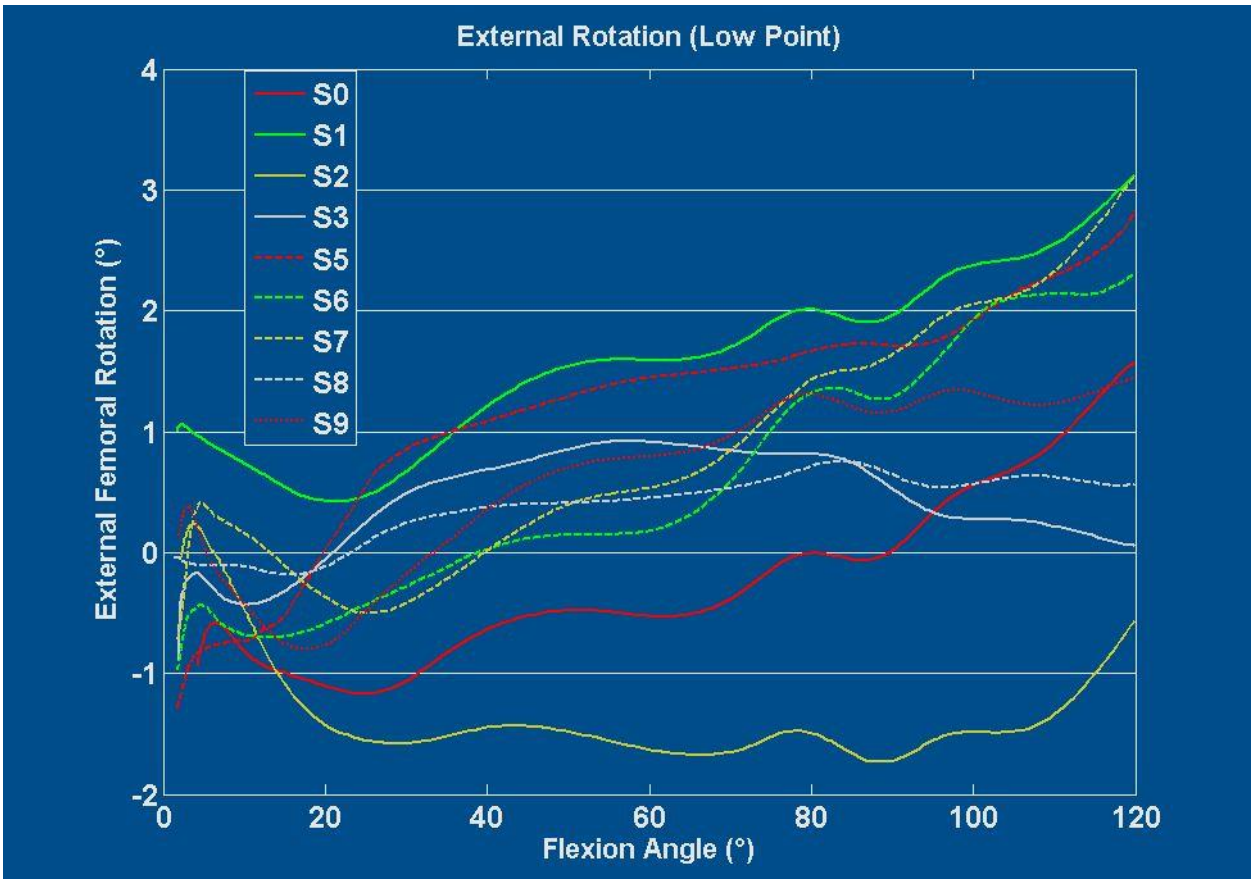


Figure 5-19: Axial rotation (Low Point) for ten subjects implanted with the Sigma Stabilized + during a DKB activity.

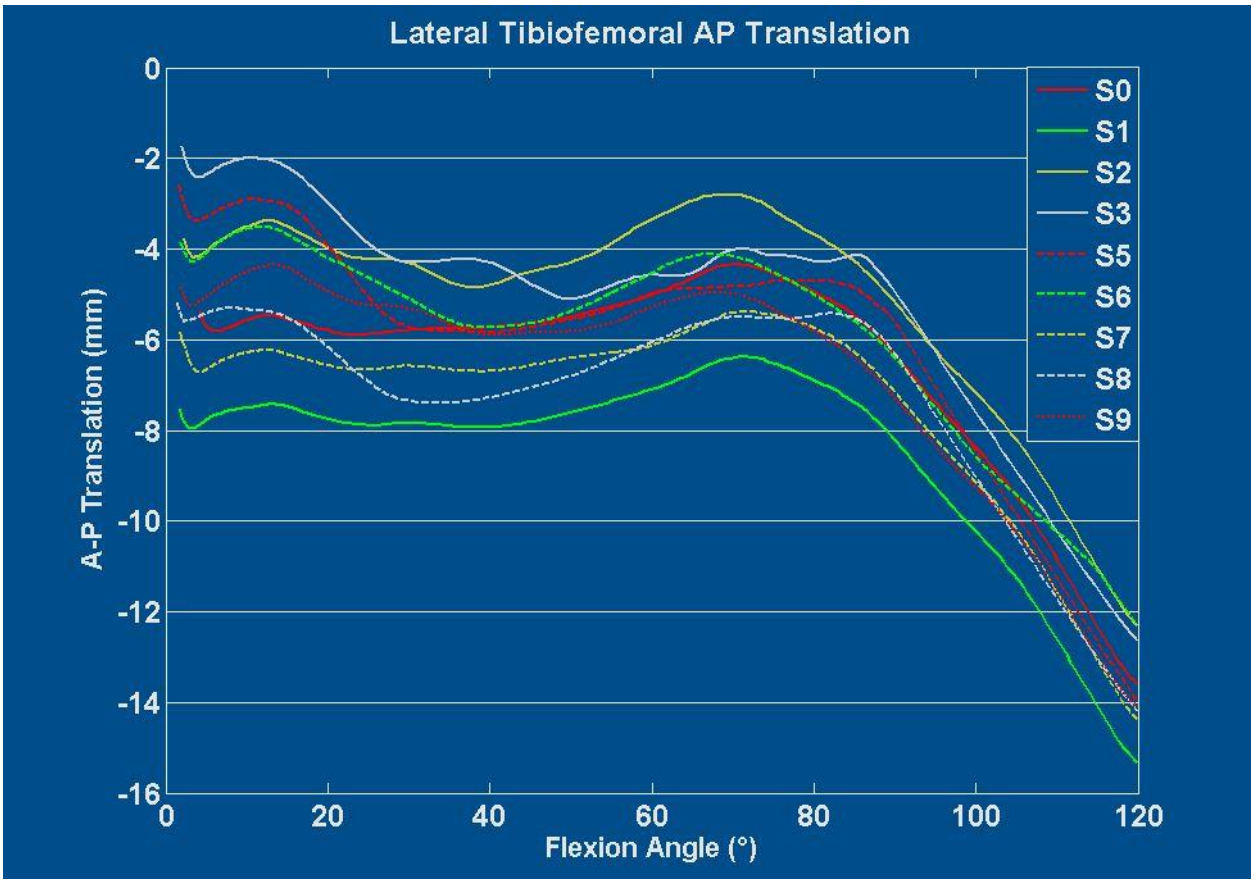


Figure 5-20: LAP for ten subjects implanted with the Sigma Stabilized + during a DKB activity.

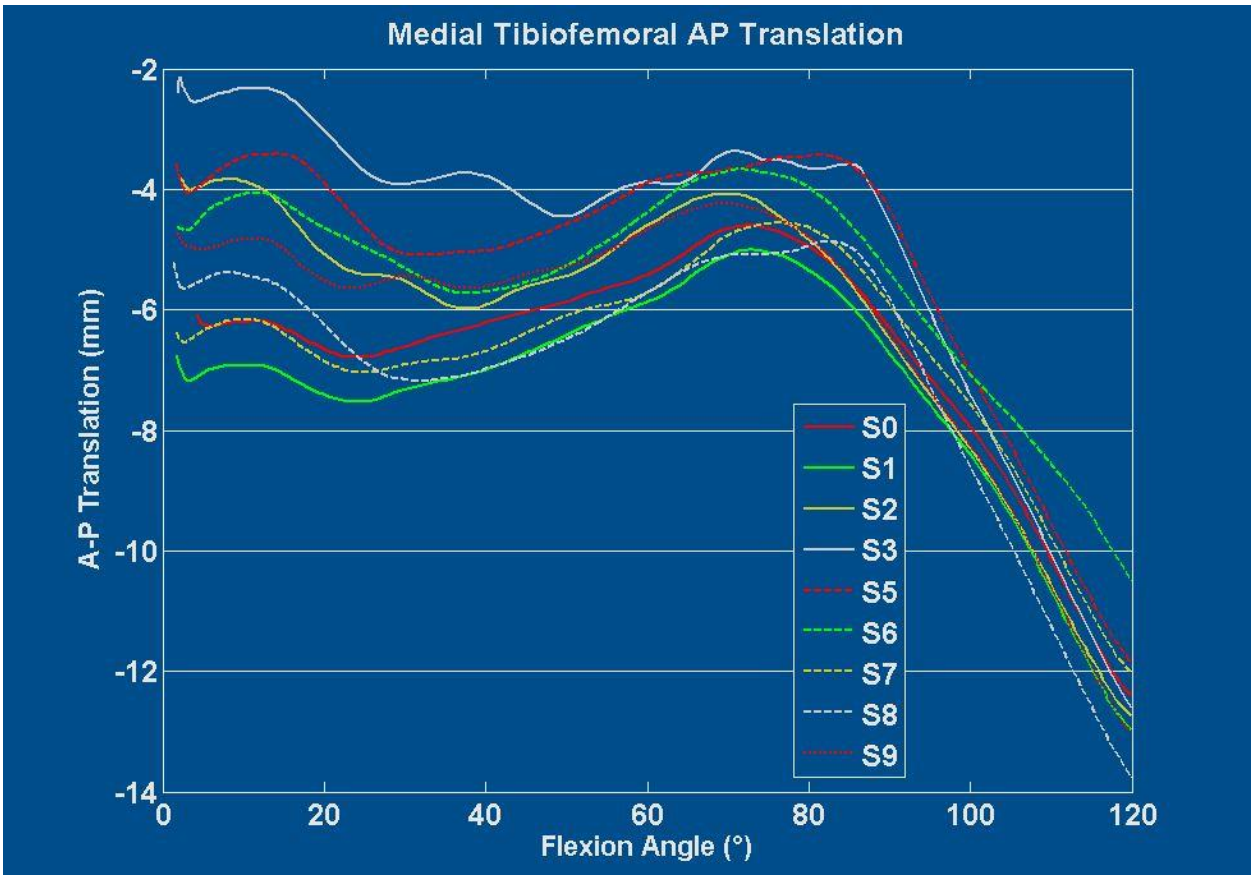


Figure 5-21: MAP for ten subjects implanted with the Sigma Stabilized + during a DKB activity.

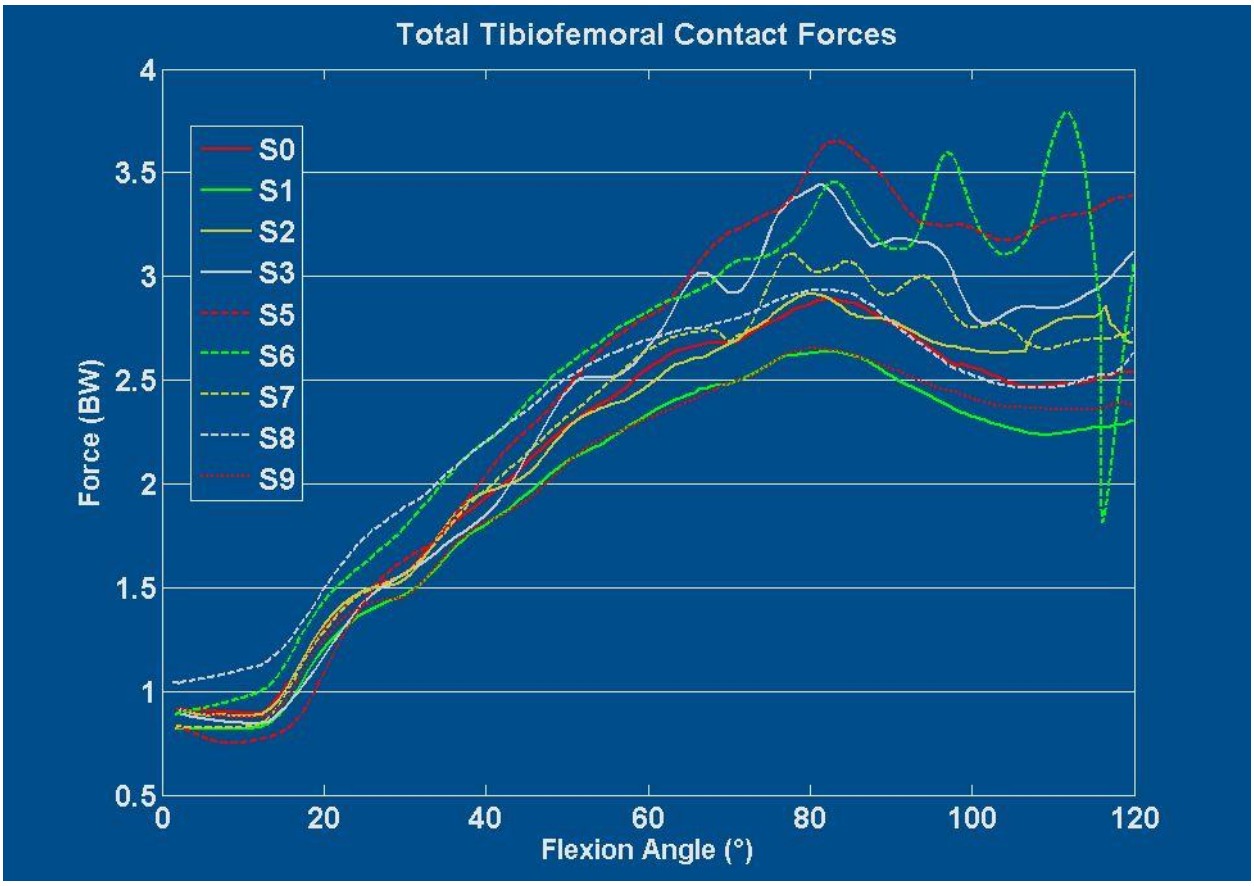


Figure 5-22: Total knee force for ten subjects implanted with the Sigma Stabilized + during a DKB activity.

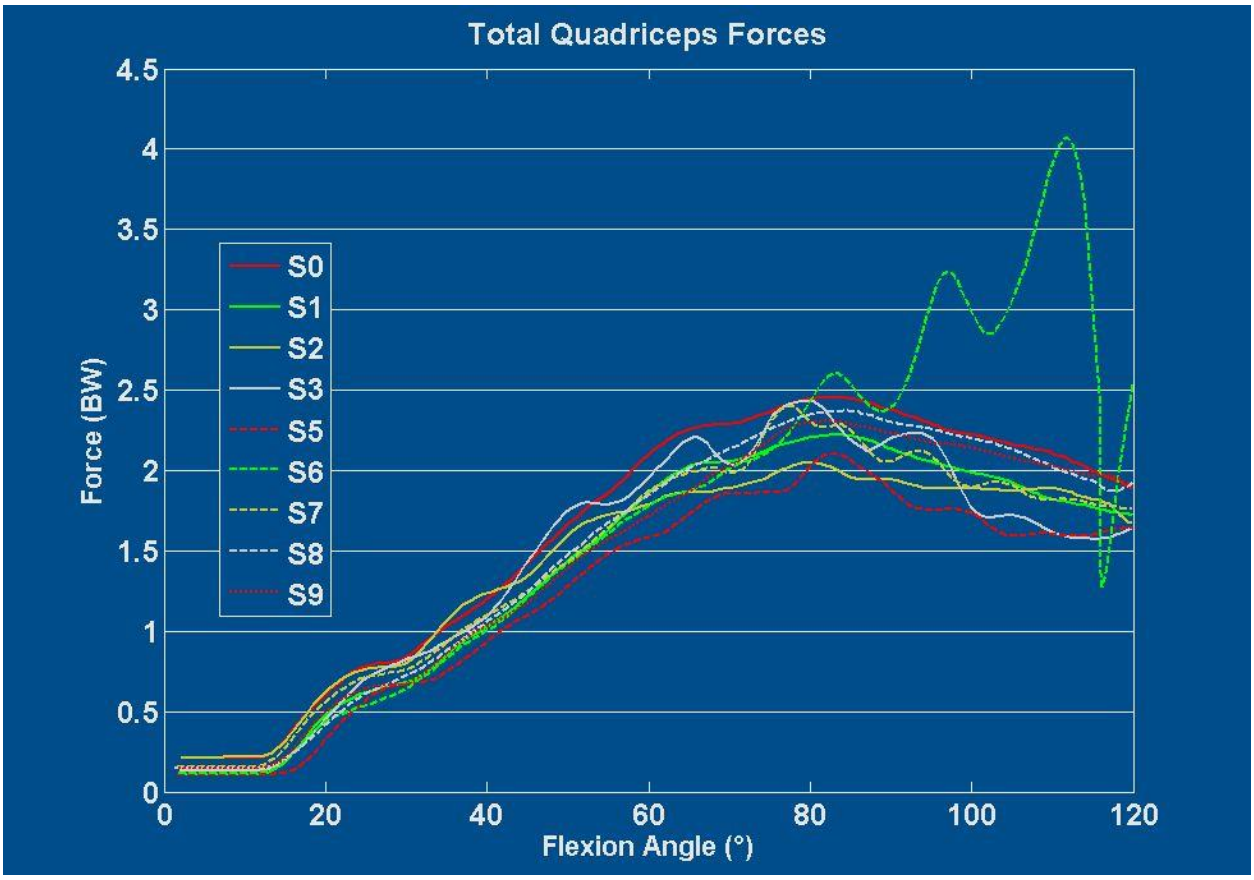


Figure 5-23: Total quad force for ten subjects implanted with the Sigma Stabilized + during a DKB activity.

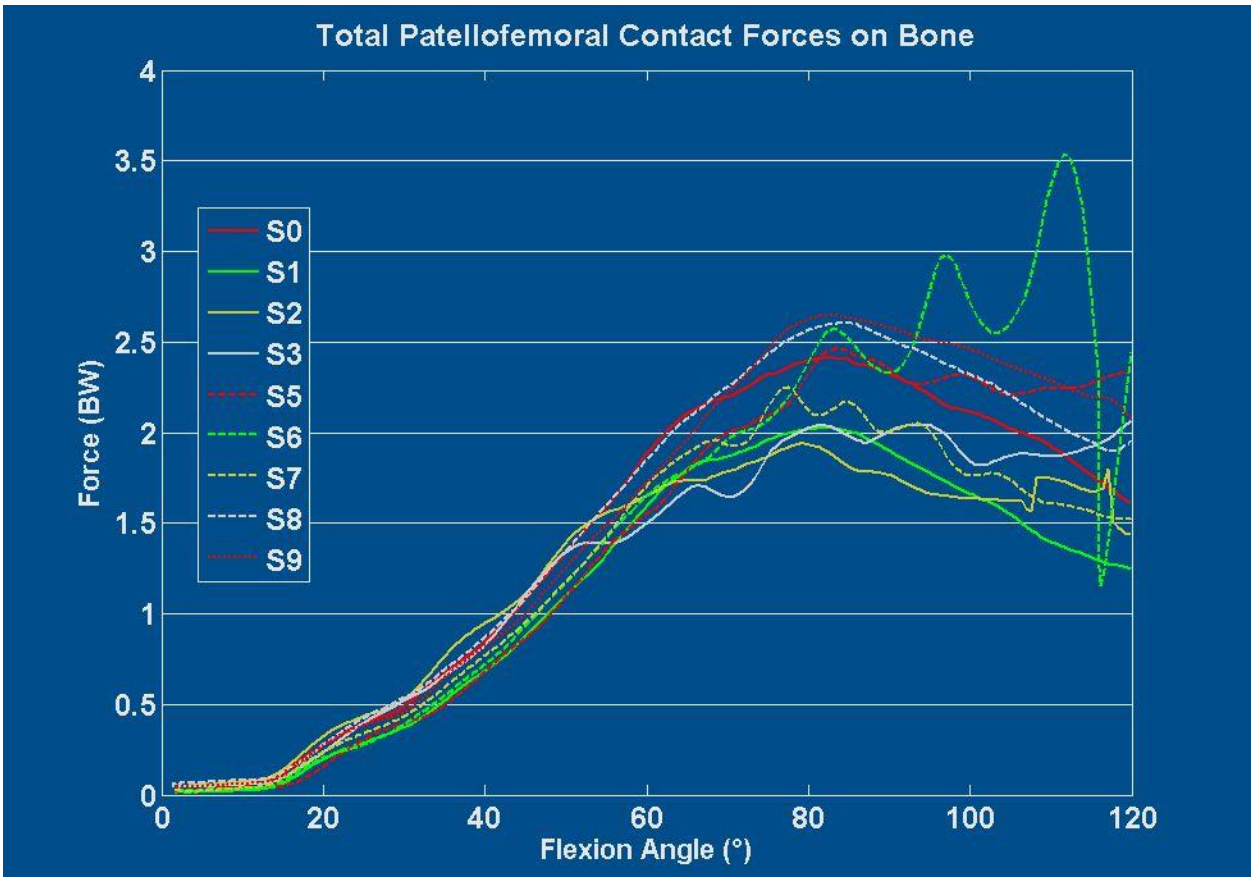


Figure 5-24: Total patellofemoral force for ten subjects implanted with the Sigma Stabilized + during a DKB activity.

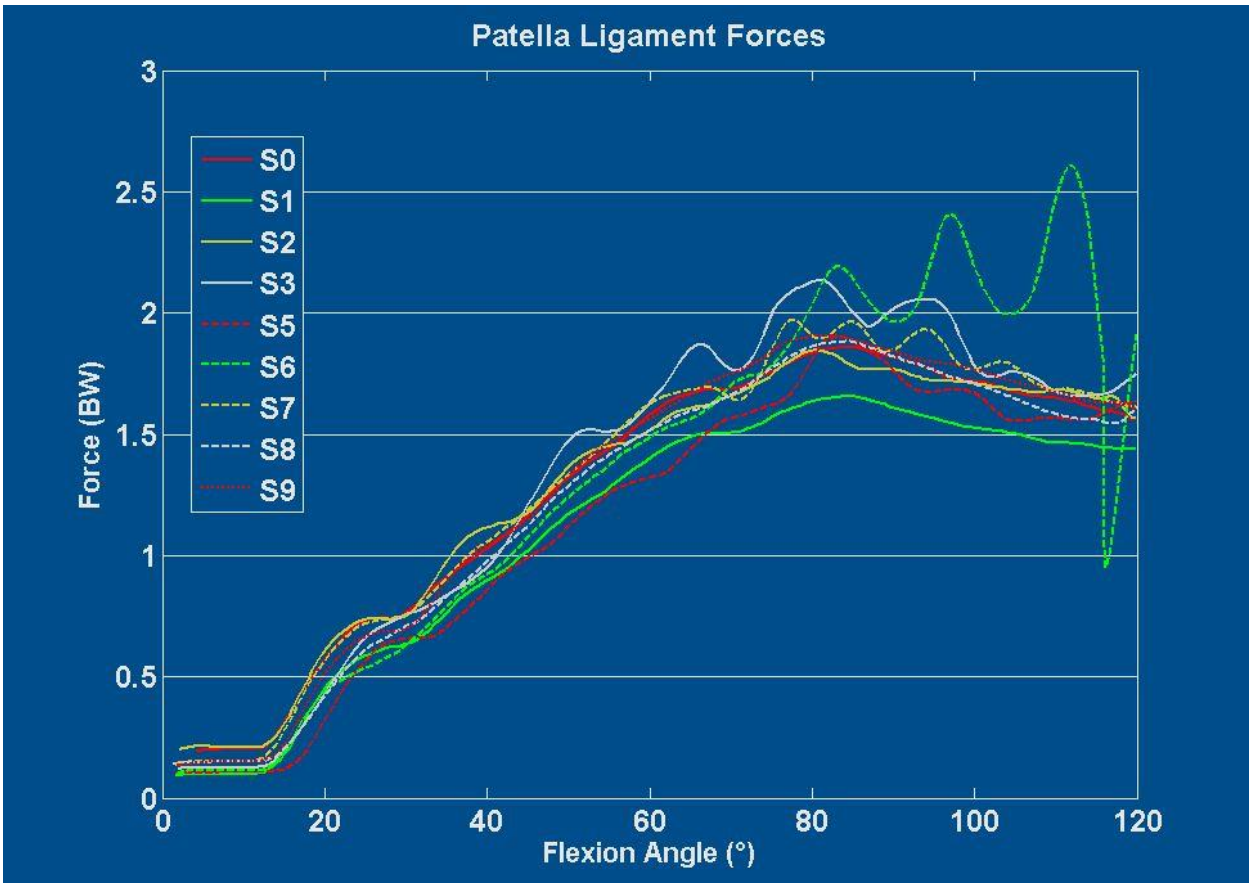


Figure 5-25: Patella ligament force for ten subjects implanted with the Sigma Stabilized + during a DKB activity.

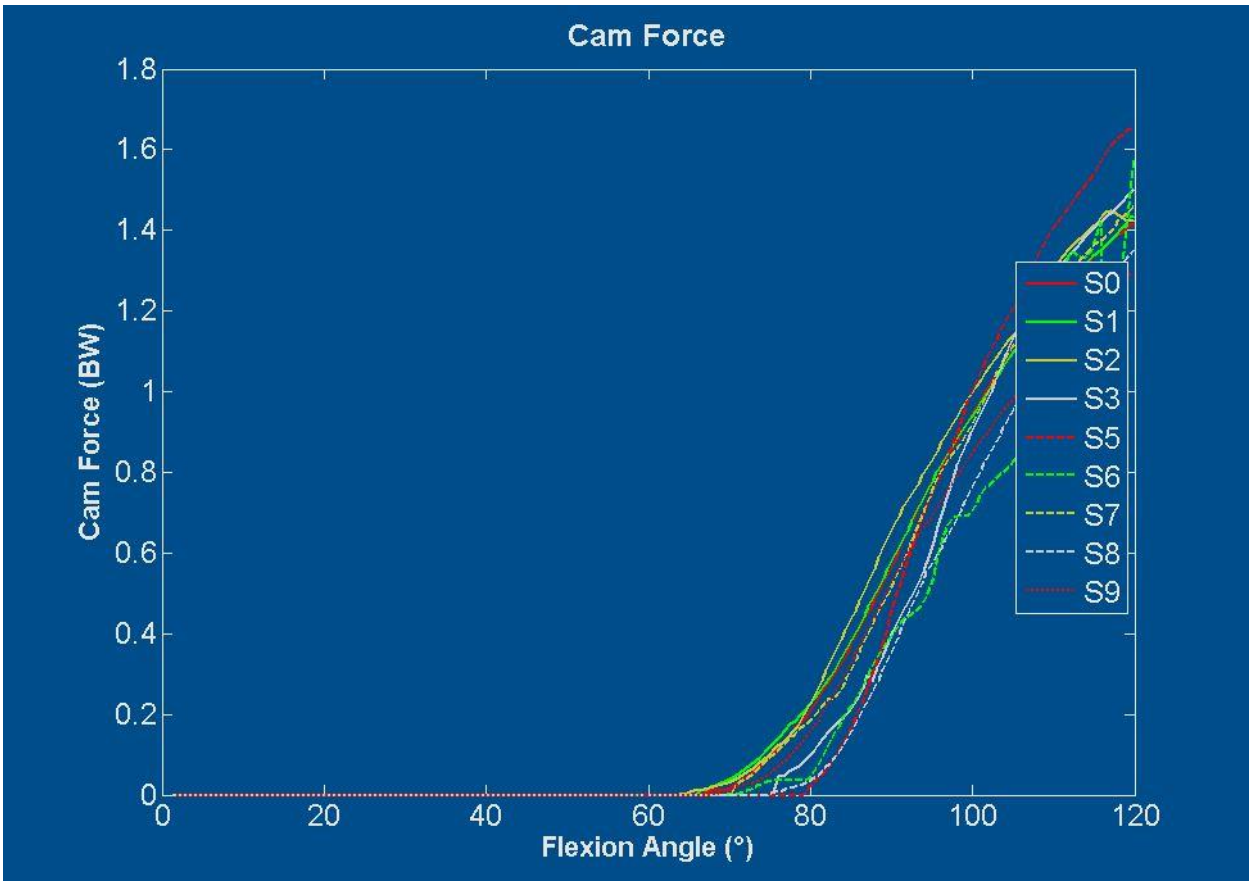


Figure 5-26: PS cam force (not including side wall forces) for ten subjects implanted with the Sigma Stabilized + during a DKB activity.

There has been no significant published analysis done on the Sigma Stabilized + implant type as it is largely used in revision cases to better stabilize the knee. This highlights one of the significant innovations of the mathematical model in this dissertation. There has been no other mathematical model to present side wall forces and the effects that it has on overall knee kinematics. As shown in the above plots, the axial rotation for subjects implanted with this implant type are all quite low ($< 3^{\circ}$). In previous studies, posterior stabilized knees have shown significantly more axial rotation. For example, Iwamoto et al. demostrated 7.4° of axial rotation on average [80], while Dessinger et al. demonstrated 7.1° of axial rotation [81]. These findings and many others suggest that the Sigma Stabilized + implant exhibits less axial rotation than the traditional PS implant. This is consistnent with the sidewall forces seen in the simulations which are designed to restrict axial rotation and keep the knee stabilized in patients who may be more at risk of soft tissue damage or implant comlications. So despite TKA designs often aiming to replicate the motion of the normal knee, in this design the limited axial rotation is considered a positive and achieves the design goals. This constrained design may prove useful to the greater orthopedic community as instability is one of the most cited reasons for implant revision surgery. This design significantly stabilizes the rotational motion of the knee with the sidewall mechanism while still allowing sufficient condylar rollback, allowing for adequate overall knee flexion. Although the Sigma Stabilized + results have consistent knee and quadricep forces with other implant types, in vivo studies may be able to confirm if patients can achieve proper knee function with this implant.

5.2.2 Unicompartmental Knee Arthroplasty

In the model, two different UKA implants were included: the Sigma UKA and the Preservation UKA. This was done largely to show the robustness of analyzing multiple UKA types in the model and to directly compare to previous literature and research conducted on these implants.

In order to accurately analyze the Sigma UKA, the model includes conditions such as retention of the ACL and non-symmetrical articulating surfaces, where one condyle has metal-polyethylene interaction while the contralateral side maintains anatomical conditions bone, cartilage and meniscus. An evaluation was conducted for the medial Sigma UKA to derive the flexion facet center (FFC) throughout flexion using subjects in the model. The FFC was set as the center of a circle fit to the articulating surface of the medial condyle. These results were then compared to a previously published in vivo fluoroscopic study that determined the FFC for multiple subjects having a medial Sigma UKA[82]. The model derived not only the kinematics for the Sigma UKA that was compared to in vivo fluoroscopic results, but also derived soft-tissue and bearing surface force profiles throughout knee flexion. The average motion for the simulated subjects in the FSMM having a Sigma UKA demonstrated anterior motion of the FFC during early flexion and a slight posterior motion in later flexion, with the FFC moving from -7.49 mm at full extension to -5.65 mm at 120° flexion. These results were then compared to previous fluoroscopy study evaluating the FFC for subjects having a Sigma UKA. The average FFC motion for subjects in the fluoroscopy study, implanted with the Sigma UKA demonstrated a similar pattern with slightly more anterior motion, with the FFC moving from -7.92 mm at full extension to -5.03 mm at 100° flexion [82] (Figure 5-27). Further evaluation of the Preservation UKA subjects in the FSMM was conducted to determine the FFC motion patterns. The average FFC motion pattern for subject implanted with the Preservation UKA showed a very similar FFC motion pattern to the Sigma UKA, with the FFC moving from -8.23 mm at full extension to -6.11 mm at 120° flexion (Figure 5-28).

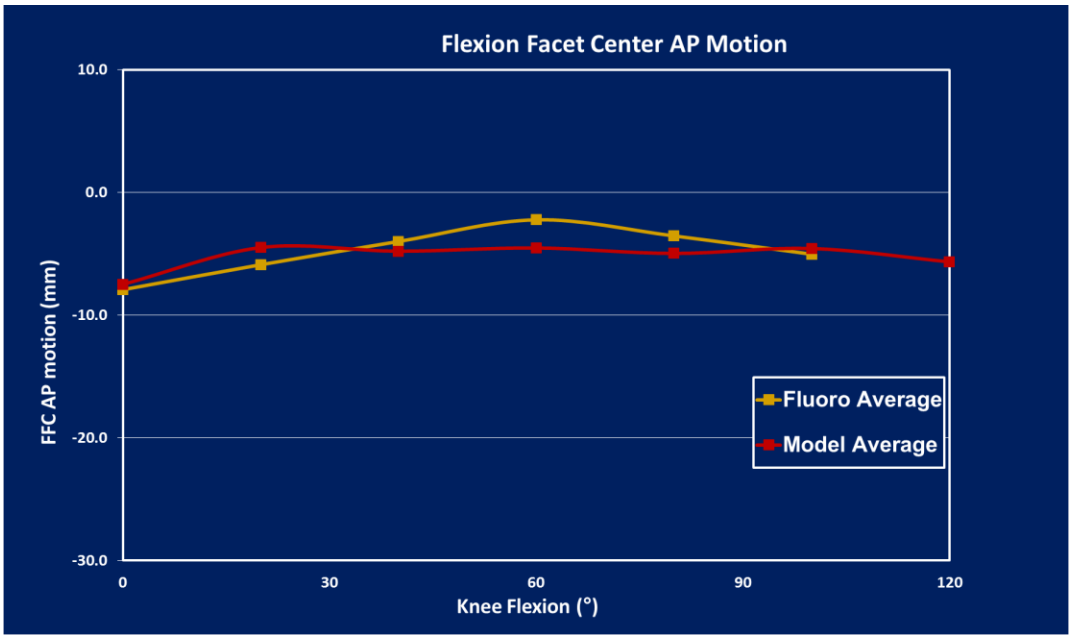


Figure 5-27: Average FFC AP motion for Sigma UKA during a DKB activity [82].

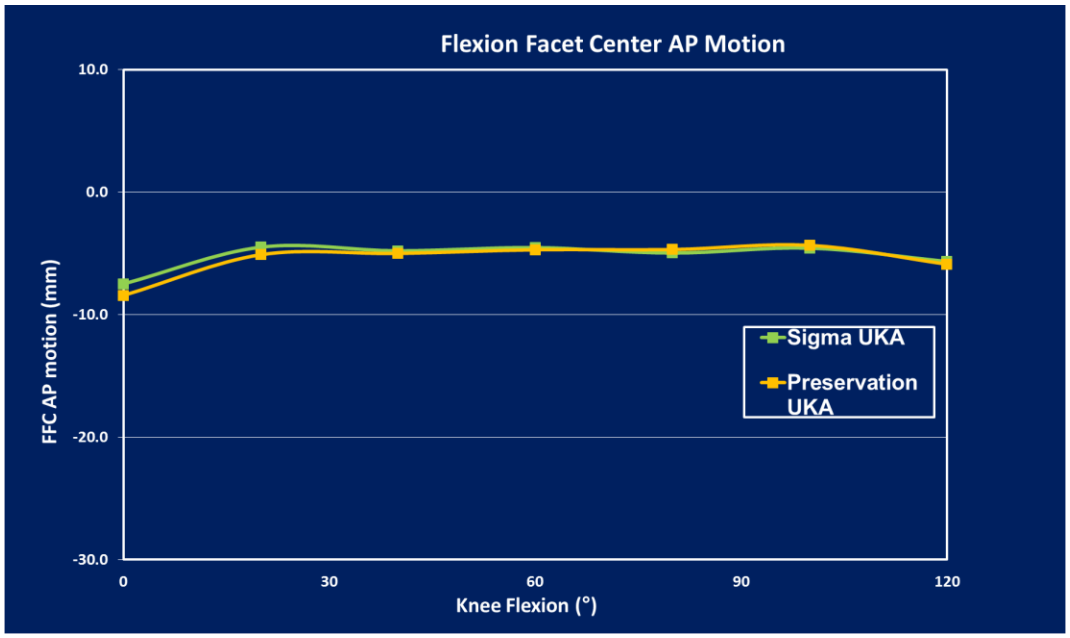


Figure 5-28: Average FFC motion for Sigma UKA and Preservation UKA during a DKB activity.

In a previous study, six subjects were fluoroscoped having a medial Preservation UKA and the in vivo kinematics were derived for each subject. The medial contact point for these subjects was determined via validated 3D to 2D registration techniques. For both groups, the average medial condyle motion for subjects moved in the posterior direction with increasing knee flexion. The modeled Preservation UKA kinematics demonstrated consistent condylar rollback with the medial contact point moving from 3.25 ± 2.14 mm at full extension to -7.51 ± 3.27 mm at 120° flexion. The average motion for the subjects in the fluoroscopic study, implanted with the Preservation UKA, demonstrated a similar pattern, although beginning the activity slightly more posterior, with the medial contact point moving from -0.13 ± 2.65 mm at full extension to -5.58 ± 1.98 mm at 100° flexion (Figure 5-29). Subjects in the fluoroscopy study averaged less range-of-motion, whereas one the advantages of the FSMM is that the evaluated subjects produced simulations to 120 degrees of knee flexion. The differences observed between the model and fluoroscoped patient are expected as there are different bone geometries and soft tissue attachments between the subjects in the model and the subjects in the fluoroscopy study. Furthermore, it is hypothesized that the integrity of the ACL in the fluoroscoped patients may be compromised in some cases as these patients were of advanced age while presenting a degree osteoarthritis. This would result in a more posterior condylar position at full extension.

5.2.3 Kinetic Comparison for UKAs

Various forces were also derived using the FSMM for both the Sigma and Preservation UKA subjects. The average bearing surface force for subjects having a Sigma UKA demonstrated an increase in force from 1.91 xBW at full extension to 3.52 xBW at 120° flexion. The Preservation UKA subjects revealed a similar pattern and demonstrated an increase from 1.92 xBW at full extension to 3.60 xBW at 120° flexion (Figure 5-30).

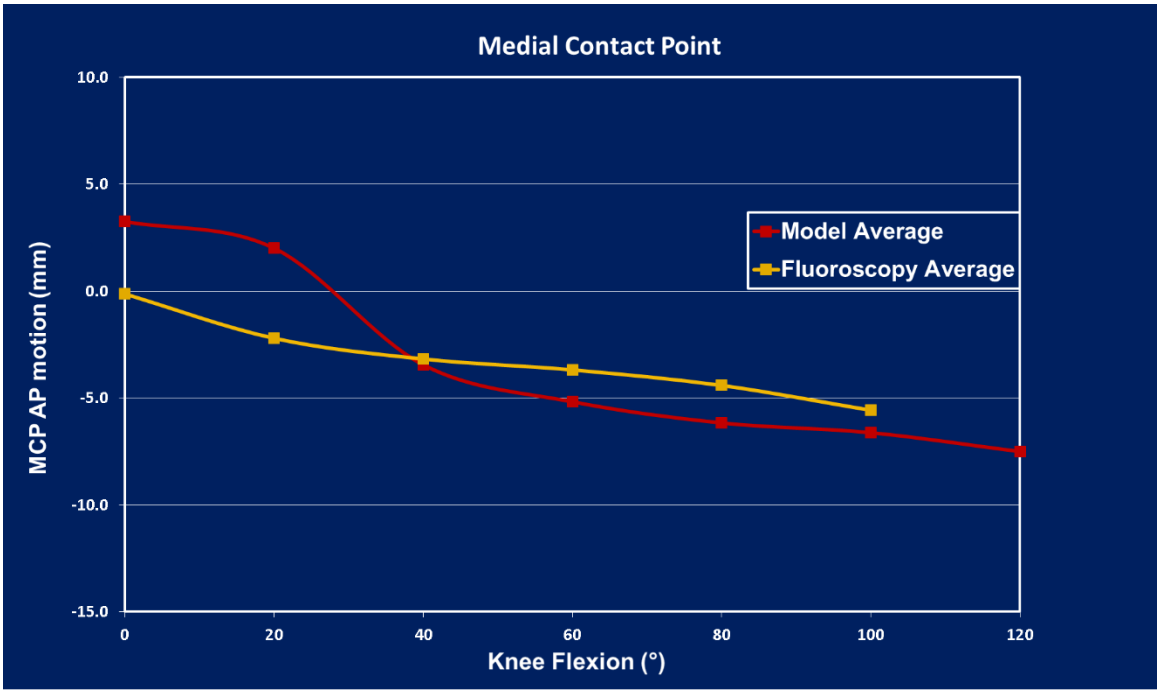


Figure 5-29: Average medial contact point for Preservation UKA during a DKB activity using modeling and fluoroscopy techniques.

The average quadriceps force for subjects in the FSMM having a Sigma UKA revealed an increase from 0.41 xBW at full extension to 2.78 at 120° flexion, while the average Preservation UKA subjects had a similar pattern and experienced an increase from 0.42 xBW at full extension to 2.76 xBW at 120° flexion (Figure 5-31). The patellofemoral interaction forces were also evaluated for both UKA. Patellofemoral forces occurring between the patella and the lateral non-implanted bone for the Sigma UKA subjects were 0.11 xBW at full extension and increased to a peak force of 2.44 xBW at 100° flexion, while the Preservation UKA subjects had a force of 0.12 xBW at full extension and increased to a peak force of 2.40 xBW at 100° flexion. Sigma subjects experienced patellofemoral forces occurring between the UKA components, with an initial force of 0.07 xBW at 60° flexion and increases to 0.99 xBW at 120° flexion, while the Preservation UKA subjects experienced a force of 0.11 xBW at 80° flexion and increased to 0.88 xBW at 120° flexion (Figure 5-32). Ligament forces are critically important for knee performance and not well defined in the literature for UKA. ACL forces demonstrated a plateau during early flexion and decreased after 60° flexion. This trend was evident in both UKA groups with the Sigma UKA subjects having an ACL force of 0.70 xBW at full extension, decreasing to 0.42 xBW at 60° flexion.

The Preservation UKA revealed ACL forces of 0.68 xBW at full extension, decreasing to 0.41 xBW at 60° flexion (Figure 5-33). Although the average pattern for ACL force for both UKA's interestingly similar, there is variability in this force when comparing various subjects (Figure 5-34). PCL forces were minimal at full extension, decreasing during midflexion, and then increasing in later flexion. The Sigma UKA PCL force was 0.18 xBW at full extension and 0.92 xBW at 120° flexion, while the Preservation UKA subjects had a force of 0.19 xBW at full extension and 0.96 xBW at 120° flexion (Figure 5-35).

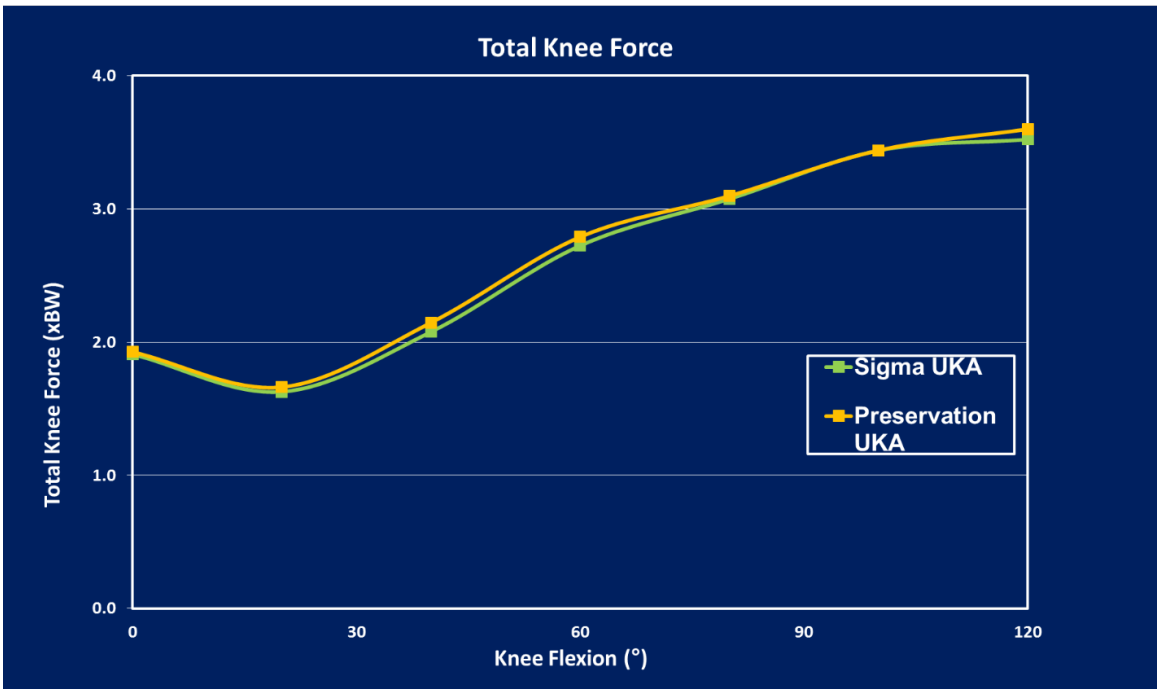


Figure 5-30: Average total knee force for Sigma and Preservation UKA during a DKB activity.

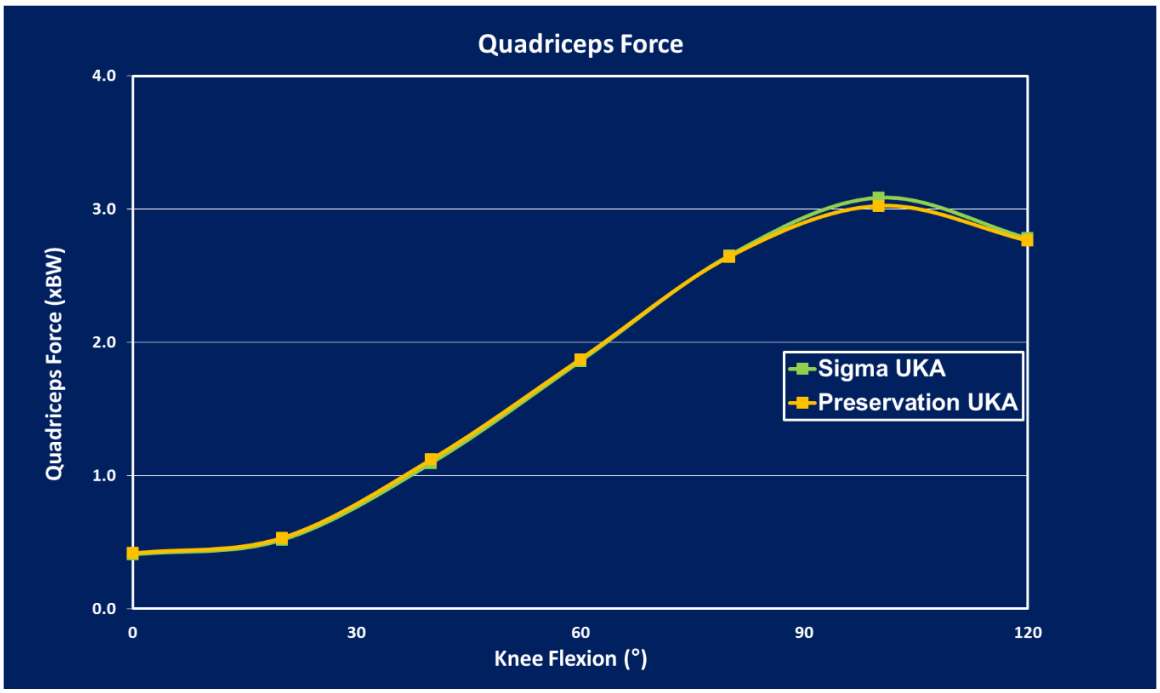


Figure 5-31: Average quadriceps force for Sigma and Preservation UKA during a DKB activity.

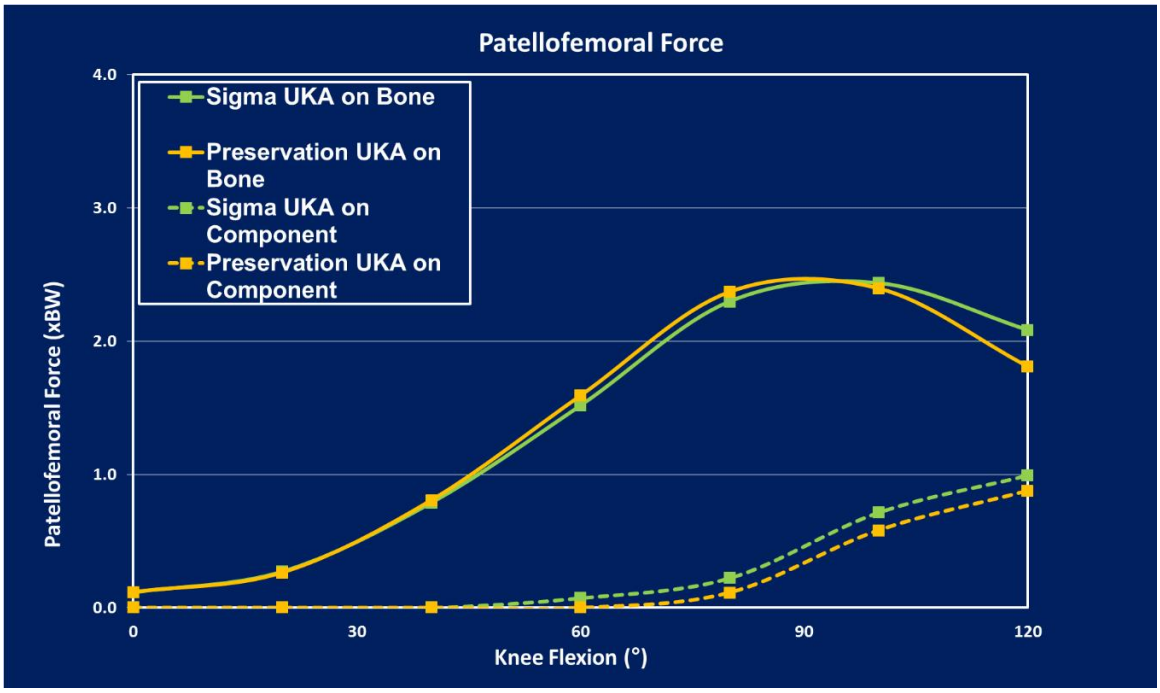


Figure 5-32: Average Patellofemoral force on bone and component for Sigma and Preservation UKA during a DKB activity.

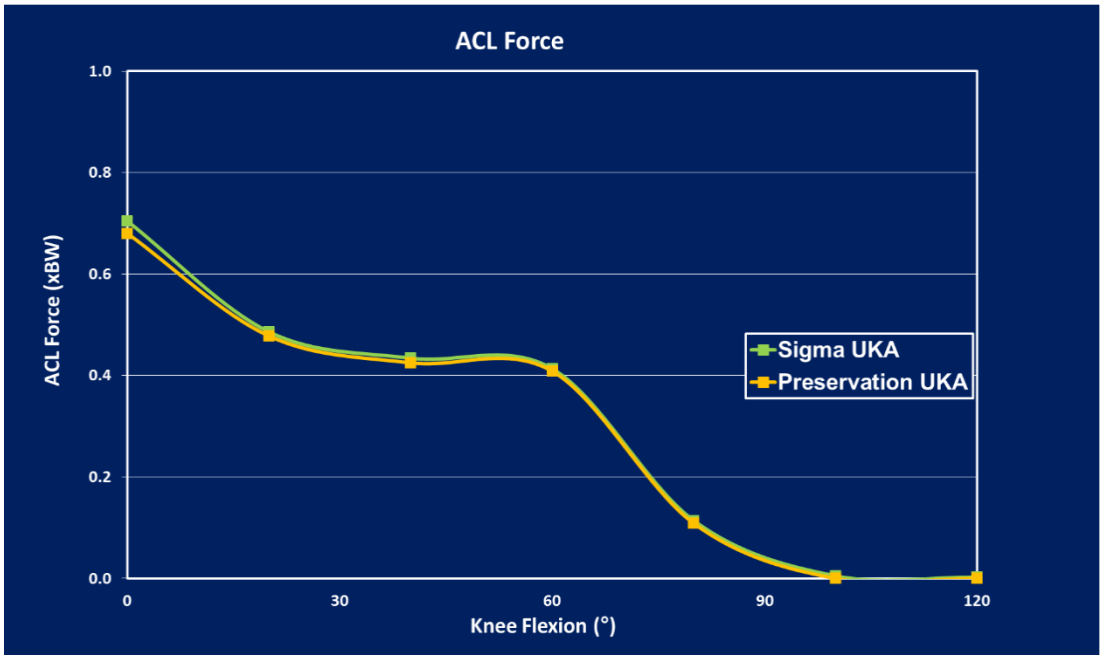


Figure 5-33: Average ACL force for Sigma and Preservation UKA during a DKB activity.

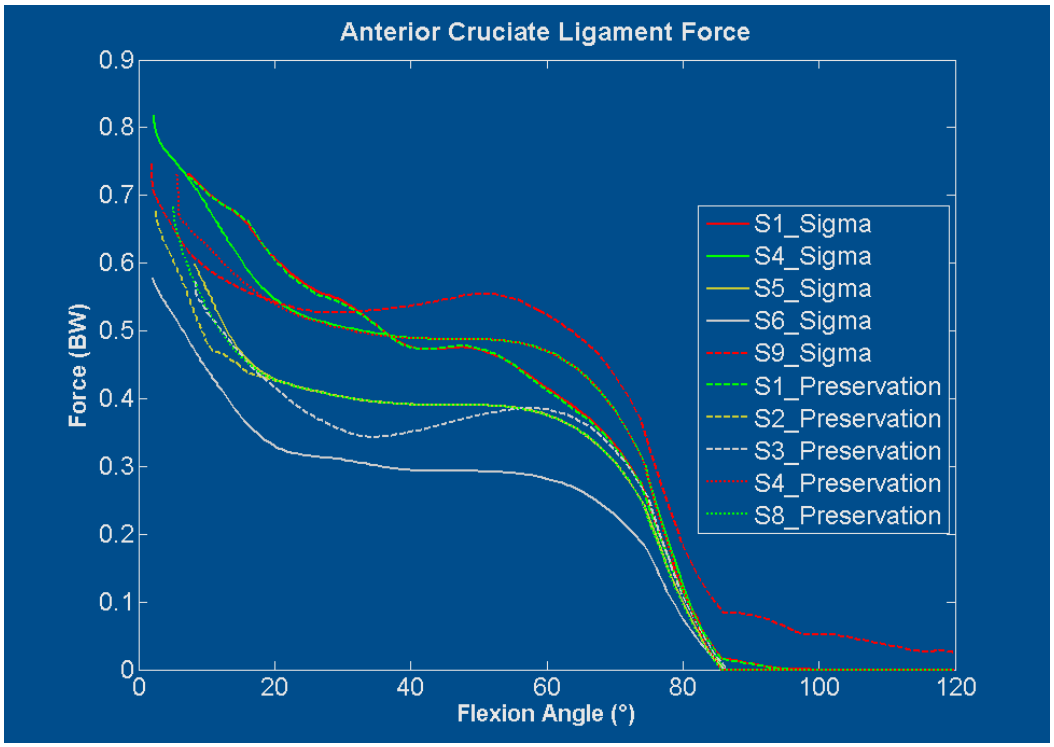


Figure 5-34: ACL force patterns for multiple subjects having a Preservation UKA and Sigma UKA.

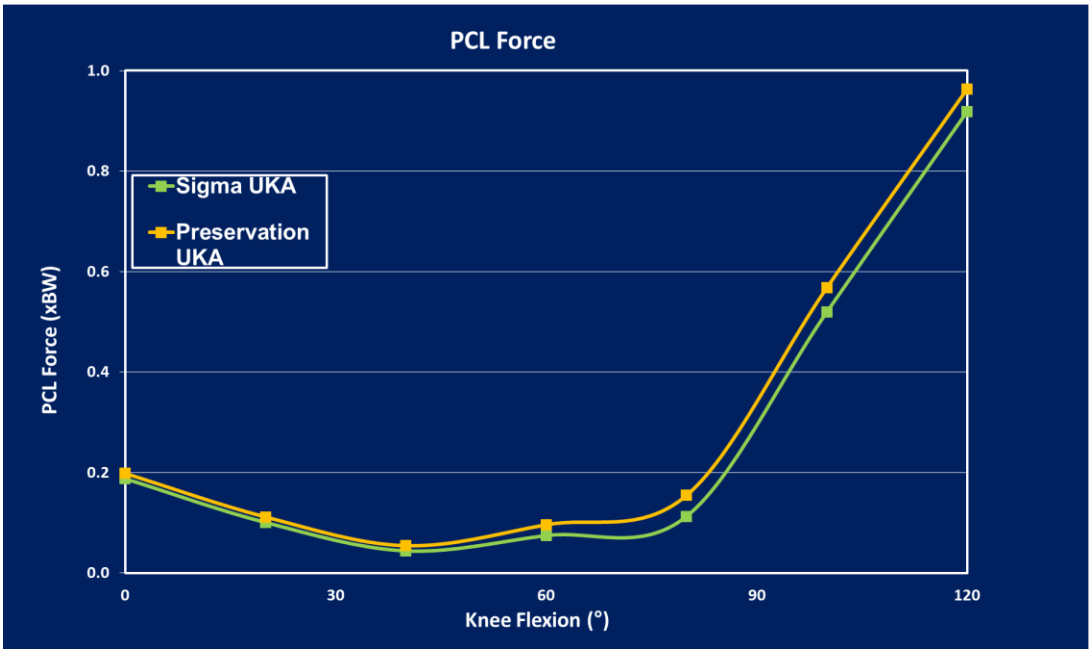


Figure 5-35: Average PCL force for Sigma and Preservation UKA during a DKB activity.

5.2.4 Analyzing the Role of the Cruciate Ligaments in UKA Subjects

To further analyze the role that the ACL plays in kinematics, one subject in the model, implanted with a Preservation UKA, performed the DKB activity with an intact ACL and with a ruptured ACL. The two simulations showed a distinct difference of medial contact point at full extension, with the ACL intact simulation beginning at 4.8 mm and the ACL removed simulation beginning at -2.8 mm. The ACL intact simulation showed consistent rollback with MCP translating to -8.11 mm at 120° flexion. The ACL ruptured simulation showed excessive medial rollback and then anterior sliding in late flexion, with the MCP translating to -21.1 mm at 80° flexion and then sliding anteriorly to -11.2 mm at 120° flexion (Figure 5-36). From a previous fluoroscopy study, a subject with an intact ACL and a ruptured ACL performed a deep knee bend [83]. The ACL intact subject began the activity at 6.19 mm and showed consistent rollback to -4.36 mm at 90° flexion. The subject with the ruptured ACL began more posteriorly at -6.78 mm and rolled back to -12.71 mm at 45° flexion. Anterior sliding occurred later in flexion, with the medial contact point slide to -2.12 mm at 90° flexion (Figure 5-37).

Although in vivo ACL forces have proven difficult to directly measure, the findings for the ACL force using the UKA FSMM are consistent with other findings in the literature. Other research has shown similar patterns, with ACL forces remaining high in early flexion, decreasing in midflexion, and ultimately going to zero in deep flexion [84]. Although there is much variability in reported peak ACL forces during a DKB, other literature has reported peak ACL forces in the normal knee at 0.55 x BW, with the implanted knee demonstrating higher forces [85, 86]. Our model may have higher magnitudes due to the more anterior positioning of the medial condyle at full extension, which is more consistent with what is seen in subjects with a healthy ACL [36].

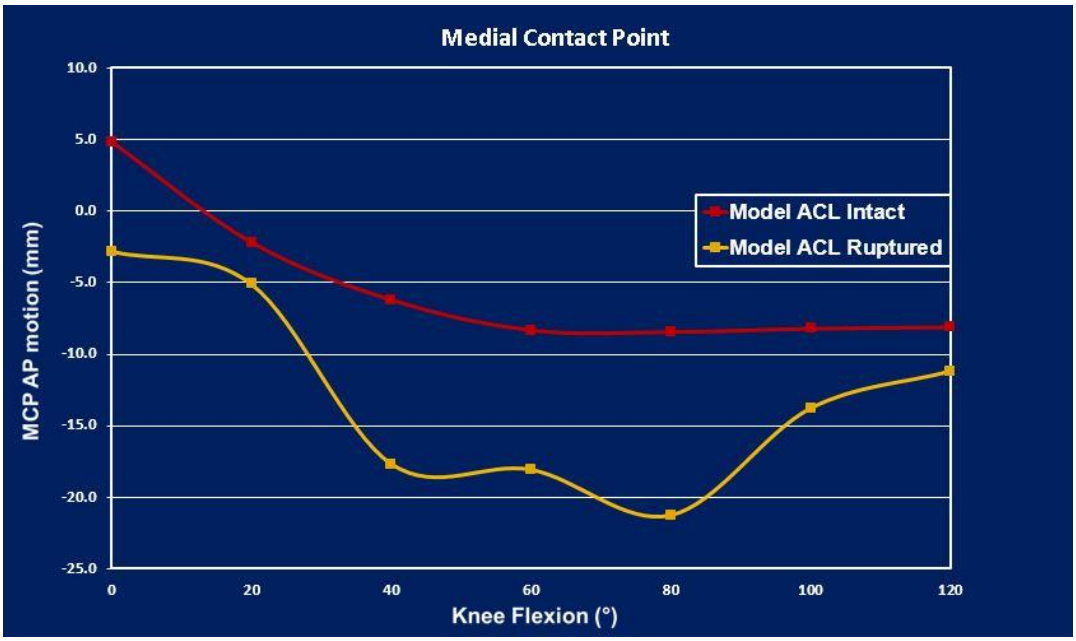


Figure 5-36: AP translation of the medial contact point for a subject implanted with a Preservation UKA with an intact and with a ruptured ACL analyzed in the FSMM.

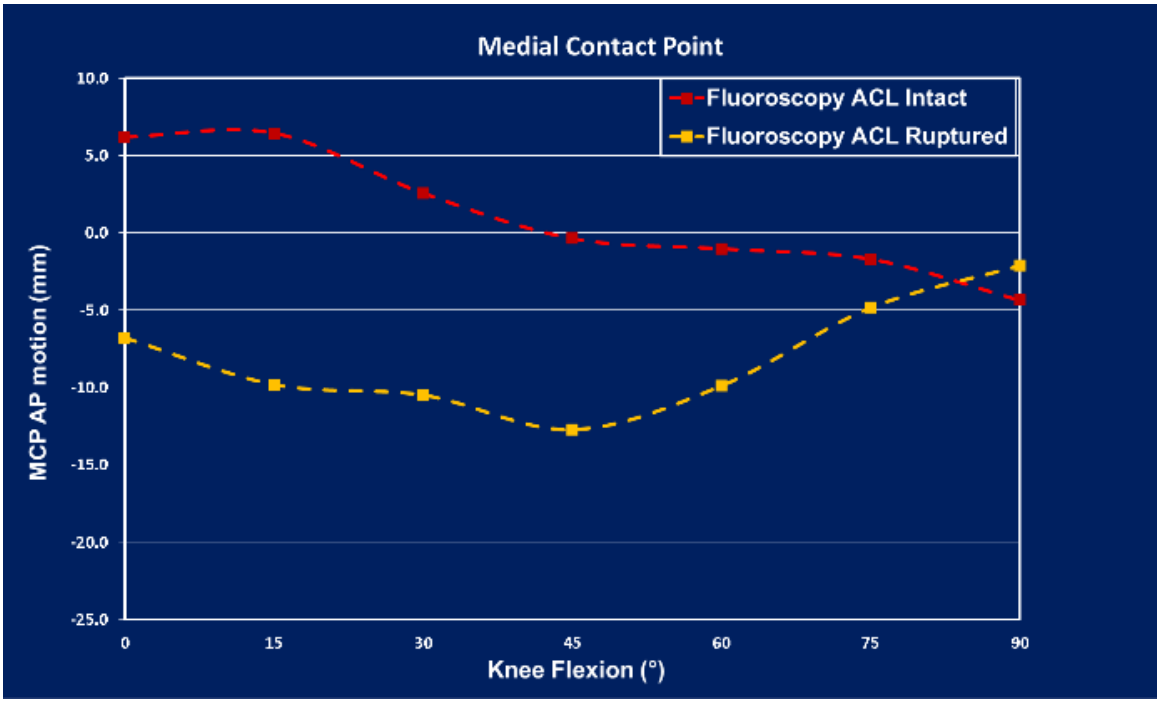


Figure 5-37: A subject implanted with a different UKA analyzed using fluoroscopy with an intact and a ruptured ACL [87].

5.2.5Step Down Activity for the UKA

To better contextualize the results of the step down activity, the results of one subject for a step down and a deep knee bend activity were compared. Overall, the kinematics were fairly similar, with the medial contact point AP motion starting at 4.22 mm for the SD activity and 5.24 mm for the DKB activity at full extension, while the medial contact point moved to 0.15 mm at 60° flexion for the SD activity and -0.09 mm at 60° for the DKB activity (Figure 5-38). The lateral contact point AP motion was also quite similar between the two activities. The lateral contact point AP motion starts at 2.62 mm for the SD activity and 3.31 mm for the DKB activity at full extension, while the lateral contact point moved to - 4.01 mm at 60° flexion for the SD activity and -5.23 mm at 60° for the DKB activity (Figure 5-39). The total knee forces remained slightly higher for the step down throughout the activity with the total knee force starting at 2.38 xBW for the SD activity and 1.91 xBW for the DKB activity at full extension, while the total knee force increased to 3.42 xBW at 60° flexion for the SD activity and 2.76 x BW at 60° for the DKB activity (Figure 5-40). These differences in knee force are likely due to the increased tibial flexion during the step down activity, as well as the increased pelvic tilt which moves the torso center of mass more anterior. The quadriceps forces for the two activities remained very similar with the total quadriceps force starting at 0.67 xBW for the SD activity and 0.48 xBW for the DKB activity at full extension, while the total quadriceps force increased to 1.18 xBW at 60° flexion for the SD activity and 1.56 x BW at 60° for the DKB activity (Figure 5-41).

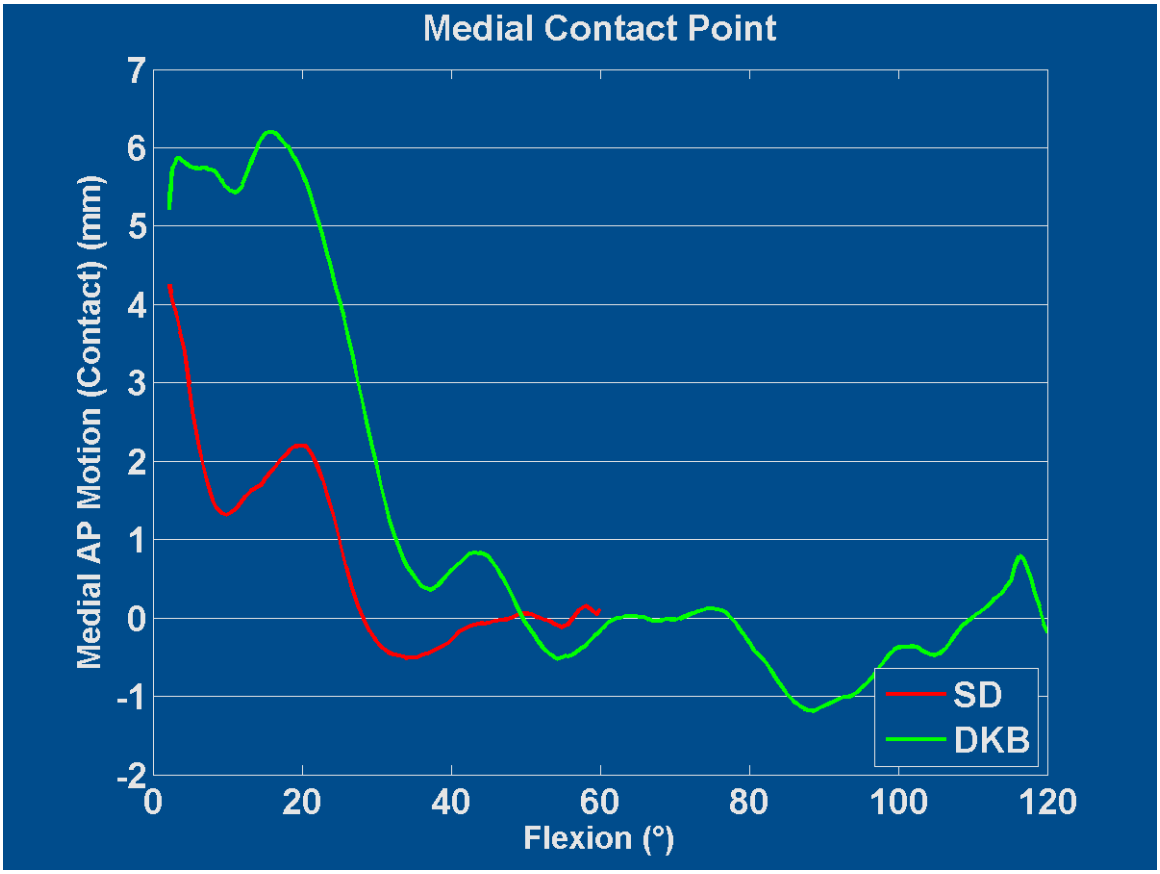


Figure 5-38: Medial contact point AP motion for a UKA subject performing a step down and DKB activity.

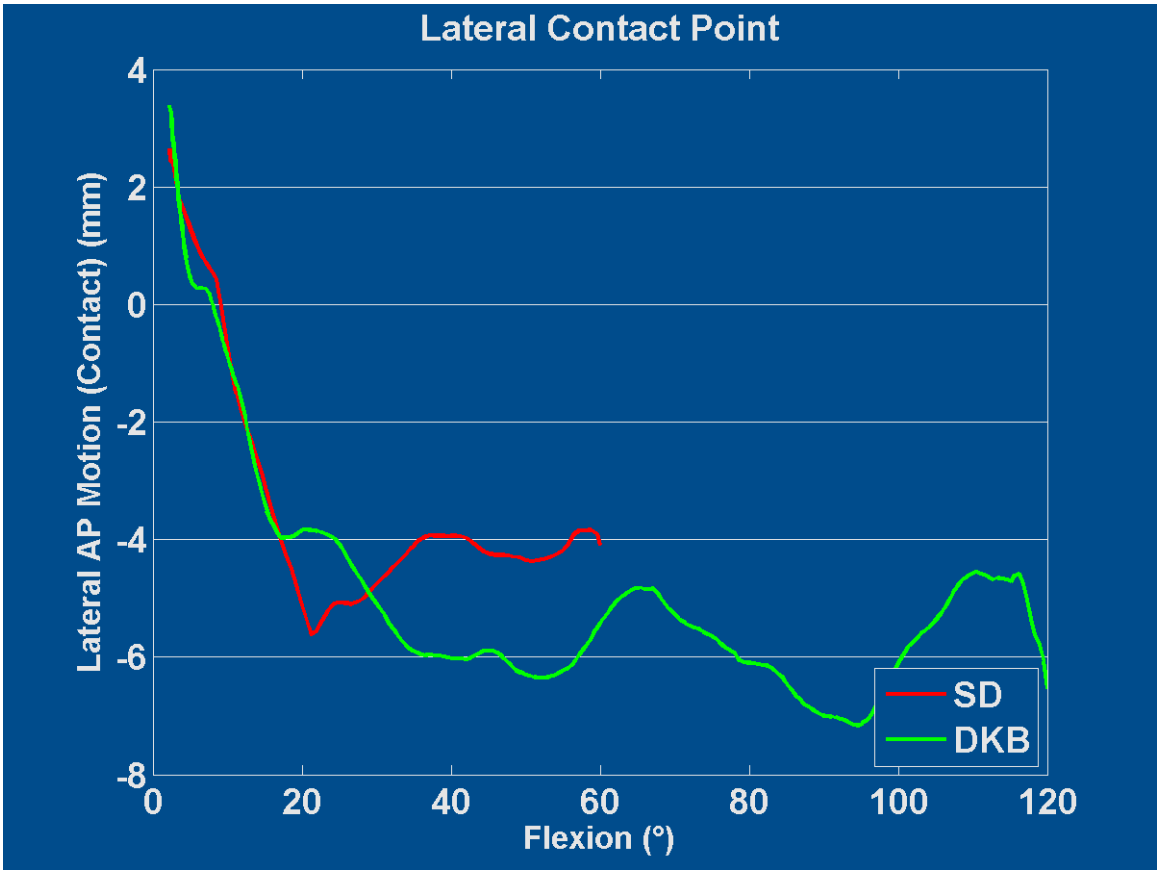


Figure 5-39: Lateral contact point AP motion for a UKA subject performing a step down and DKB activity.

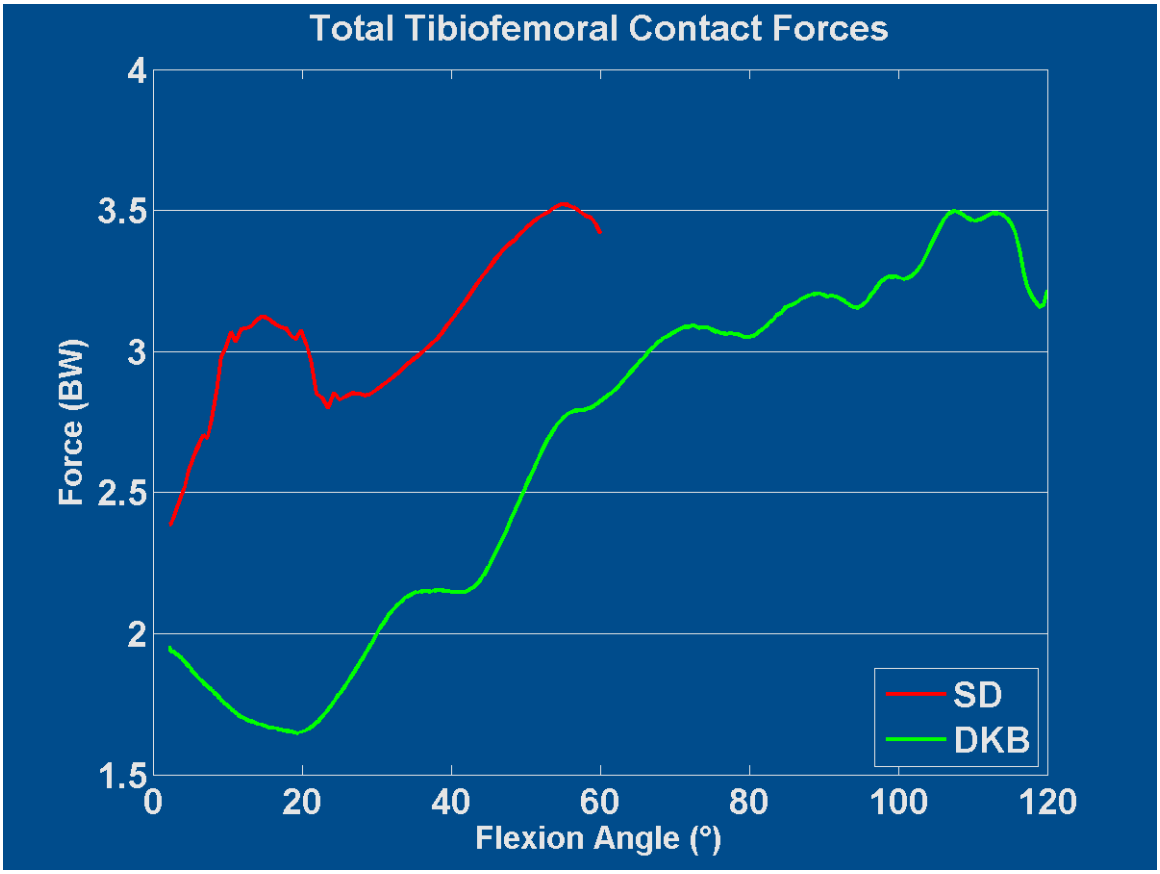


Figure 5-40: Total knee force for a UKA subject performing a step down and DKB activity.

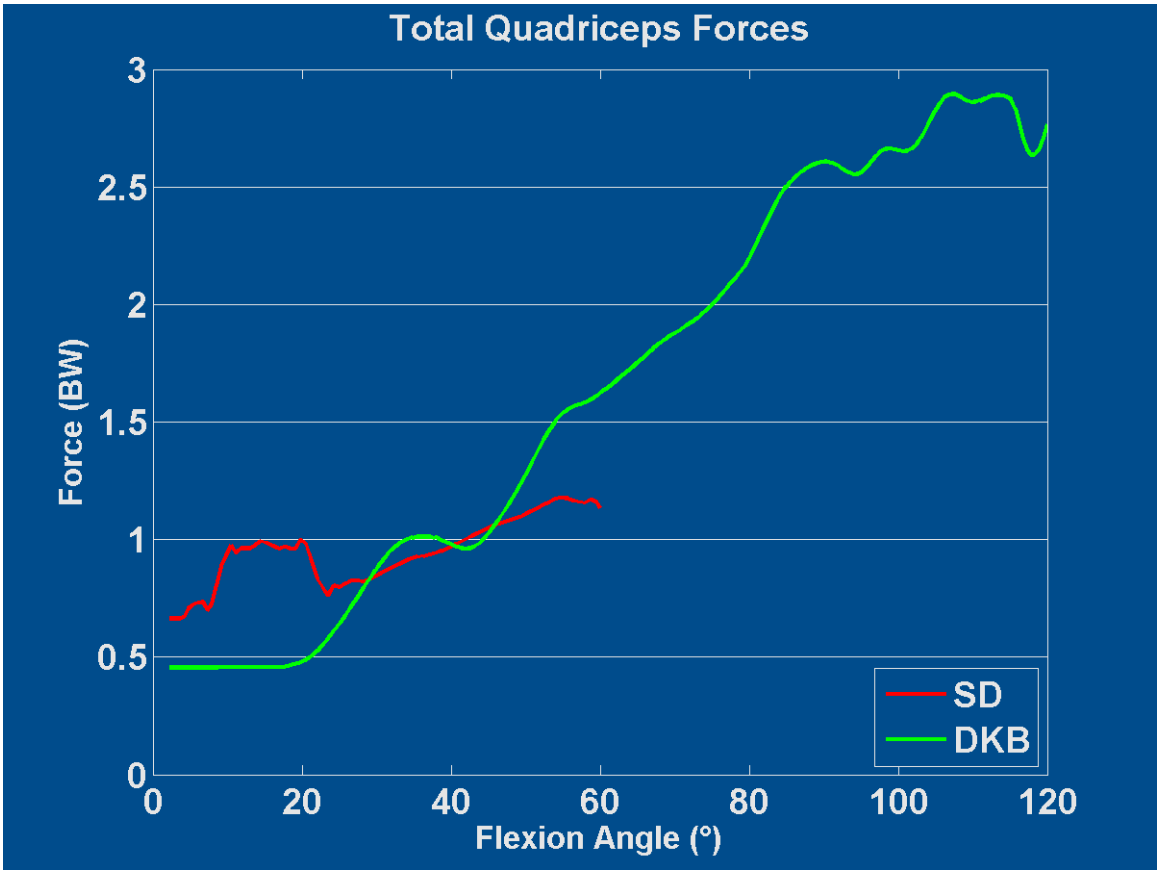


Figure 5-41: Total quadriceps force for a UKA subject performing a step down and DKB activity.

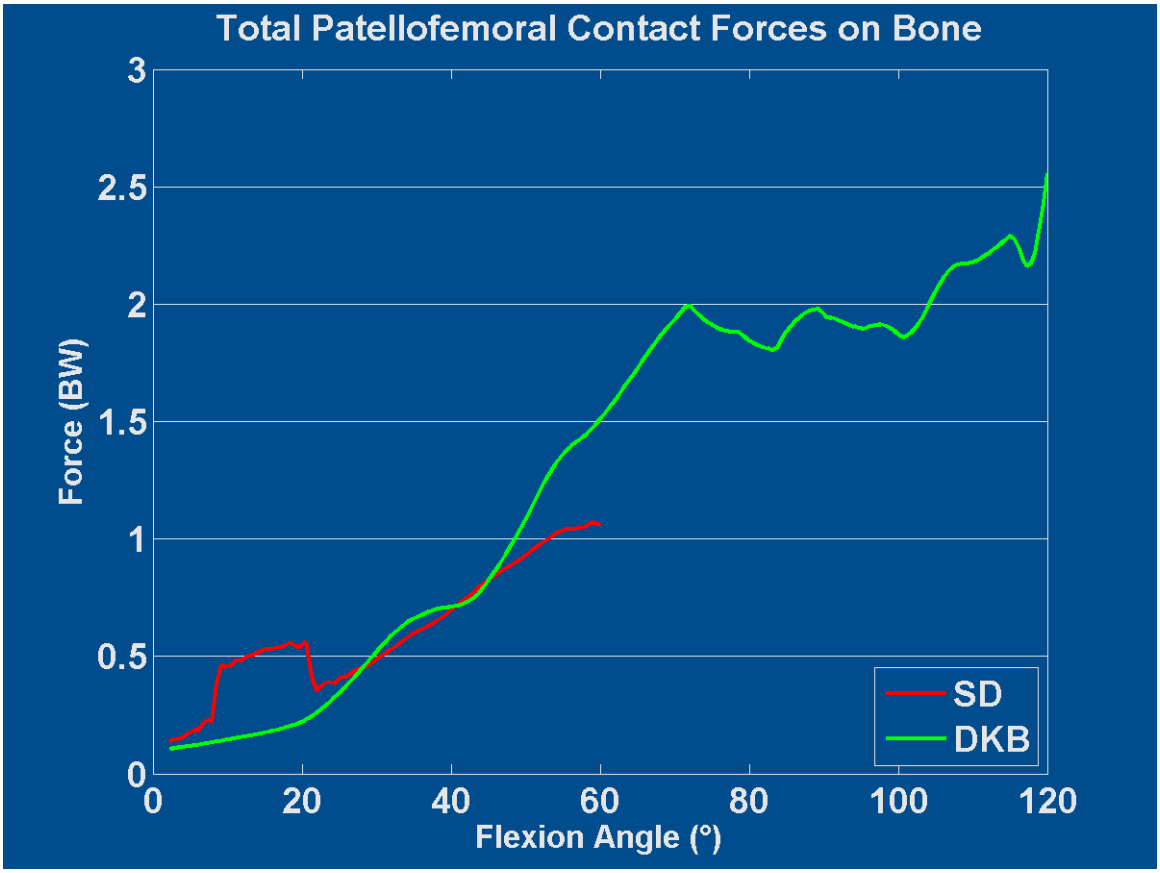


Figure 5-42: Patellofemoral force on the bone for a UKA subject performing a step down and DKB activity.

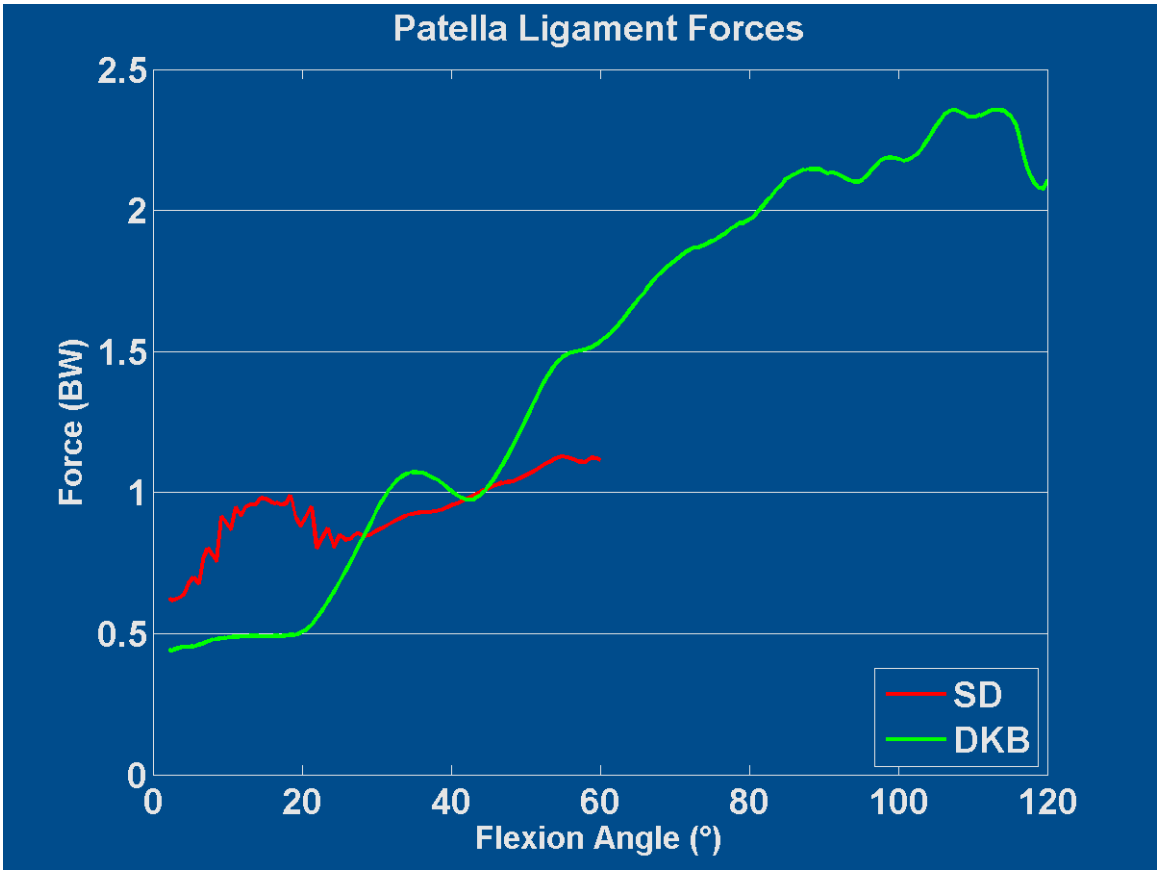


Figure 5-43: Patella ligament force for a UKA subject performing a step down and DKB activity.

The patellofemoral forces for the two activities remained very similar with the patellofemoral force starting at 0.12 xBW for the SD activity and 0.10 xBW for the DKB activity at full extension, while patellofemoral force increased to 1.06 xBW at 60° flexion for the SD activity and 1.49 x BW at 60° for the DKB activity (Figure 5-42). The patella ligament forces for the two activities remained very similar with the patella ligament force starting at 0.61 xBW for the SD activity and 0.10 xBW for the DKB activity at full extension, while patella ligament force increased to 1.06 xBW at 60° flexion for the SD activity and 1.49 x BW at 60° for the DKB activity (Figure 5-43).

5.3 Incorporating New Activities into the Model

5.3.1 Gait Results

Gait is vastly different from any other activities in the model. For the purposes of this model, only the stance phase is analyzed. The activity begins at heel strike, with the knee slightly flexed. As the activity continues, the knee further flexes as the leg accepts more weight. During midstance the knee begins to extend again, and ultimately flexes again at toe off. The knee flexion profile used during our gait activity can be seen in Figure 5-44.

Two different implant types were assessed, the Attune CR and Attune PS. Kinematic results for gait can be found in Figure 5-45. Overall there is much less condylar movement and rotation in comparison with a DKB activity. The axial rotation begins at -0.3° at heel strike for CR and 0.2° for PS and internally rotates to -3.5° around halfway through stance phase for CR and -3.1° for PS. In the second half of the activity the knee rotates externally to -0.4° for CR and -0.7° for PS and then slightly rotates internally to -1.2° at toe off for CR and -1.5° for PS. Both LAP and MAP show fairly similar trends for both implant types. They both demonstrate an anterior translation of close to 3 mm before a slight posterior translation of close to 1 mm.

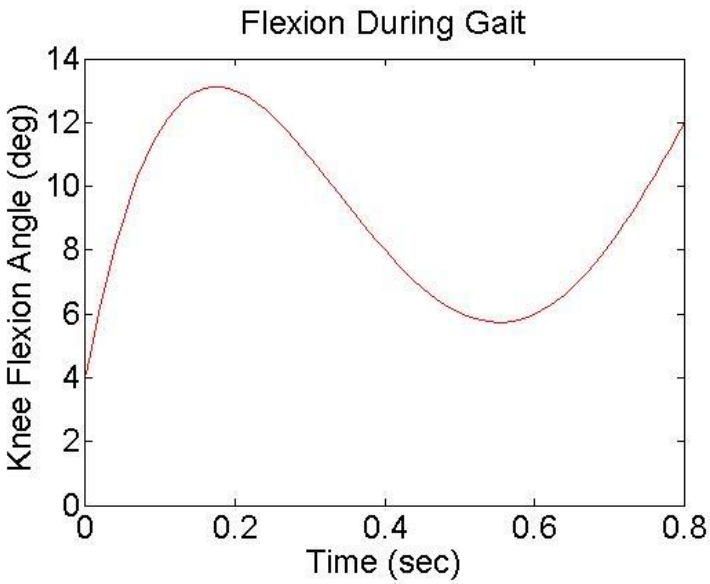


Figure 5-44: Knee flexion profile during gait activity.

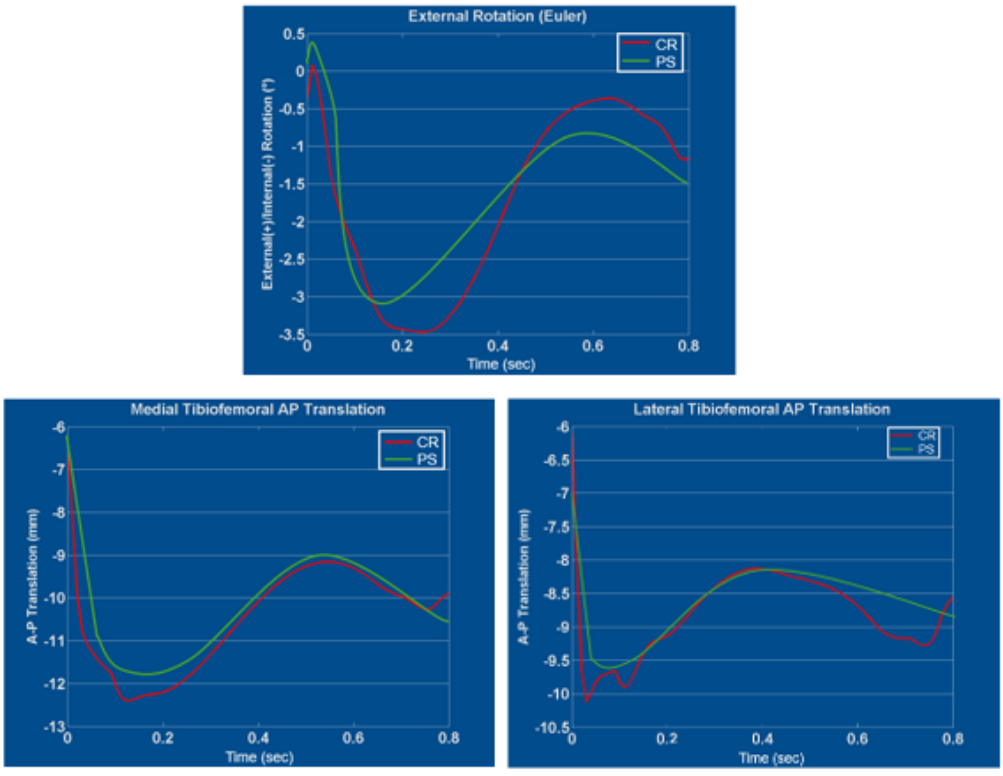


Figure 5-45: Axial rotation (top), MAP (left), and LAP (right) during a gait activity.

While understanding the motion of the knee during gait is important, it is also valuable to understand the forces that are occurring during the activity. A summary of kinetic results for gait can be found in Figure 5-46. One of the most important results regarding gait is the knee force during the activity. One hallmark of gait is an M-curve in the knee force graph. The first peak of the M-curve is a result of the loading response of the leg, while the second is a result of the pushing off towards toe-off. The gait activity in the model has a distinct M-curve in its knee force graph. The first peak reaches 2.23 xBW for CR and 2.25 xBW for PS, while the second peaks at 2.28 xBW for CR and 2.30 xBW for PS. The patellofemoral force remained quite low throughout the activity. Starting at close to 0 xBW at heel strike for both implants, the patellofemoral force peaks at 0.31 xBW for CR and 0.33 for PS and then drops back down to below 0.01 xBW for both implants. The activity finishes with a slight increase to 0.08 xBW at toe off for both implants. Patella ligament force shows a fairly similar trend to the patellofemoral force, but at a higher magnitude. The patella ligament force begins close to 0 xBW at heel strike for both implants, and then increases to a peak of 1.13 xBW for CR and 1.15 for PS before dropping to 0.01 xBW later in the activity for both implants. The activity finishes with an increase of 0.34 xBW at toe off for CR and 0.38 for PS. Overall, the kinetic results are consistent with literature. A prominent M-curve demonstrates the acceptance of weight during that activity and a distinct pushing off in the later stages of the activity. The patellofemoral and patella ligament forces peak early in the activity and remain lower in the second half of the activity. They both show peaks during the weight acceptance phase of gait, so they may play an important role in that phase of the activity.

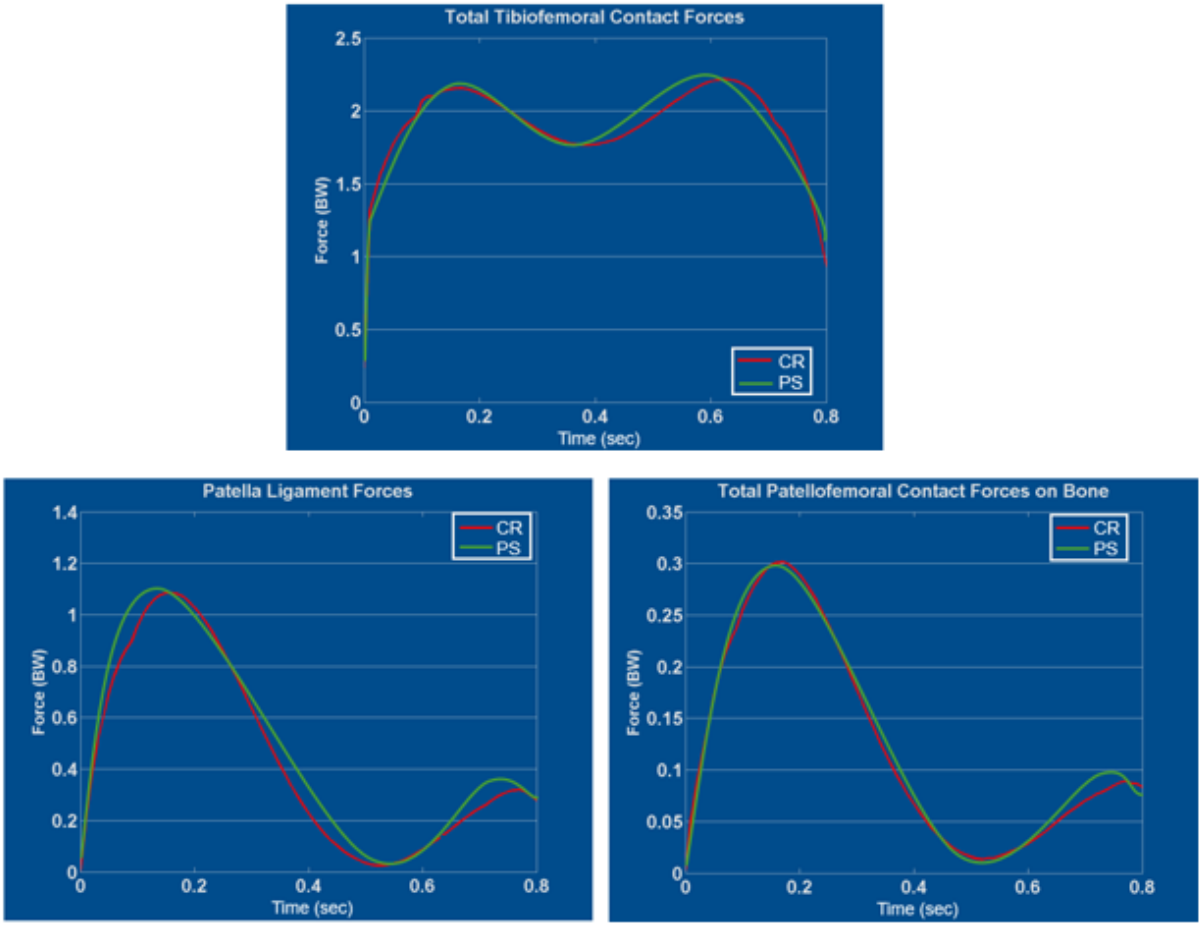


Figure 5-46: Total knee force (top), patella ligament force (left), and patellofemoral force (right) during a gait activity.

Although previously analyzed activities, such as deep knee bend, show valuable results over a large range of flexion, gait is the most common daily activity for patients. This makes gait an important activity to understand and analyze for orthopedic companies. Utilizing mathematical modeling to analyze gait is especially useful since gathering fluoroscopic data on gait has proven difficult. Additionally, gathering in person data can be challenging since differences have been observed in treadmill gait and overground gait [88].

Studies have shown that the peak knee forces during gait are between 2 and 3 xBW [89]. The results shown above are consistent with these findings. For orthopedic companies, it is important to establish that knees implanted with their device will not have a significant increase in knee force as this may lead to increased component wear and potential complications in the future. The addition of gait to this model allows for this analysis to be quickly completed on any unique TKA design. This type of evidence can be utilized in a device's design process as it goes through quality testing.

In addition to femorotibial mechanics, patellofemoral mechanics is also an important aspect to overall joint performance. In other studies, the peak patellofemoral joint forces have been reported 0.9 ± 0.4 xBW. While this is slightly higher than the 0.33 xBW reported, the sample size is currently quite small. Further analysis on more subjects will be important to confirm the accuracy of the model. Abnormalities in the patellofemoral joint have been shown to alter gait [89]. The development of the gait activity in the model could lead to future investigations into patellofemoral pain syndrome and other conditions.

5.4 Contact Mapping Results

5.4.1 Femorotibial Contact Mapping

Having reliable contact area and stress data is critical to understanding potential wear patterns and component longevity in TKAs and UKAs. The femorotibial joint undergoes the highest contact forces which can reach over 3 xBW in deep flexion. In this model, the femorotibial contact mapping tool was utilized to calculate both the medial and lateral femorotibial contact areas and stresses for 10 subjects implanted with an Attune PS during a deep knee bend activity. The average medial contact area was 201.22 mm^2 at 0° flexion and steadily decreased to 104.22 mm^2 at 120° flexion. The average lateral contact area was 247.54 mm^2 at 0° flexion and steadily decreased to 103.28 mm^2 at 120° flexion (Figure 5-47). Other literature has shown this decrease in femorotibial contact areas, with one study showing total femorotibial contact areas beginning at 368.22 mm^2 at 0º flexion and decreasing to 129.54 mm^2 at 120º flexion[90]. The average medial contact stress was 1.3 MPa at 0° flexion and increases to 12.1 MPa at 120° flexion. The average lateral contact stress was 1.7 MPa at 0° flexion and increases to 9.0 MPa at 120° flexion (Figure 5-48). Medial contact stresses were higher than lateral contact stresses, which is consistent with other literature which has shown peak medial contact forces of 22 MPa and peak lateral contact forces of 13 MPa in other implants [5].

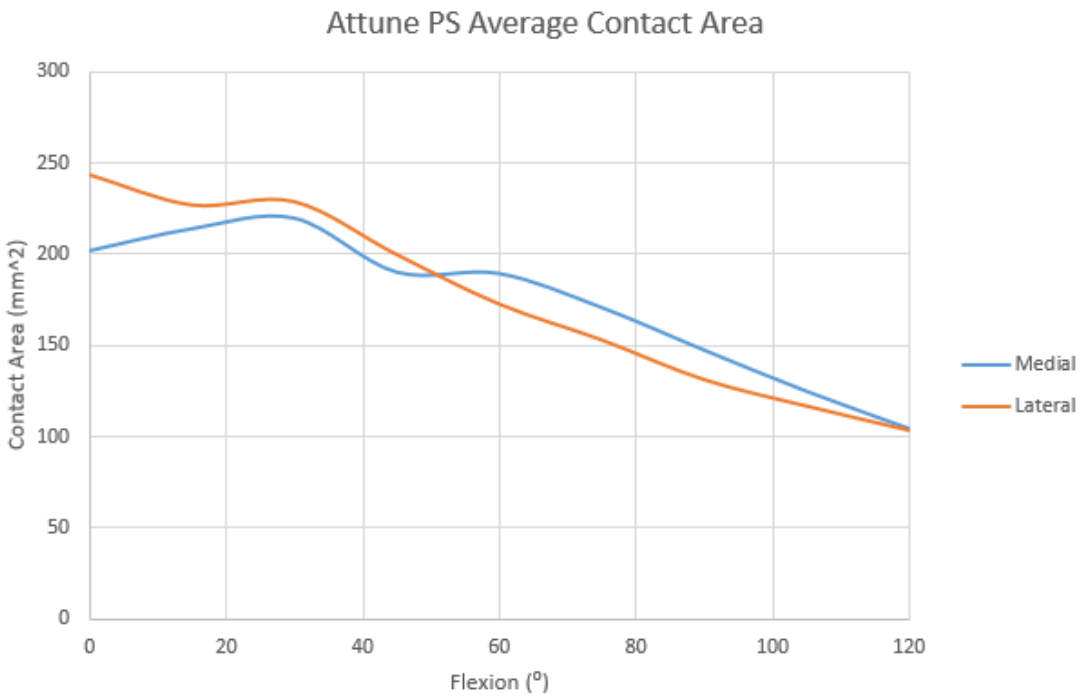


Figure 5-47: Average Attune PS contact areas during a DKB activity.

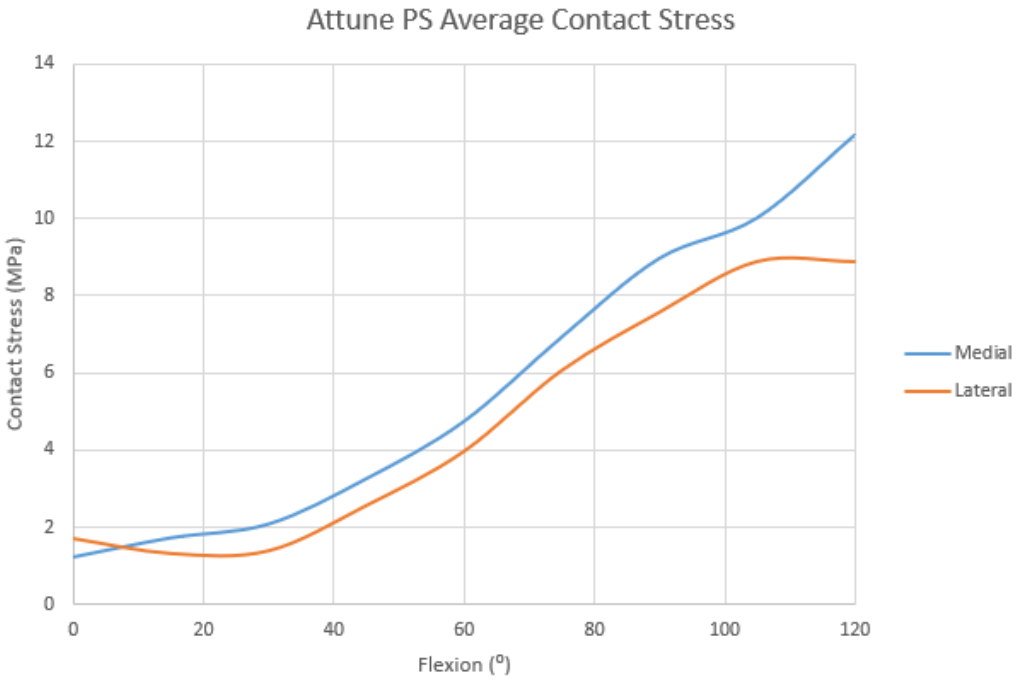


Figure 5-48: Average Attune PS contact stress during a DKB activity.

5.4.2 Cam/Post Contact Mapping

The shape of the cam/post mechanism is important to its performance and purpose in a TKA design. An analysis was conducted on two different PS implant types with differently shaped posterior posts: the Sigma PS and the Attune PS. The Attune PS has a rounded post, while the Sigma PS has a flat post (Figure 5-49). The shape of this post has significant effects on the contact areas and contact stresses. In early cam/post engagement the flat post TKA shows higher contact areas with an area of 85.56 mm^2 at 85º flexion. However, edge loading occurs as the axial rotation of the femur increases leading to a decrease in contact area with a contact area of 28.22 mm^2 at 120º flexion. The rounded post TKA shows a contact area of 32.54 mm^2 at 85º flexion, but shows an increased contact area as flexion increases, with a contact area of 52.25 mm^2 at 120º flexion (Figure 5-50). The flat post TKA shows a maximum contact stress of 38.51 MPa, while the rounded post TKA shows a maximum contact stress of 19.25 MPa (Figure 5-51).

5.4.3Patellofemoral Contact Mapping

In order to contextualize some of the model's patellofemoral contact results, experimental data was gathered by Depuy to assess patellofemoral contact mechanics. In order to do this, a femoral component was mounted to a u-shaped bracket, while the patella surface was equipped with a TekScan sensor (Figure 5-52). An axial load was applied to the femur via TestStarIIm, and the femur component was rotated to eight set orientation, 0°, 15°, 30°, 45°, 60°, 90°, 120° and 145° knee flexion. Once set up, the following forces were used to assess patellofemoral contact: 700N for 0° and 15° and 30°, 961N for 45°, 1308N for 60°, 2195N for 90°, 2779N for 120° and 2593N for 145°. Although the force values used and component orientations are different from what occurs in the model, this experimental data can be used as good baseline data in which to compare model results with.

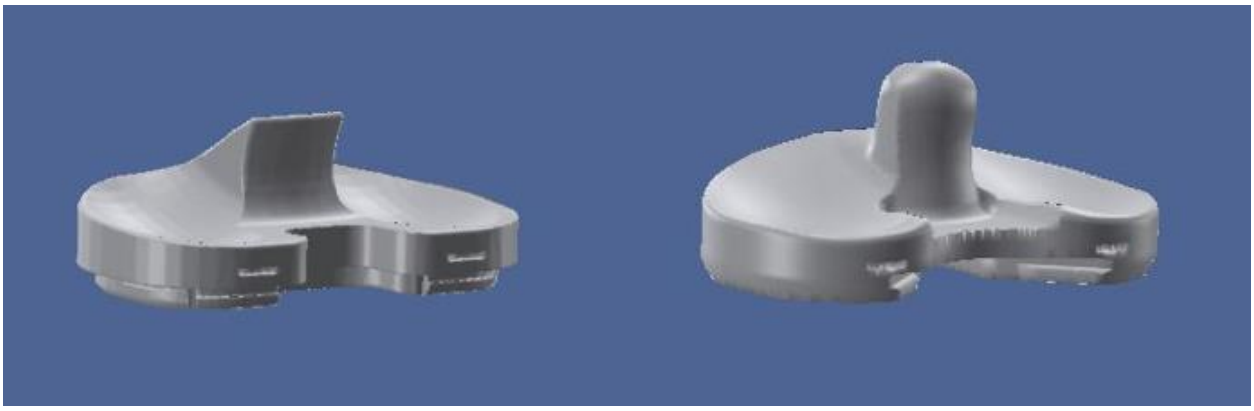


Figure 5-49: Post geometry of Sigma PS (left) and Attune PS (right).

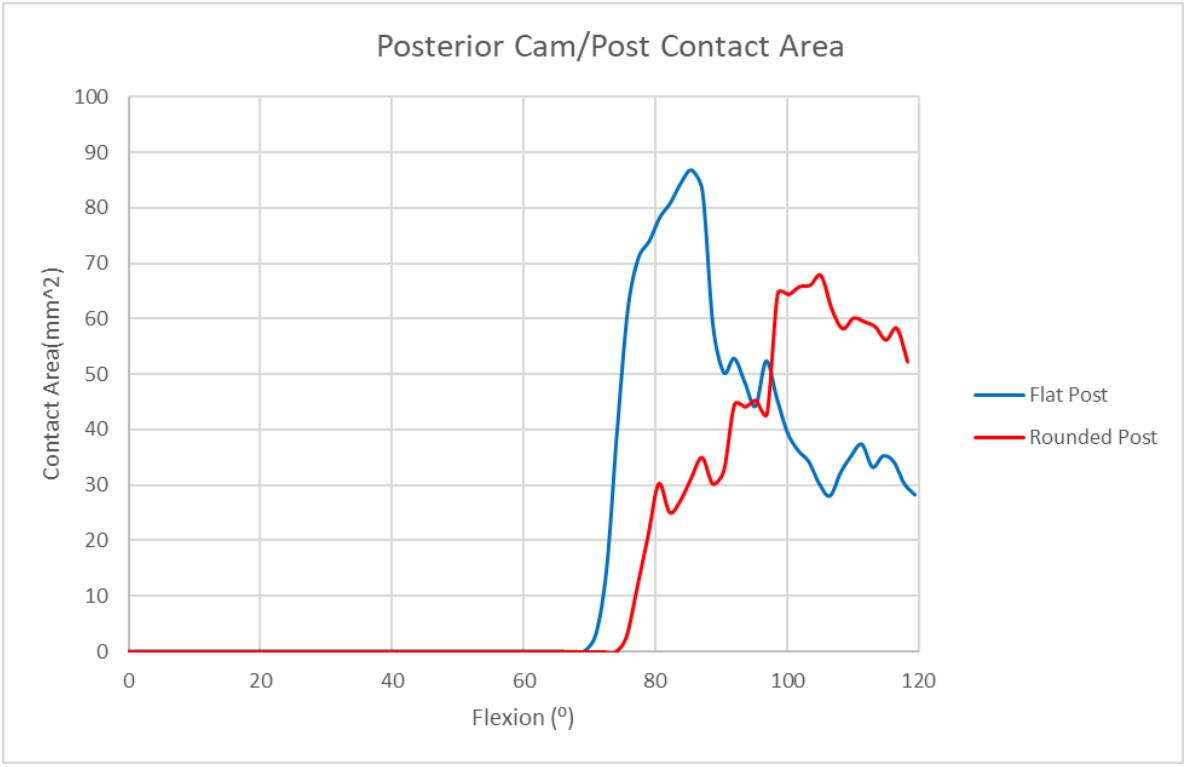


Figure 5-50: Cam/Post contact area of Sigma PS and Attune PS during a DKB activity.

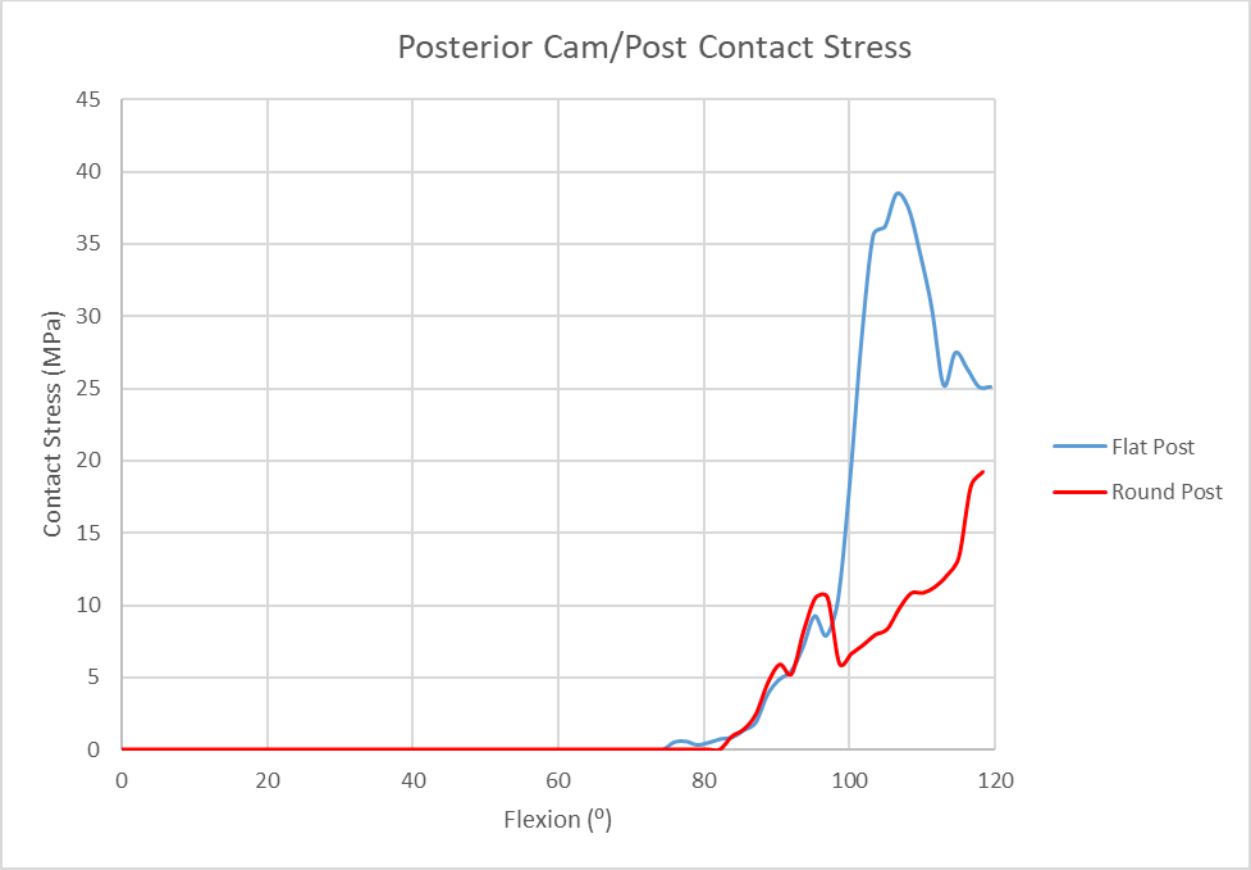


Figure 5-51: Contact Stress for a Sigma PS and Attune PS TKA during a DKB activity.

The total average contact areas for each flexion value is shown in Figure 5-53. The average maximum stress for each flexion value is shown in Figure 5-54. It can be seen that the average maximum stress is higher than the stress values calculated in the model. However, the model calculates average stress, while the experimental data shows maximum stress. So rather than reporting the highest stress of an individual face in the contact area, the model reports the average overall stress for the entire contact area. Figure 5-55 was created to show the average stress based upon the experimental contact area information and the experimental loads being used in a similar way that the model reports stress. This data in Figure 5-55 is much closer to the model patellofemoral stress data, with an experimental maximum average of 25.32 MPa compared to a theoretical maximum average of 25.16 MPa. Although different loads and orientations are being used, the overall stress figures are still fairly similar throughout the activity.

This experimental foundation allows for the theoretical modeling results to be directly compared, as the patellofemoral contact mechanics can change significantly depending on which implant type is being used. The patellofemoral contact mechanics were obtained for four activities of daily living, including chair rise, DKB, step down, and step up. As shown in the experimental setup, patellofemoral contact area steadily increased with flexion until roughly 80˚, then the patella contact splits onto both the medial and lateral condyles (Figure 5-56), resulting in a lower contact area. All four activities demonstrate fairly similar contact areas from 0˚ to 60˚ knee flexion. In deep flexion, chair rise plateaus, while DKB decreases (Figure 5-57). This difference may be because the chair rise activity begins in deep flexion and moves towards full extension, while the DKB activity moves towards deep flexion.

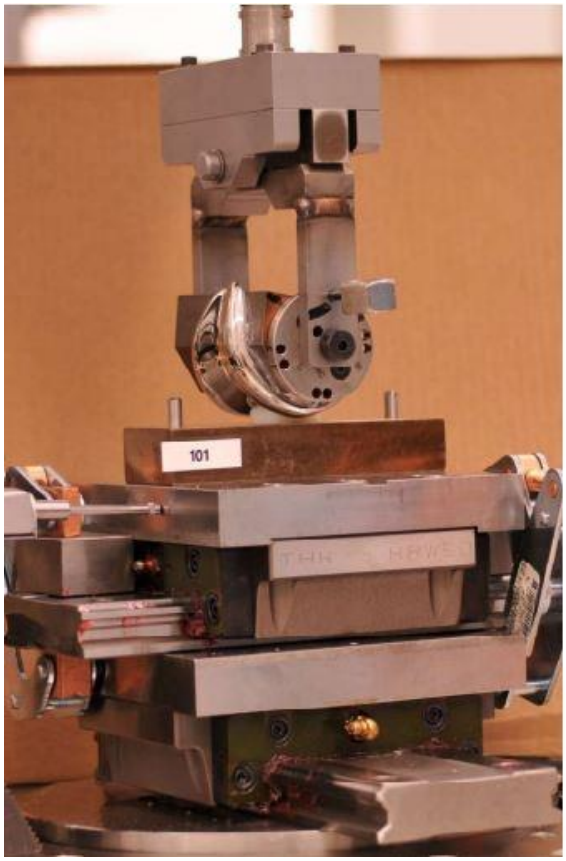


Figure 5-52: Experimental setup for patellofemoral contact testing.

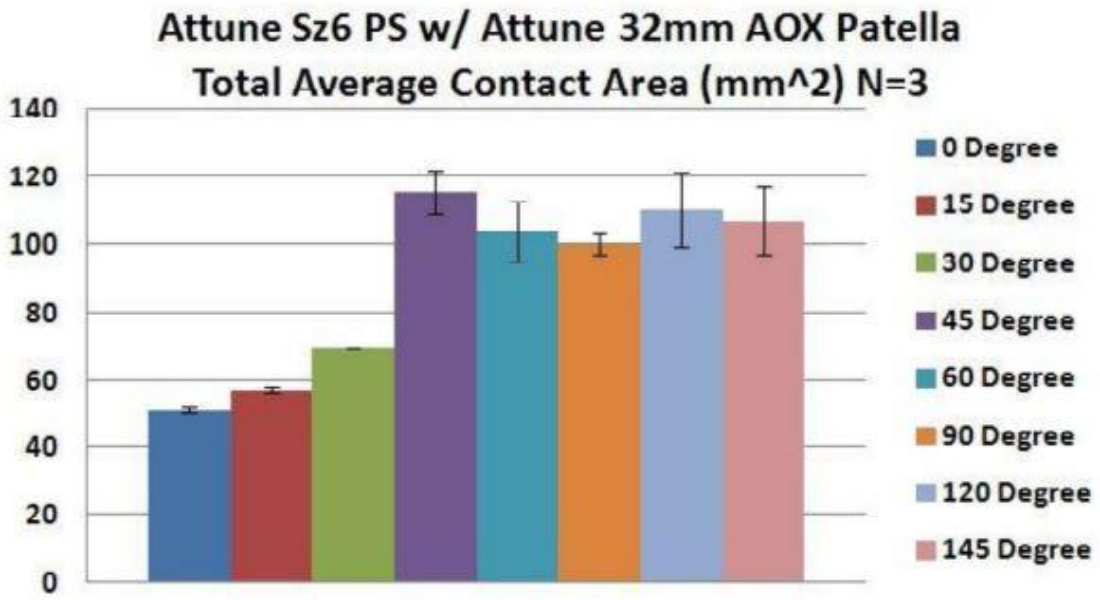


Figure 5-53: Average experimental patellofemoral contact areas.

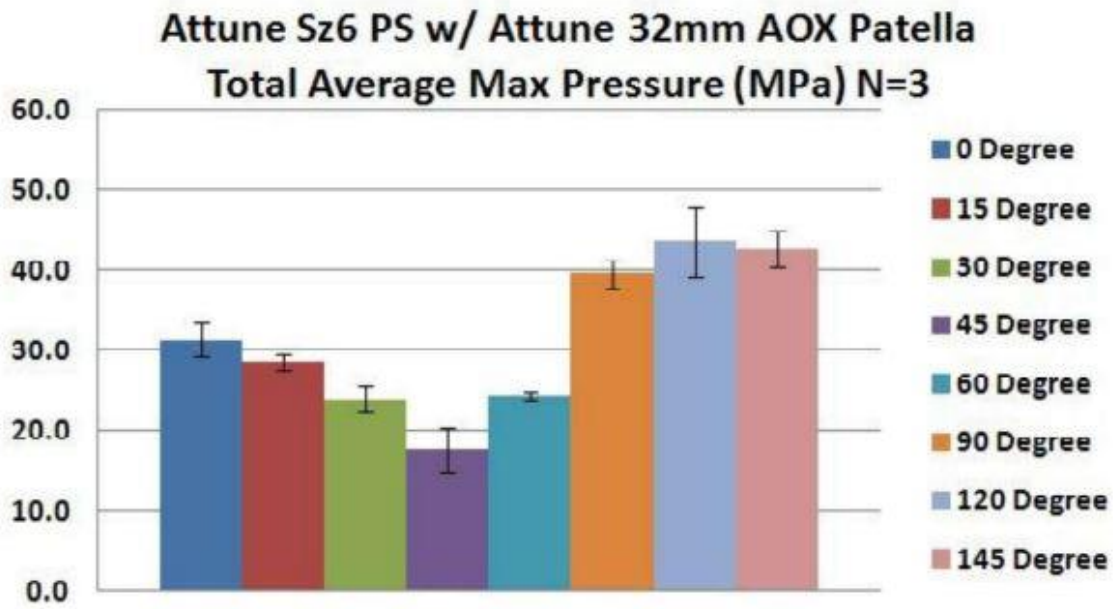


Figure 5-54: Average maximum experimental patellofemoral contact stresses.

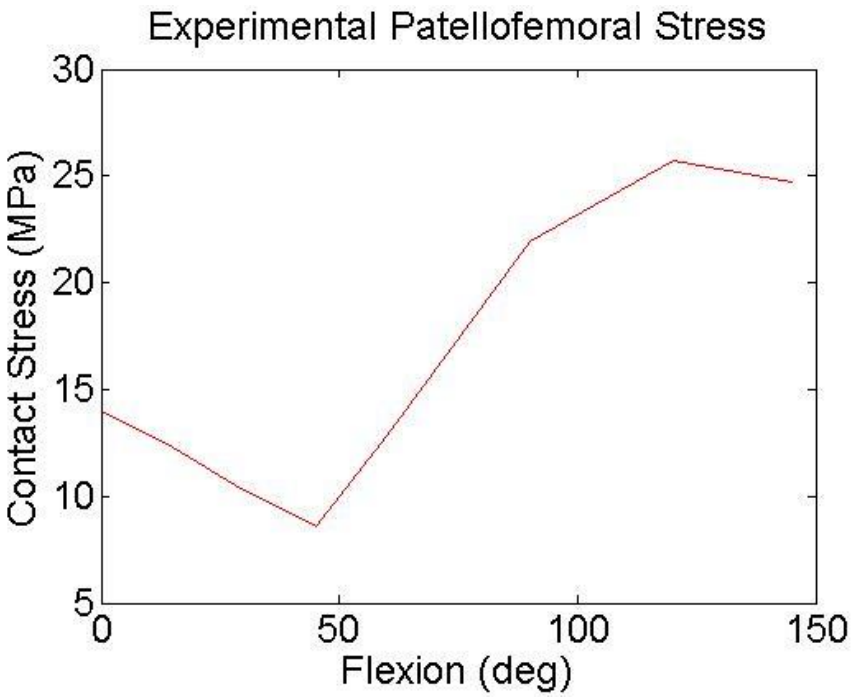


Figure 5-55: Average experimental patellofemoral contact stress using a TestStarIIm controller.

The lowering contact area in deep flexion, along with the increased patellofemoral forces in deep flexion results in a higher patellofemoral stress. As with the contact area plots, the contact stresses remain fairly consistent across the four activities up to 60˚ flexion. In deeper flexion, the DKB activity shows the highest contact stress, peaking at ~22 MPa, while the chair rise contact stress peaks at ~ 10 MPa (Figure 5-58).

The model's patellofemoral contact mechanics compared well with the contact mechanics from the experimental setup. the differences observed expected due to the slightly different loads applied to the system. The peak average contact stress of 25 MPa in the experimental setup showed minimal differences with the 22 MPa peak contact stress in the model. The model's patellofemoral contact area was slightly higher throughout the activity, but in line with other patellofemoral contact area studies [91]. The patellofemoral joint has the potential of experiencing large amounts of overall contact stress. With this in mind, continuing to focus on the patellofemoral joint during the design and implementation phase of TKA will help further improve implant longevity and postoperative outcomes.

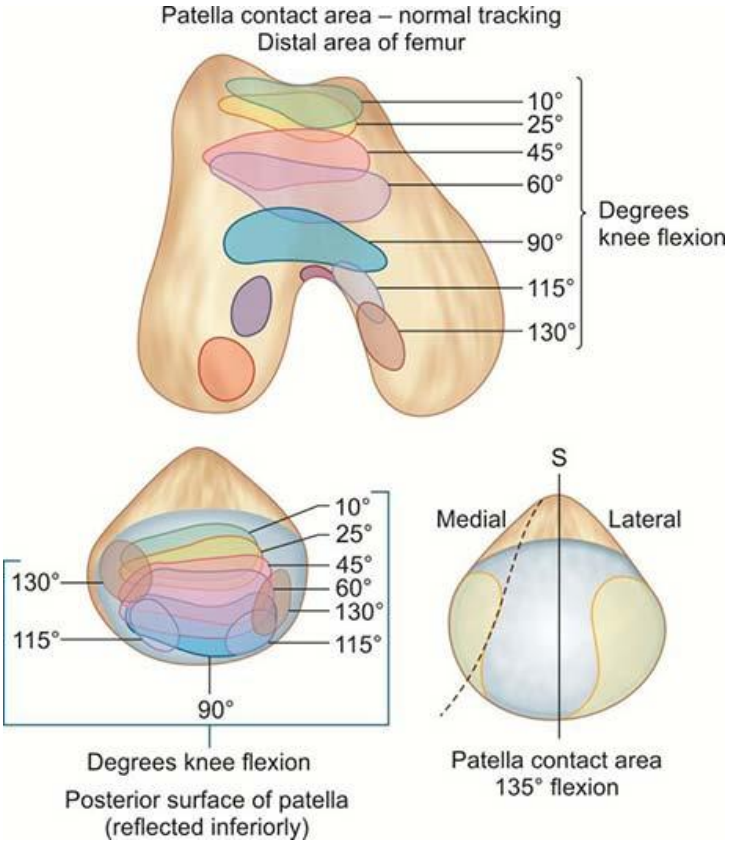


Figure 5-56: Normal patella tracking in the healthy knee (https://www.jaypeedigital.com/book/9789352501670/chapter/ch11)

.

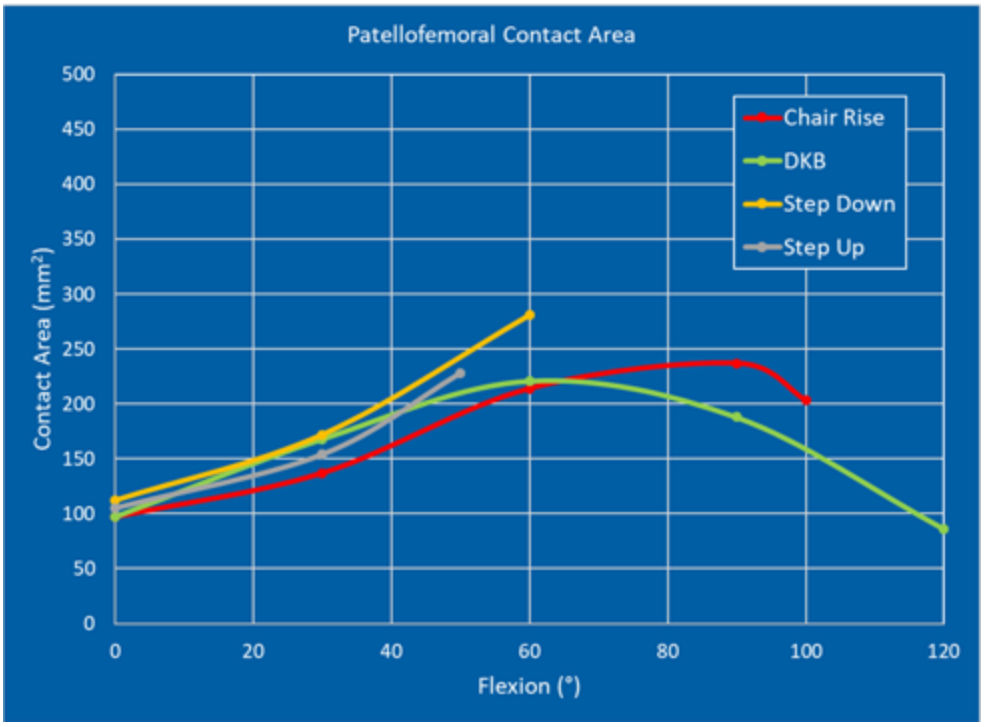


Figure 5-57: Patellofemoral contact area for four activities of daily living.

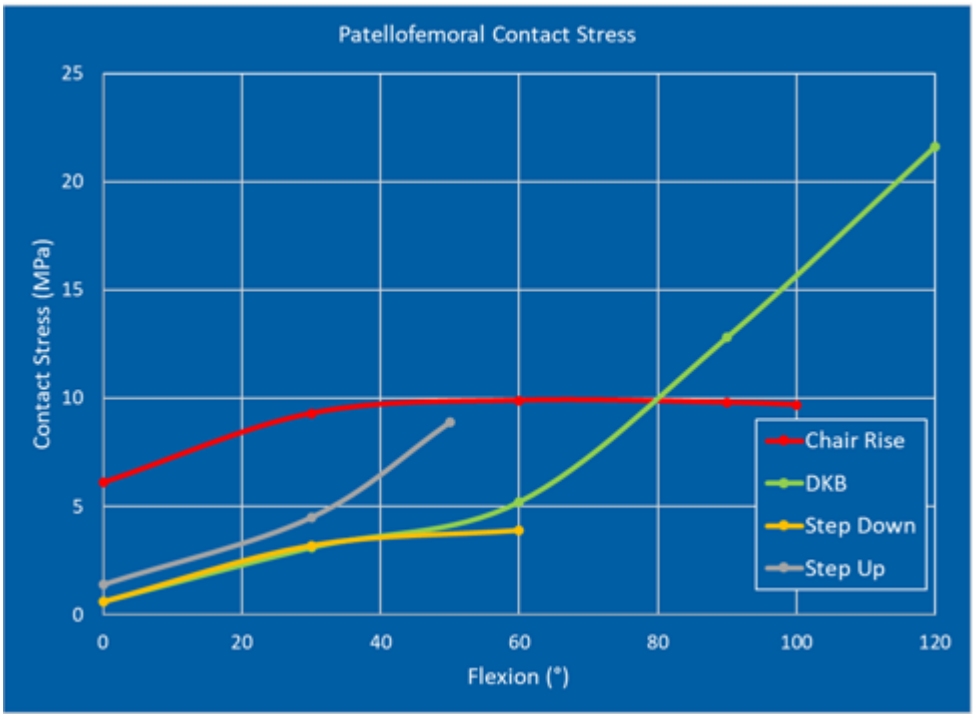


Figure 5-58: Patellofemoral contact stress for four activities of daily living.

Chapter 6 Summary

Throughout this dissertation, several novel additions to the existing forward mathematical model of the knee were made. These additions improved the functionality of the model as well as expanded the model's functionality and analysis capabilities. These additions contributed to the overall knowledge of biomechanics in orthopedics and will be a useful tool for future analysis on knee implants. This improved mathematical model allows for a more ethical and safer environment for testing implant designs, investigating soft tissue forces, and understanding contact mechanics. This model allows for more implant types and activities to be analyzed, allowing more comprehensive testing to be done before implanting the device and potentially putting patients at risk.

The patellofemoral contact capabilities have been improved through the development of a new representation of the two surfaces in the patellofemoral joint. The contact can now be calculated and displayed with the patellofemoral contact separating into two distinct patches on the anterior aspect of either condyle. This advancement allows for a more accurate patellar tracking and a more accurate patellofemoral force magnitude and direction. Since the patellofemoral joint and femorotibial joint are closely connected, the changes in the patellofemoral joint will allow for more accurate analysis of the entire knee.

A sophisticated contact mapping algorithm was developed to calculate contact areas and contact stresses at the bearing surfaces of the knee. A variety of contact types including femorotibial, patellofemoral, cam/post, and side wall contact were included. This advancement provides important information on the contact mechanics of the knee. This is often a point of interest for orthopedic companies, allowing for predictions of edge loading and the expected wear of

components to be better understood. The contact mapping algorithm also allows for potential failure modes to be identified early in the design process. Ultimately this will lead to safer implants for patients and surgeons alike.

The addition of a gait activity to the model allows for the most common activity of daily living to be analyzed. This advancement is quite significant, as it allows for better understanding of an activity which is very different from any other existing activities in the model which either involves only flexion or extension. The gait activity required a significant rework of the model's code as rather than simply loading or unloading the joint, this activity incorporates weight acceptance and the transfer of weight onto the contralateral leg. Despite not going through the full range of motion of the knee, the addition of a gait activity to the model allows for a more commonly performed activity to be better understood. This allows for the model to complete more comprehensive analyses of the knee and expand the knowledge of knee biomechanics.

A new implant type, the Sigma Stabilized +, was added to the model. This unique implant type strives to constrain axial rotation of the knee, for patients having compromised collateral ligaments, while still allowing for sufficient overall flexion. This implant incorporates a side wall constraint mechanism to prevent excessive axial rotation. Since this design feature is unique to this implant, custom code was developed to account for this extra contact type. This addition to the model further improves its versatility and is very useful for the investigation of this implant design and other revision TKAs. Revision TKAs offer an alternative for subjects which sustained damage to their knee or have compromised soft tissues surrounding the joint. These implants allow for a larger patient population to be treated and for more patients to have a good outcome with a TKA.

Multiple UKA implant types were also added into the model. These UKA designs allow for only one compartment of the knee to be resurfaced while keeping the other compartments native. This

results in a mixture of native and implanted structures which proves complicated to model. The model allows for various discoveries which can be difficult to investigate in vivo. For example, the roles of the cruciate ligaments in the UKA can be further understood by using this model since the ligament properties can be manually modified to further investigate the roles of each individual ligament. Also commonly associated issues with UKAs, such as patellar maltracking, can be delved into by combining the recently added patellofemoral contact detection improvements with these new UKA implant types.

Advancements in the representation of soft tissue structures have also been made in the model. The addition of the posterior capsule allows for more stability in the knee at full extension and may further the understanding of the effects a posterior capsule release may have on the overall mechanics of the knee. Improved MCL attachment profiles have also allowed for anatomically correct force profiles to drive proper kinematics in the joint. By further investigating the effects various attachment point positions have on the force profile of the MCL, a better understanding of the overall ligament can be acquired. These findings can be directly tied to clinically significant applications. For example, the native joint line can often be changed during a TKA or UKA surgery. The MCL analysis done allows for the effects of changing the joint line may have on ligaments to be better understood. The benefits of improved soft tissue representation seeps into many aspects of the model including more accurate kinematics, kinetics, and contact mechanics.

Throughout this dissertation, hundreds of simulations have been completed. These simulations have allowed for a greater understanding of the biomechanics of the knee and the effects of TKA designs features. This model has provided improved representation of soft tissues as well as expanding its capabilities to other activities and implant types. Detailed contact mapping allows for better understanding of wear patterns and implant longevity. In summary, the advancements

made in this dissertation make the FSM a powerful tool which can be a valuable asset to the orthopedic community.

6.1 Assumptions

The human knee joint is extremely complex and modeling every aspect of it can seem to be overwhelming, but we chose to assess one aspect at a time, essentially "peeling an onion one layer at a time". For this FSM, assumptions had to be made in order to solve the variables of interest in the system. One assumption in the model is the simplification of bodies in the model. The femur, tibia, foot, pelvis, etc., each had their masses determined as a proportion of the entire body mass of the average person based upon literature. These proportions may vary between individuals, but for the uses of this model, the ratios remained constant across the ten subjects in the model. All bone models were created from 3D reconstructions of CT scans. The soft tissue attachment points were determined based upon the average person's attachment sites in literature. These points were best chosen for each subject on a case-by-case basis. It is also important to note that the contralateral leg is not directly modeled but has its resultant forces and torques applied onto the pelvis. While this is a logical representation, there may be differences in how a subject may perform an activity that results in different contralateral leg forces. However, these contralateral forces are assumed to be consistent across the various subjects in the model. Furthermore, assumptions were made about the motion at other joints of the lower limb including the ankle and hip. While part of these assumptions is related to the activity type being performed, different individuals likely perform the same activity in slightly different ways. This variability was not accounted for in the model.

Another assumption in the model pertains to the representation of soft tissues. Ligament properties were determined based upon literature and remained consistent across subjects. In actuality, these

properties may vary between individuals as natural joint laxity can often differ between genders. Muscles were represented as bundles of fibers. The overall muscle forces were distributed across the fibers based upon constant values.

This model incorporates a reduction method to incorporate the three major muscle groups: the quadriceps, hamstrings, and gastrocnemius. While other muscles surround the knee, including only these three muscle groups allows for a simpler system, as this assumes that the quadriceps muscle is the primary driver and the hamstring and gastrocnemius muscles are stabilizers. These muscles can be specified or controlled via a PID controller based upon the activity type. Since these are the main contributors to overall leg motion, the model remains accurate despite neglecting some of the smaller soft tissue structures of the leg.

6.2 Limitations

Despite this model's many capabilities, it still has some limitations. The model can only analyze the activities included in the GUI. While these activities continue to expand, more demanding activities like running or abrupt change of direction are not available for analysis, but these are not activities recommended for patients with a TKA. These activities may stress and test the knee joint, but again, clinicians discourage overly intense activities for subjects with knee implants. Another limitation of this model is that it only has ten subjects available for analysis. Establishing a large enough database of subjects to properly represent various populations across the world would be ideal, however this is currently not included in the model. There are also limitations surrounding the representation of the non-implanted side in UKA simulations. While some accommodations were made to address the presence of cartilage in the non-implanted side of the knee, the meniscus is not properly represented. The meniscus provides stability to the knee and may prevent excessive

translation or rotation of the native side. The meniscus has very complex physical properties and would require very different modeling techniques than the current rigid body assumptions that are currently in use.

While the model's focus is the knee joint, more information surrounding the adjacent joints, the hip and ankle, could improve the model's accuracy and offer information on overall lower limb kinematics and kinetics. No detailed contact mechanics are available for these joints as well as fewer soft tissue representations, but they are included in other models that have been developed by our research group. The model also is limited by the speed of analysis. Currently, a DKB activity may take roughly 10 minutes to complete. To complete a detailed analysis in contact mapping algorithm, an additional 2-3 minutes is required for each contact type. While this simulation time is often quicker than many other models, the time simulations take to run may slow the overall analysis.

Clinically, there are also some limitations to the use of the model. In order to perform TKA surgery, there are multiple surgical methods surrounding the balancing of ligaments including gap balancing and measured resection techniques. Currently the model does not allow for easy interchangeability between these techniques to allow for the effects of surgical methodology to be closely studied. While it is possible to manually make these changes in the model, it would take significant time and effort to properly establish simulations which accurately depict changes in ligament balancing techniques. Another important indicator of implant success is the range of motion patients are capable of achieving. It is not well understood what makes a patient limit their motion. This could be due to high quadriceps forces, the presence of knee pain, or the constraints of other soft tissues surrounding the joint. With this in mind, the model cannot accurately predict the range of motion of subjects and runs DKB activities to 120° knee flexion to allow the study of

mechanics in deep flexion. Despite these limitations, the UKA simulations showed good agreement with UKA fluoroscopic studies so the role of the meniscus in knee biomechanics may require further study to be included in the model.

6.3 Future Work

Despite the many improvements made to the model in this dissertation, there is still room for future advancements. Some of these advancements involve making the user's experience with the model a smoother one. Currently the correct default KSIM must first be selected to run a simulation. This default KSIM determines the subject, implant type, and activity. Switching between implant types or activities is not as quick of a process as it could be. The development of an implant database would allow for the user to select the desired implant and size from a drop-down menu. This would automatically load in the new implant's three-dimensional model as well the proper bone cuts and surfaces required for analysis. This implant database would be especially useful when trying to choose the correct implant size or when comparing results of different implant types. Along with this database, the option of choosing alignment types could be another useful addition. Currently, there is much debate surrounding which alignment type will produce the best patient outcomes [6]. If the model could offer simulations of the same implant and subject with different alignment options including mechanical, anatomical, kinematic, and others, this would be of great interest to the orthopedic community.

Another topic of future work is the inclusion of Monte Carlo analysis. This would allow for several simulations to run at once to conduct more thorough and systematic sensitivity analyses. The created plots would help illuminate the roles each variable has in the model and demonstrate how changing a variable may change results. This addition could be especially useful for early design feature investigations and sensitivity analysis of variables of interest.

Finally, the addition of the normal knee into the model would help contextualize the simulation results of implanted subjects. As mentioned in the limitations section, the lack of the meniscus and other soft tissues in the current version of the model makes simulations of the normal knee not entirely accurate. Accounting for these structures would allow for direct comparisons between implanted and native knee kinematics and kinetics. This could prove to be a powerful analysis, as the golden standard for TKAs is the normal knee. However, everyone's knee will perform differently. Incorporating the normal knee into the model would allow for changes in results based purely on the implant's design to be better identified. This would make the strengths and limitations of an implant type very clear to orthopedic researchers.

Overall, the model has many capabilities to provide the orthopedic community with insightful information on TKA and UKA implant performance. Despite its limitations, there is no competing model which can provide the breadth of analysis this model provides, as well as subject-specific and implant-specific details. The future of this model is promising and will prove to be a valuable resource for years to come.

Works Cited

1. Aglietti, P. and P.P.M. Menchetti, *Biomechanics of the patellofemoral joint*, in *The patella*. 1995, Springer. p. 25-48.
2. HUNGERFORD, D.S. and M. Barry, *Biomechanics of the patellofemoral joint.* Clinical Orthopaedics and Related Research (1976-2007), 1979. **144**: p. 9-15.
3. HEHNE, H.-J., *Biomechanics of the patellofemoral joint and its clinical relevance.* Clinical Orthopaedics and Related Research®, 1990. **258**: p. 73-85.
4. Sharma, A., et al., *In vivo contact pressures in total knee arthroplasty.* The Journal of arthroplasty, 2007. **22**(3): p. 404-416.
5. Sharma, A., et al., *High-flexion TKA designs: what are their in vivo contact mechanics?* Clinical Orthopaedics and Related Research®, 2007. **464**: p. 117-126.
6. Sharma, A., et al., *In vivo patellofemoral forces in high flexion total knee arthroplasty.* Journal of biomechanics, 2008. **41**(3): p. 642-648.
7. Saxby, D.J., et al., *Tibiofemoral Contact Forces in the Anterior Cruciate Ligament-Reconstructed Knee.* Medicine and science in sports and exercise, 2016. **48**(11): p. 2195-2206.
8. Cleather, D.J. and M.B. Czasche, *Knee forces during landing in men and women.* Journal of Human Kinetics, 2019. **68**(1): p. 177-192.
9. Richard, V., *Multi-body optimization method for the estimation of joint kinematics: prospects of improvement*. 2016, Ph. D.). Claude Bernard University Lyon 1.
10. Fu, F.H., et al., *Biomechanics of knee ligaments: basic concepts and clinical application.* JBJS, 1993. **75**(11): p. 1716-1727.
11. Woo, S.L., et al., *Biomechanics of knee ligaments.* The American journal of sports medicine, 1999. **27**(4): p. 533-543.
12. Woo, S.L.-Y., et al., *Biomechanics of knee ligaments: injury, healing, and repair.* Journal of biomechanics, 2006. **39**(1): p. 1-20.
13. Germany, C., *How Does the Knee Work?* Institute for Quality and Efficiency in Health Care 2020.
14. Andriacchi, T.P., C.O. Dyrby, and T.S. Johnson, *The use of functional analysis in evaluating knee kinematics.* Clinical Orthopaedics and Related Research®, 2003. **410**: p. 44-53.
15. Komistek, R.D., D.A. Dennis, and M. Mahfouz, *In vivo fluoroscopic analysis of the normal human knee.* Clinical Orthopaedics and Related Research®, 2003. **410**: p. 69-81.
16. Kim, H.Y., et al., *Screw-home movement of the tibiofemoral joint during normal gait: three-dimensional analysis.* Clinics in orthopedic surgery, 2015. **7**(3): p. 303.
17. Feng, Y., et al., *Motion of the femoral condyles in flexion and extension during a continuous lunge.* Journal of Orthopaedic Research, 2015. **33**(4): p. 591-597.
18. Neuprez, A., et al., *Patients' expectations impact their satisfaction following total hip or knee arthroplasty.* PLoS One, 2016. **11**(12): p. e0167911.
19. Jacobs, C.A. and C.P. Christensen, *Factors influencing patient satisfaction two to five years after primary total knee arthroplasty.* The Journal of arthroplasty, 2014. **29**(6): p. 1189-1191.
20. Healy, W.L., et al., *Complications of total knee arthroplasty: standardized list and definitions of the Knee Society.* Clinical Orthopaedics and Related Research®, 2013. **471**(1): p. 215-220.
21. Devers, B.N., et al., *Does greater knee flexion increase patient function and satisfaction after total knee arthroplasty?* The Journal of arthroplasty, 2011. **26**(2): p. 178-186.
22. Mirulla, A.I., et al., *Assessment of paradoxical anterior translation in a CR total knee prosthesis coupling dynamic RSA and FE techniques.* Journal of Experimental Orthopaedics, 2021. **8**: p. 1-7.
23. Food, U. and D. Administration, *A history of medical device regulation & oversight in the United States.* 2019.
24. Walter, J.P. and M.G. Pandy, *Dynamic simulation of knee-joint loading during gait using force-feedback control and surrogate contact modelling.* Medical Engineering & Physics, 2017. **48**: p. 196-205.
25. Choi, Y.-J. and H.J. Ra, *Patient satisfaction after total knee arthroplasty.* Knee surgery & related research, 2016. **28**(1): p. 1.
26. Bahce, E. and E. Emir, *Investigation of wear of ultra high molecular weight polyethylene in a soft tissue behaviour knee joint prosthesis wear test simulator.* Journal of Materials Research and Technology, 2019. **8**(5): p. 4642-4650.

27. Manal, K. and T.S. Buchanan, *An electromyogram-driven musculoskeletal model of the knee to predict in vivo joint contact forces during normal and novel gait patterns.* Journal of biomechanical engineering, 2013. **135**(2): p. 021014.
28. Reynaud, V., et al., *Core outcome measurement instruments for clinical trials of total knee arthroplasty: a systematic review.* Journal of clinical medicine, 2020. **9**(8): p. 2439.
29. Marya, S. and R. Thukral, *Knee Replacement*. 2011: JP Medical Ltd.
30. Kennedy, F.E., et al., *Tribological conditions in mobile bearing total knee prostheses.* Tribology International, 2013. **63**: p. 78-88.
31. Wittig, U., et al., *Higher use of fixed-bearing over mobile-bearing and posterior-stabilized over medial pivot designs in total knee arthroplasty (TKA): a systematic comparative analysis using worldwide arthroplasty registers from England and Wales, Australia, Norway, New Zealand, Germany and Switzerland.* Archives of Orthopaedic and Trauma Surgery, 2023. **143**(2): p. 1021-1029.
32. Ferguson, K., et al., *A comparison of lateral release rates in fixed-versus mobile-bearing total knee arthroplasty.* Journal of Orthopaedics and Traumatology, 2015. **16**: p. 87-90.
33. Huang, C.-H., J.-J. Liau, and C.-K. Cheng, *Fixed or mobile-bearing total knee arthroplasty.* Journal of orthopaedic surgery and research, 2007. **2**: p. 1-8.
34. Bhan, S., et al., *A comparison of fixed-bearing and mobile-bearing total knee arthroplasty at a minimum follow-up of 4.5 years.* JBJS, 2005. **87**(10): p. 2290-2296.
35. Fitzpatrick, C.K., et al., *Mechanics of post-cam engagement during simulated dynamic activity.* Journal of Orthopaedic Research, 2013. **31**(9): p. 1438-1446.
36. Grieco, T.F., et al., *In vivo kinematic comparison of a bicruciate stabilized total knee arthroplasty and the normal knee using fluoroscopy.* The Journal of arthroplasty, 2018. **33**(2): p. 565-571.
37. Smith, L., et al. *IN VIVO KINEMATICS COMPARISON BETWEEN SUBJECTS HAVING A POSTERIOR CRUCIATE-RETAINING TOTAL KNEE ARTHROPLASTY OR A BICRUCIATE-RETAINING TOTAL KNEE ARTHROPLASTY AND THE NORMAL KNEE DURING DEEP KNEE BEND*. in *Orthopaedic Proceedings*. 2020. Bone & Joint.
38. Migliorini, F., et al., *Mobile bearing versus fixed bearing for unicompartmental arthroplasty in monocompartmental osteoarthritis of the knee: a meta-analysis.* Journal of clinical medicine, 2022. **11**(10): p. 2837.
39. Murakami, K., et al., *In vivo kinematics of gait in posterior-stabilized and bicruciate-stabilized total knee arthroplasties using image-matching techniques.* International Orthopaedics, 2018. **42**: p. 2573-2581.
40. Burger, J.A., et al., *Bearing design influences short-to mid-term survivorship, but not functional outcomes following lateral unicompartmental knee arthroplasty: a systematic review.* Knee Surgery, Sports Traumatology, Arthroscopy, 2019. **27**: p. 2276-2288.
41. Migliorini, F., et al., *Unicompartmental versus total knee arthroplasty for knee osteoarthritis.* European Journal of Orthopaedic Surgery & Traumatology, 2019. **29**: p. 947-955.
42. Bayo, E., *A finite-element approach to control the end-point motion of a single-link flexible robot.* Journal of Robotic systems, 1987. **4**(1): p. 63-75.
43. Breen, A.C., *Measurement of joint kinematics utilising video-fluoroscopy*, in *Human Orthopaedic Biomechanics*. 2022, Elsevier. p. 623-635.
44. Needham, R., J. Stebbins, and N. Chockalingam, *Three-dimensional kinematics of the lumbar spine during gait using marker-based systems: a systematic review.* Journal of medical engineering & technology, 2016. **40**(4): p. 172-185.
45. Holliday, W., et al., *Static versus dynamic kinematics in cyclists: A comparison of goniometer, inclinometer and 3D motion capture.* European Journal of Sport Science, 2017. **17**(9): p. 1129-1142.
46. Pandy, M.G. and N. Berme, *A numerical method for simulating the dynamics of human walking.* Journal of biomechanics, 1988. **21**(12): p. 1043-1051.
47. Wagner, H., et al., *Optimization reduces knee-joint forces during walking and squatting: Validating the inverse dynamics approach for full body movements on instrumented knee prostheses.* Motor Control, 2022. **27**(2): p. 161-178.
48. Narayanaswami, P., et al., *Critically re-evaluating a common technique: accuracy, reliability, and confirmation bias of EMG.* Neurology, 2016. **86**(3): p. 218-223.
49. Holder, J., et al., *A systematic review of the associations between inverse dynamics and musculoskeletal modeling to investigate joint loading in a clinical environment.* Frontiers in bioengineering and biotechnology, 2020. **8**: p. 603907.

50. Thelen, D.G. and F.C. Anderson, *Using computed muscle control to generate forward dynamic simulations of human walking from experimental data.* Journal of biomechanics, 2006. **39**(6): p. 1107-1115.
51. Tsai, L.-W., *The mechanics of serial and parallel manipulators.* Robot Analysis, John Wiley & Sons, Inc, 1999.
52. Dhaher, Y.Y. and L.E. Kahn, *The effect of vastus medialis forces on patello-femoral contact: a model-based study.* J. Biomech. Eng., 2002. **124**(6): p. 758-767.
53. Kiapour, A., et al., *Finite element model of the knee for investigation of injury mechanisms: development and validation.* Journal of biomechanical engineering, 2014. **136**(1): p. 011002.
54. Srinivas, G.R., A. Deb, and M.N. Kumar, *A study on polyethylene stresses in mobile-bearing and fixed-bearing total knee arthroplasty (TKA) using explicit finite element analysis.* Journal of Long-Term Effects of Medical Implants, 2013. **23**(4).
55. Khasian, M., et al., *A validated forward solution dynamics mathematical model of the knee joint: can it be an effective alternative for implant evaluation?* The Journal of Arthroplasty, 2020. **35**(11): p. 3289-3299.
56. Sharif Shourijeh, M. and J. McPhee, *Forward dynamic optimization of human gait simulations: a global parameterization approach.* Journal of Computational and Nonlinear Dynamics, 2014. **9**(3): p. 031018.
57. Liu, J., et al., *Rigid model-based 3D segmentation of the bones of joints in MR and CT images for motion analysis.* Medical physics, 2008. **35**(8): p. 3637-3649.
58. Levinson, D.A. and T.R. Kane, *AUTOLEV—a new approach to multibody dynamics*, in *Multibody systems handbook*. 1990, Springer. p. 81-102.
59. Carretero, J.M., et al., *Exploring bone volume and skeletal weight in the Middle Pleistocene humans from the Sima de los Huesos site (Sierra de Atapuerca, Spain).* Journal of Anatomy, 2018. **233**(6): p. 740-754.
60. Wang, J., et al., *Law of dynamic deformation of bone.* Chinese Medical Journal, 2019. **132**(21): p. 2636-2637.
61. Martins, J., et al., *A numerical model of passive and active behavior of skeletal muscles.* Computer methods in applied mechanics and engineering, 1998. **151**(3-4): p. 419-433.
62. Avis, D. and D. Bremner. *How good are convex hull algorithms?* in *Proceedings of the eleventh annual symposium on Computational geometry*. 1995.
63. Edelsbrunner, H., T.S. Tan, and R. Waupotitsch. *An o (n 2log n) time algorithm for the minmax angle triangulation*. in *Proceedings of the sixth annual symposium on Computational geometry*. 1990.
64. Brewe, D.E. and B.J. Hamrock, *Simplified solution for elliptical-contact deformation between two elastic solids.* 1977.
65. Adravanti, P. and S. Vasta, *Varus-valgus constrained implants in total knee arthroplasty: indications and technique.* Acta Bio Medica: Atenei Parmensis, 2017. **88**(Suppl 2): p. 112.
66. Kim, K.T., et al., *Long-term clinical results of unicompartmental knee arthroplasty in patients younger than 60 years of age: minimum 10-year follow-up.* Knee surgery & related research, 2018. **30**(1): p. 28.
67. Vasso, M., A. Antoniadis, and N. Helmy, *Update on unicompartmental knee arthroplasty: current indications and failure modes.* EFORT open reviews, 2018. **3**(8): p. 442-448.
68. Sylvester, A.D., S.G. Lautzenheiser, and P.A. Kramer, *Muscle forces and the demands of human walking.* Biology Open, 2021. **10**(7): p. bio058595.
69. LaCour, M.T., M.D. Ta, and R.D. Komistek, *Development of a hip joint mathematical model to assess implanted and non-implanted hips under various conditions.* Journal of Biomechanics, 2020. **112**: p. 110051.
70. Passmore, E., H.K. Graham, and M. Sangeux, *Defining the medial-lateral axis of the femur: Medical imaging, conventional and functional calibration methods lead to differences in hip rotation kinematics for children with torsional deformities.* Journal of Biomechanics, 2018. **69**: p. 156-163.
71. Wiik AV, A.A., Brevadt M, Jones G, Cobb J., *Abnormal ground reaction forces lead to a general decline in gait speed in knee osteoarthritis patients.* World J Orthop, 2017. **8(4)**: p. 322-328.
72. Wijdicks, C.A., et al., *Structural properties of the primary medial knee ligaments.* The American journal of sports medicine, 2010. **38**(8): p. 1638-1646.
73. Jacob, G., et al., *Percutaneous arthroscopic assisted knee medial collateral ligament repair.* Arthroscopy Techniques, 2020. **9**(10): p. e1511-e1517.
74. Steinbrück, A., et al., *Posterior cruciate ligament balancing in total knee arthroplasty: a numerical study with a dynamic force controlled knee model.* Biomedical Engineering Online, 2014. **13**: p. 1-13.
75. Farshidfar, S.S., et al., *The effect of modelling parameters in the development and validation of knee joint models on ligament mechanics: a systematic review.* PLoS One, 2022. **17**(1): p. e0262684.
76. Nasseri, A., et al., *Modelling the loading mechanics of anterior cruciate ligament.* Computer Methods and Programs in Biomedicine, 2020. **184**: p. 105098.

77. Smale, K.B., et al., *Effect of implementing magnetic resonance imaging for patient-specific OpenSim models on lower-body kinematics and knee ligament lengths.* Journal of biomechanics, 2019. **83**: p. 9-15.
78. Sancheti KH, S.P., Shyam AK, Joshi R, Patil K, Jain A, *Factors affecting range of motion in total knee arthroplasty using high flexion prosthesis: A prospective study.* Indian J Orthop., 2013. **Jan**.
79. Shelburne, K.B. and M.G. Pandy, *A Dynamic Model of the Knee and Lower Limb for Simulating Rising Movements.* Computer Methods in Biomechanics and Biomedical Engineering, 2002. **5**(2): p. 149-159.
80. Iwamoto, K., et al., *Comparison of in vivo kinematics of total knee arthroplasty between cruciate retaining and cruciate substituting insert.* Asia-Pacific Journal of Sports Medicine, Arthroscopy, Rehabilitation and Technology, 2021. **26**: p. 47-52.
81. Dessinger, G., et al., *IN VIVO DETERMINATION OF KNEE KINEMATICS FOR SUBJECTS IMPLANTED WITH A POSTERIOR-STABILIZED TOTAL KNEE ARTHROPLASTY DESIGNED FOR GENDER AND ETHNICITY.* Orthopaedic Proceedings, 2020. **102-B**(SUPP_1): p. 137-137.
82. Zumbrunn, T., et al., *Medial unicompartmental knee arthroplasty in ACL-deficient knees is a viable treatment option: in vivo kinematic evaluation using a moving fluoroscope.* Knee Surgery, Sports Traumatology, Arthroscopy, 2020. **28**: p. 1765-1773.
83. Haas, B.D., et al., *Kinematic comparison of posterior cruciate sacrifice versus substitution in a mobile bearing total knee arthroplasty.* The Journal of arthroplasty, 2002. **17**(6): p. 685-692.
84. Beynnon, B.D., et al., *The strain behavior of the anterior cruciate ligament during squatting and active flexion-extension: a comparison of an open and a closed kinetic chain exercise.* The American Journal of Sports Medicine, 1997. **25**(6): p. 823-829.
85. Kulas, A.S., T. Hortobágyi, and P. DeVita, *Trunk position modulates anterior cruciate ligament forces and strains during a single-leg squat.* Clinical biomechanics, 2012. **27**(1): p. 16-21.
86. Toutoungi, D., et al., *Cruciate ligament forces in the human knee during rehabilitation exercises.* Clinical biomechanics, 2000. **15**(3): p. 176-187.
87. Argenson, J.-N.A., et al., *In vivo determination of knee kinematics for subjects implanted with a unicompartmental arthroplasty.* The Journal of arthroplasty, 2002. **17**(8): p. 1049-1054.
88. Guan, S., et al., *In vivo six-degree-of-freedom knee-joint kinematics in overground and treadmill walking following total knee arthroplasty.* Journal of Orthopaedic Research, 2017. **35**(8): p. 1634-1643.
89. Arazpour, M., et al., *The Effect of Patellofemoral Pain Syndrome on Gait Parameters: A Literature Review.* (2345-4644 (Print)).
90. Kitisak, K., N. Siroros, and C. Rungsiyakull, *Finite Element Analysis in Posterior Stabilized Total Knee Arthroplasty on Kneeling.* International Journal of Pharma Medicine and Biological Sciences, 2016. **5**(1): p. 67.
91. Hinterwimmer, S., et al., *Patella kinematics and patello-femoral contact areas in patients with genu varum and mild osteoarthritis.* Clinical Biomechanics, 2004. **19**(7): p. 704-710.

Vita

Seth Campbell Coomer was born July 22, 1994 in Nashville, Tennessee. He inherited his love for math and science from his parents who both had careers in STEM. In high school Seth was involved in both varsity cross country and soccer while also enrolling in advanced placement classes. In the fall of 2013 Seth was accepted into the University of Tennessee's Honors Program and started his undergraduate work in biomedical engineering.

During undergrad Seth completed pre-med requirements in addition to his biomedical engineering workload in hopes of attending medical school. However, Seth fell in love with problem solving and research, ultimately deciding to pursue a graduate degree in biomedical engineering. In his first semester of graduate school, he enrolled in an advanced biomechanics class which led to a position in the Center for Musculoskeletal Research lab in January 2019.

Once in CMR, Seth began work on the inverse modeling of patellofemoral kinematics in the implanted and normal knee. He was also involved in the fluoroscopic analysis of hundreds of subjects across the US and Europe. Seth's main work was the development of a forward mathematical model of the knee, resulting in multiple peer-reviewed journal articles and presentations at international orthopedic conferences. Outside of academics, Seth is an avid sports fan and closely follows Tennessee sports teams and European soccer. Seth continues to play soccer and guitar recreationally. He also enjoys exploring the outdoors with his dog Casey and traveling to new places. Seth plans to continue his research work in industry as he has taken a position at Medical Metrics, developing diagnostic tools for the spine.